2018

Analysis of Viscoelestic Properties of Elastomers Using Molecular Modeling

Suvrajyoti Kar
University of Rhode Island, kar.suvraj@gmail.com

ANALYSIS OF VISCOELASTIC PROPERTIES OF ELASTOMERS USING MOLECULAR MODELING

BY

SUVRAJYOTI KAR

A DISSERTATION SUBMITTED IN PARTIAL FULFILLMENT OF THE REQUIREMENTS FOR THE DEGREE OF

DOCTOR OF PHILOSOPHY

IN

CHEMICAL ENGINEERING

UNIVERSITY OF RHODE ISLAND

2018

DOCTOR OF PHILOSOPHY DISSERTATION

OF

SUVRAJYOTI KAR

APPROVED:

Dissertation Committee:

Major Professor Michael L. Greenfield

Arijit Bose

David G. Taggart

Nasser H. Zawia

DEAN OF THE GRADUATE SCHOOL

UNIVERSITY OF RHODE ISLAND

2018

ABSTRACT

The goal of this research is to quantify and analyze elastomer chain conformations and their role in affecting rubber tire viscoelastic properties through the development of novel numerical methods. The hypothesis is that changes in the statistical mechanics of chain conformations at the microscopic scale provide a direct molecular link towards quantifying macroscopic properties of elastomers. The molecular level investigation began with simulating chains in the unperturbed state to study the impact of chain size and temperature on overall chain size statistics. To understand changes in the chain conformations under stress, a numerical model was developed that encompasses effects from multiple forms of deformation. The probabilistic approach implemented in this work allowed for molecular level understanding of chain behavior.

Flory's Rotational Isomeric State (RIS) approach was used to generate numerous uncorrelated, isolated, random conformations of amorphous cis- and trans-1,4-polybutadiene single chains under unperturbed conditions of different molecular weights and over a range of temperatures. Probability density distributions of squared end-to-end distances of these chains were quantified to study size properties. Characteristic ratios were in good agreement with prior experimental and

theoretical findings, and increased with increasing molecular weight of cis and trans chains, with this effect being more pronounced for trans than for cis chains. Chain swelling was observed on heating indicated by an increasing characteristic ratio with temperature and positive temperature coefficients for both cis and trans chains. Chain size and shape properties were mutually dependent, with most changes in shape occurring due to changes along the principal direction. A larger relative increase in probability density distribution of unlikely larger chains and a smaller relative decrease in probability density distribution of more likely smaller chains resulted in increased average chain size and characteristic ratios with increasing temperature. This has been termed the "*taut conformation effect*" and had a significant impact on chain swelling with heating. This effect motivated further work into investigating its presence in other polymers such as polypropylene and polystyrene which is discussed in chapter 4.

After the unperturbed state of chain ensembles were analyzed through size and shape studies, the perturbed or deformed state of the ensembles were explored through molecular modeling techniques to exert and quantify external stresses. Uniaxial, equibiaxial deformation and shear were applied to unperturbed chain ensembles which resulted in changes in their probability density distributions and

elastic free energy. The approach for computing changes in elastic free energy involved developing a probability-based numerical method that can be applied across multiple forms of deformation. In order to determine the accuracy of the numerical method, it was initially applied to generated Gaussian chains and compared against known analytical equations. The numerical results and known analytical solutions of Gaussian chains were in excellent agreement and hence the numerical model was extended to computing elastic free energy change, force, and stress on RIS cis- and trans-1,4-polybutadiene chains. Compression forces were much greater than tension forces. Equibiaxial and uniaxial stresses were equivalent in a single extension direction, and greater than shear. Forces and stresses increased with deformation and showed dependence on chain volume and temperature. Significant variation was observed in moduli with chain repeat unit size while only minor variations were observed with temperature. Fewer repeat unit size chains correspond to lower molecular weight between cross-links causing a more tightly cross-linked chain network. This resulted in greater moduli as compared to chains of more repeat units. A slight linear increase in moduli with temperature of chains of the same repeat unit size was observed. Young's and shear moduli computed from the numerical model were in good agreement with experimental results. The novelty

in this approach is the ability to incorporate polymer-polymer and polymer-filler interactions.

The "*taut conformation effect*" was identified as a significant contributor to chain size behavior for polybutadiene, and its presence in vinyl polymers, such as polypropylene and polystyrene, were investigated. Random conformations of numerous single chains of amorphous, isotactic polypropylene and polystyrene were generated using Flory's RIS approach. Characteristic ratios were in decent agreement with prior experimental and theoretical results. These ratios increased with molecular weight and were higher for polystyrene than polypropylene. Chain heating resulted in shrinkage for both polypropylene and polystyrene, indicated by decreasing characteristic ratios and negative temperature coefficients, which were in decent agreement with experimental results. Probability density distribution and chain size subset analysis indicated that only the least probable long size chains or taut conformations showed a decrease in probability density distribution and characteristic ratio with temperature. The most probable medium size chains hardly showed any change in their probability density distributions and characteristic ratios with temperature, while short size chains showed marginal increase. Hence, much like polybutadiene chains, less probable taut chain conformations had a sig-

nificant impact on the average chain size indicating "*taut conformation effect*".

The primary focus of this dissertation was analyzing chain conformation statistics. In addition to that work, rheology experiments were performed on asphalt systems, and models were developed in order to predict the experimental results. Rheological studies were done to analyze viscoelastic properties of asphalt binders from different sources and under various aging conditions. Time-temperature superposition (TTS) was applied to frequency sweep data to produce master curves, and discrete and continuous Maxwell models were applied to predict stress relaxation modulus, relaxation and retardation time distributions, and creep compliance. Moduli increased upon aging indicating increased binder stiffness. Zero-shear viscosities decreased with increasing temperature for all binders due to increasing molecular motion and flexibility. At shorter times, stress relaxation moduli and creep compliance were similar for all binders, but with increasing time, unaged binders relaxed more rapidly than aged binders. Low creep compliance at shorter times corresponded to the absence of any configurational re-arrangements of asphalt binders. TTS allowed for computation of creep compliance at very low temperatures (-18°C) to predict Pressure Aging Vessel (PAV) aged binder stiffness and resistance to thermal cracking at such low temperatures. Two binder samples were

analyzed and showed similar low temperature flexibilities. The low temperature stiffness results predicted by our rheological model were in good agreement with bending beam rheometer experimental results, hence corroborating the efficiency of our model.

This work encompasses three significant contributions to the scientific community. For polybutadiene, polypropylene and polystyrene, the impact of less likely, taut conformations on the overall chain size was identified and termed the "*taut conformation effect*". A probability-based, reliable numerical tool was developed to predict mechanical properties of elastomers subjected to multiaxial deformations. Finally, an example of applying rheology models to experimental data was shown by accurately predicting asphalt binder stiffness and resistance to low temperature thermal cracking.

ACKNOWLEDGMENTS

I would like to thank my advisor Dr. Michael Greenfield for his constant encouragement and valuable guidance throughout my Graduate School career. He has always encouraged me to strive for the best, to think outside the box, and push the boundaries of my knowledge. Our meetings ranged from an hour update to an evening marathon leaving both of us exhausted, but they were always fruitful and fulfilling. Thanks to him, I had the opportunity to travel all over the USA presenting our research, to network with other professional scientists, and work on projects in various aspects of my field. As I move beyond the realm of Graduate School, he has been instrumental in guiding me on a path towards a professional career. The experience I have gained from him is invaluable and will hold me in good stead for the future.

I want to thank my wonderful committee members Dr. Arijit Bose, Dr. David Taggart, and my dissertation defense chair Dr. Yana Reshetnyak for their precious input and time. Their comments and suggestions have helped make this dissertation possible.

In addition to inputs and guidance on my dissertation, I have had the fortune of attending two classes with Dr. Bose. He has always been very supportive with

my ideas and very encouraging in his demeanor. I will fondly remember all our conversations regarding science, cricket and beyond. I am also thankful for his role in helping my wife, Julie Cuddigan, get her first industrial job.

Dr. Taggart has always been open to discussions and meetings with a smile on his face. He has a wonderfully caring personality that shines through. I have always felt very comfortable approaching him regarding any questions and he patiently answered them all.

Dr. Reshetnyak very graciously accepted my request to be the chair of my committee. I had taken a biophysics course with her which was enriching and she was always available to answer any questions I had regarding the course material. I connected with her vast knowledge of polymer physics and am fortunate to have her as the chair of my committee.

I want to thank Brenda and Sheryl from the Chemical Engineering Department and Dean's Office respectively for their timely help whenever I needed them. They were the first individuals from Chemical Engineering that I had met at URI and will never forget the times we have spent together.

I am thankful to each and every member of the Chemical Engineering Department at URI, especially my labmate Faramarz. He has been a good friend and I

wish him all the best on his journey towards completing his PhD dissertation.

During my time at URI, I served as the President of the Indian Student Association and helped build upon South East Asian cultural awareness in the URI community. "*Diwali*" or the Indian Festival of Lights became one of the most popular and widely attended events at URI and gained many laurels under my leadership. I would like to thank each and every member of the Indian Student Association family that made this possible.

I also had the fortune of pursuing my passion for cricket and the honor of leading a cricket team. Being a team sport, it allowed me to meet and play with individuals from various cultures and walks of life.

Throughout my time at URI, I have been fortunate to meet many wonderful people who have had a profound influence on my life, whether it be my colleagues in the Chemical Engineering Department or other departments, in the Graduate School, in the Indian Student Association or even in the field of cricket. I shall always cherish these times and memories.

DEDICATION

I dedicate this dissertation to my parents, Chitralekha and Subhash, and my wife, Julie.

Ma and Baba, thank you for instilling virtues in me, teaching me that there is no alternative to hard work and how important it is to be kind, caring and patient in life. Everything I will ever achieve in life will always be dedicated to you.

Julie, you are my significant other in the truest term. It is safe to say that this dissertation would not have been possible without your help, support and love. From March 2nd, 2015 when we first met till now, you have made my life better, more meaningful and fun.

Ma, Baba and Julie - I love you!

PREFACE

The following work is presented in manuscript format in accordance with the guidelines set by the University of Rhode Island Graduate School. This dissertation consists of five manuscripts, one of which was published in the journal Polymer and four have been prepared for submission to peer reviewed journals.

Chapter 1 is a manuscript "Sizes and shapes of simulated amorphous cis- and trans-1,4 polybutadiene". This was published in the journal Polymer in 2015.

Chapter 2 is a manuscript "Simulating stress-strain behavior by using individual chains. 1. Uniaxial deformation of amorphous cis- and trans-1,4-polybutadiene". This is prepared for submission to the journal Polymer.

Chapter 3 is a manuscript "Simulating stress-strain behavior by using individual chains. 2. Biaxial deformation and shear of amorphous cis- and trans-1,4-polybutadiene". This is prepared for submission to the journal Polymer.

Chapter 4 is a manuscript "Size Distribution Analysis of Simulated Amorphous Vinyl Polymer Chains: Polypropylene and Polystyrene". This is prepared for submission to the journal Polymer.

Chapter 5 is a manuscript "Fitting Viscoelastic Models to Bitumen Shear Rheometry Data to Predict Rheological Properties". This is prepared for submis-

sion to the journal Construction and Building Materials.

TABLE OF CONTENTS

LIST OF TABLES

LIST OF FIGURES

Figure **Page**

CHAPTER 1

"Sizes and shapes of simulated amorphous cis- and trans-1,4-polybutadiene"

by

Suvrajyoti Kar, Michael L Greenfield *

Department of Chemical Engineering, University of Rhode Island, Kingston, RI - 02881, USA

Polymer

Volume 62

Year 2015

Pages 129-138

*Corresponding author email: greenfield@uri.edu

Abstract

Controlling loss modulus can decrease tire rolling resistance. Deformation forces in elastomers depend on chain conformation. As a first step toward screening chemical effects on these, isolated single cis- and trans-1,4-polybutadiene chains of uncorrelated random conformations under unperturbed conditions are generated using Flory's Rotational Isomeric State approach, with discrete rotational states defined by Mark, Abe, and Flory. Averages and distribution of squared end-to-end distance, radius of gyration, and shape parameters are studied for chains ranging from 15 to 120 repeat units at 343 K and for the 50-unit chain at temperatures of 275 K to 400 K. The calculated characteristic ratios are in good agreement with experimental and prior computed values. Only small absolute changes in chain size probability densities with temperature are found. A larger relative increase in probability density of unlikely larger chains and a smaller relative decrease in probability density of more likely smaller chains result in increased average chain size and characteristic ratios with increasing temperature. Within subdivisions of the size distribution, larger chains show an increase in characteristic ratio with temperature, while smaller and medium size chains show little change with temperature. This previously unreported effect is stronger for trans than for cis chains.

Eigenvalues of the radius of gyration matrix quantify chain shapes along principal directions. Averaged shape measures differ between cis and trans chains, and most shape changes arise along the longest principal direction. Joint correlations between chain size and shape show they are mutually dependent.

Keywords: Rotational Isomeric State Chain conformation, size distribution, 1,4-polybutadiene, squared radius of gyration, Gaussian, chain polymer shape.

1.1 Introduction

Vehicle tires are an important application of rubber worldwide. Methods that improve fuel economy by decreasing rolling resistance without compromising wear resistance and traction have been reported [1, 2, 3, 4]. Rolling resistance results from the energy a tire absorbs as it revolves and deflects when in contact with the road.

This paper takes steps toward understanding how elastomer chains contribute to rolling resistance. Its basis is an assumption that rolling resistance on the macroscale connects directly to energy losses from changes in chain conformations on the microscale. This paper is part of an overall project to quantify how differences in chain conformations in the presence of interactive fillers lead to entropy differences during deformation, which lead to changes in energy losses that con-

tribute to rolling resistance. In this approach, studying and understanding the statistical mechanics of chain conformations provide a molecular link toward understanding the role of chain conformations in determining rolling resistance.

A rubber tire comprises one or more different types of elastomers such as styrene-butadiene rubber (SBR), polybutadiene, or polyisoprene. In addition to elastomers, tires include materials such as reinforcement fillers, curing agents, processing oil, antidegradant, stearic acid, etc.[5]. Here we focus on unfilled polybutadiene as an initial case. Each single chain can represent an elastomer chain, a butadiene component within an SBR block copolymer, or a butadiene subchain between cross links.

Burkhart [6] reviewed structurally realistic elastomer models that were developed from the mid-1960s to the 1990s. He documented rubber elasticity theories and molecular simulations that included molecular mechanics, Flory's Rotational Isomeric State (RIS) method [7, 8], Monte Carlo, and molecular dynamics. The review includes both single chain and bulk elastomer simulations. The RIS method is efficient for sampling single-chain conformations and thus appeared in early literature. Molecular dynamics or Monte Carlo simulation methods in later papers account for chain-chain interactions that arise in bulk systems.

Mark [9, 10] and Abe and Flory [11] used the RIS method to generate random conformations of cis- and trans-1,4-polybutadiene chains. Mark's work focused on computing characteristic ratios of chains and using comparisons with experimentally obtained values to determine model parameters. Abe and Flory computed properties that included strain-birefringence coefficients and coefficients of rotational isomerization under stretching. Both groups obtained temperature coefficients of mean-squared end-to-end distance and compared intramolecular energies among different rotational isomeric states per repeat unit of polybutadiene. Kajiwara and Burchard [12] used a Monte Carlo implementation of the RIS model to simulate several polymers, including polybutadienes and polyisoprenes. They found that characteristic ratios for 120 to 150 skeletal carbon atoms reached infinite chain limits.

Groups starting with Mattice and co-workers have compared single chain conformations to bulk structures. Li and Mattice [13] generated single cis-1,4-polybutadiene chains of 99 repeat units at 300 K using a Monte Carlo method followed by minimization. Instead of using discrete rotational states with fixed torsional angles around single bonds, Li and Mattice used a continuous distribution of torsion angles. They found low energy states similar to those suggested

by Mark [9, 10], and torsion angle probability distributions were similar within single chain and bulk structures. Kim, Misra, and Mattice [14] used that same methodology to study amorphous structures of trans-1,4-polybutadiene, isotactic 1,2-polybutadiene, and a random butadiene copolymer. They found few CH–CH_2 torsions in cis configurations. Gestoso et al. [15] used end-bridging Monte Carlo simulations to simulate cis-1,4-polybutadiene in the melt and as single chains. They found similar end-to-end distances, single-chain structure factor, and torsion angle distributions for both cases.

Complementary results have been found for bulk systems of polybutadiene from molecular dynamics simulations. Predictions include density, dynamic structure factor, and torsion angle distribution [16, 17, 18, 19, 20, 21, 22, 23]. Smith and Paul [24] developed a united atom (UA) force field for molecular dynamics simulation of 1,4-polybutadiene systems based on ab initio quantum chemistry. They computed characteristic ratios for chains within bulk polybutadiene. Smith et al. [20] quantified differences among neutron spin echo scattering, molecular dynamics simulation, and the Rouse model, noting non-Gaussian distributions of segment-segment distances.

Some studies have focused on correlations in conformational changes. Gee and

Boyd [18] found similar conformational transition rate activation energies in single chain and bulk systems, while torsion angle correlation rates showed a higher activation energy in the bulk. A cooperative kinetics approach models how relaxation rate about one torsion angle in polybutadiene impacts relaxation of neighboring torsions [25, 26]. Correlations of this sort were found in a dynamic RIS model that was parameterized by MD results [27].

Experimental data may be interpreted to obtain chain conformation measures. Danusso et al. [28], Moraglio [29], and Abe and Fujita [30] measured intrinsic viscosity of cis-1,4-polybutadiene under theta conditions. Mark [9] extracted characteristic ratio results from these data. Mark [10] also cites intrinsic viscosity experiments published later [31] to determine the characteristic ratio of trans-1,4-polybutadiene. Hadjichristidis et al. [32] measured intrinsic viscosity under theta conditions to determine the characteristic ratio of a polybutadiene of 36% cis, 57% trans, 7% 1,2-vinyl composition. Gkourmpis and Mitchell [33] measured the structure factor of polybutadiene by neutron scattering and compared to predictions from the RIS model. Agreement between these methods was better at small wavevector (longer distances), which led them to alter the chain parameters in their model on the basis of improved agreement of predicted scattering results.

In this work we have studied size and shape properties of random chain conformations of polybutadiene by calculating the distribution of single chain conformations that arise under theta conditions. Numerous ($> 10^5$) uncorrelated random conformations of isolated cis- and trans-1,4-polybutadiene single chains were computed under unperturbed conditions. Using a single chain in each computation is justified because a flexible polymer surrounded by the same polymer takes on the same average shape as a single random polymer chain in a theta solvent or a melt [34], as confirmed in cis-1,4-polybutadiene simulations [13]. The polybutadiene chains were generated using the RIS model. Each chain realization in RIS provides an independent sample. While the standard molecular dynamics and Monte Carlo methods provide sequences of related states, the small changes that occur in each step lead to correlations that must be relaxed to sample an equilibrium distribution. The RIS method offers an advantage of generating a much larger number of uncorrelated random chain conformations in a computationally cheap manner. Using the ensemble of single-chain configurations, characteristic ratios were computed for cis- and trans-1,4 polybutadiene chains at different chain lengths and over a range of temperatures. Probability density distributions of the chains at different temperatures indicate a previously unknown result: relatively

large increases in the small absolute probabilities of the most stretched chains are responsible for increases in average chain size (i.e. chain swelling) with increasing temperature. Chain shapes at different chain lengths and over a range of temperatures were also studied. Finally, joint probability correlations between chain size and shape for cis- and trans-1,4-polybutadiene chains were considered.

1.2 Methodology

In the RIS approximation, torsions about backbone bonds are treated as existing in discrete rotational states, with each possible state chosen to coincide with a region of low potential energy. States differ in relative energy and thus in Boltzmann-weighted probability. Discrete states are defined only around bonds that allow torsion. Rotations about the double bond are not allowed.

The simulations consist of generating numerous independent chain conformations. For each chain, the set of torsion angles are chosen on the basis of relative probabilities of different local chain geometries. In total, 100,000 isolated single chains of cis- and of trans-1,4-polybutadiene were simulated at each degree of polymerization n = 15, 25, 50, 75, 100, and 120 repeat units, all at 343 K. Simulations of 100,000 chains each were carried out for a single chain length (n = 50) at temperatures T = 275, 300, 323, 343, 375, and 400 K. Ensemble averages of various

chain size and shape parameters, defined below, were calculated in order to characterize cis and trans chains over these ranges of chain length and temperature. At each condition, property averages used an equal weighting for each chain. This is appropriate because relative Boltzmann-weighted probabilities were taken into account while generating the chain conformations. Further calculations obtained correlations among chain size, length, and shape.

1.2.1 Chain Geometry and Internal Energy

The positions of all atoms in the chain are defined by the position of the chain start, the overall orientation of the chain, and the internal coordinates, i.e. the bond lengths, bond angles, and torsion angles. The chain start was always placed at $(60, 60, 80)$ Å within a box of edge lengths $(137, 137, 137)$ Å that used periodic boundary conditions. The angles that determine the overall chain orientation were chosen randomly. These choices for the chain start and orientation should not have any effect on the results. Bond lengths and bond angle supplements used in our computations were obtained from Mark [9, 10] and are shown in Tables 1 and 2. Abe and Flory [11] used the same values in their calculations. For the C–C=C–C double bond, the torsional angle (ϕ) is zero (trans) or 180° (cis).

Table 1: Bond length geometries [9]

Bond	length (Å)
C–C	1.53
C=C	1.34
C–H	1.10

Table 2: Bond angle geometries [9]

Angle	Supplement
$\angle$ CH_2–CH=CH (θ'')	55°
$\angle$ CH–CH_2–CH_2 (θ')	68°
$\angle$ CH_2–CH–H (θ''_H)	62.5°
$\angle$ CH_2–CH_2–H (θ'_H)	70°

For the C–C single bond, the torsional angle states were based on regions of low potential energy. Mark [9, 10] chose to use six discrete rotational isomeric states for each torsional bond of polybutadiene. These isomeric states correspond to $\phi = -120°$, $-60°$, $0°$, $60°$, $120°$, $180°$, with $\phi = 0°$ defined as the trans state (Flory convention [8]).

The total energy of each system was calculated as a summation of the torsional energy [8] and the dispersion interactions between non-bonded atoms. Interactions among atoms separated by 3 or fewer bonds were included within the rotational isomeric state-dependent torsional energies. Atoms separated by three or more bonds contributed to the non-bonded interaction energy, which was computed

using the Lennard-Jones (6-12) potential [35]. This short range interaction between widely spaced atoms was used to avoid direct chain overlap. Its range was restricted by using a quintic spline that started at $r_{ij} = 1.45\sigma_{ij}$ and brought the interactions to $^{LJ} = 0$ and $d^{LJ}/dr = 0$ at $r_{ij} = 2.33\sigma_{ij}$. The scaling of average chain size with the molecular weight is checked below to confirm the chains remain unperturbed. Every conformation of polybutadiene generated in our work has fixed bond lengths and bond angles, and thus the bond energies and angle energies are independent of conformation.

1.2.2 Chain Generation

Transformation matrices convert bond vectors from one reference system to another [8]. These orthogonal transformation matrices were used to determine atom positions within each single chain of polybutadiene from the internal coordinates. Four transformation matrices were used per repeat unit of polybutadiene: three for the C–C single bonds and one for the C=C double bond.

Each polybutadiene chain was built in an atom-by-atom manner by using the states chosen for three torsional angles per repeat unit (ϕ_i, ϕ_{i+1}, ϕ_{i+3}) around the three single C–C bonds, as defined in figure 1. Torsion angles ϕ_i and ϕ_{i+3} about bonds i and $i + 3$ affect positions of the pendant hydrogen atoms (H_i, $H_{i'}$, H_{i+3},

$H_{i+3'}$) attached to the backbone atoms C_i and C_{i+3}. They also directly affect positions of the next atoms along the backbone (C_{i+1}, C_{i+4}). Torsion angle ϕ_{i+1} directly affects positions of two carbon atoms (C_{i+2}, C_{i+3}) and two hydrogen atoms (H_{i+1}, H_{i+2}). The chain start and end were hydrogen atoms in place of C_{i-1} and C_{i+4} for the first and last repeat unit.

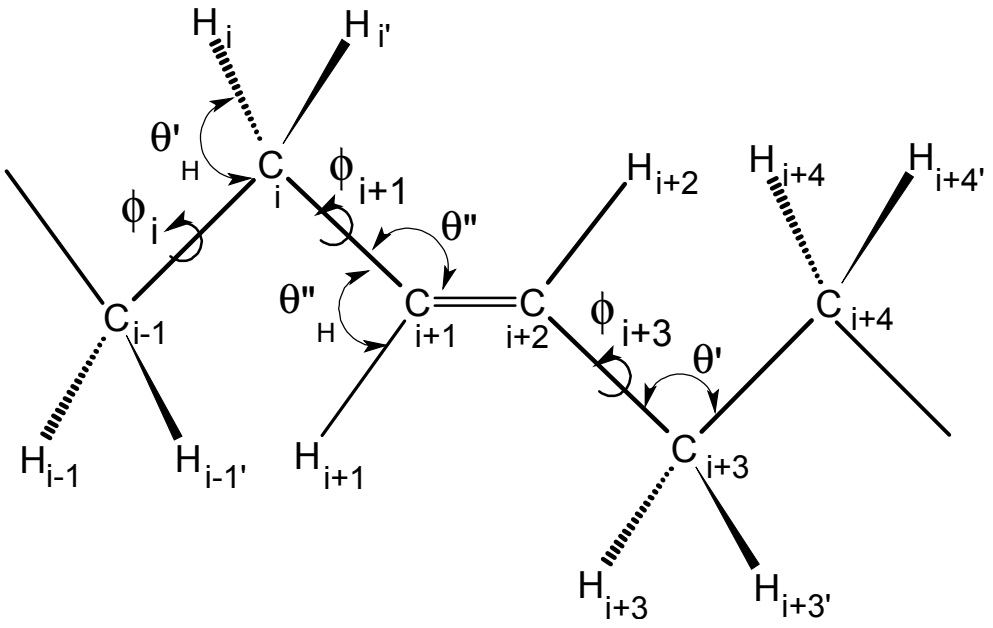

Figure 1: Trans-1,4-polybutadiene structure showing bonds, bond angles and torsion angles. Atoms from C_i to C_{i+3} and their pendant hydrogens comprise a single repeat unit. Numbering employs Flory's convention [8].

The rotational isomeric states (i.e. torsion angles) for each repeat unit were selected here by choosing randomly according to probabilities that account for relative energies of adding two consecutive torsion angles. Statistical weight matrices [8] that incorporate these relative energies for consecutive torsion angles were sug-

gested by Mark [9, 10] for 1,4-polybutadiene systems. The same set of matrices and statistical weights were used here, and chains were generated based on Boltzmann-weighted probabilities. Baysal et al. [25] found that adjacent torsions show the most angle-angle correlation, with torsions further away correlated to some extent. The partition function [8] incorporates each possible combination of rotational isomeric states of a chain. The pairwise probability of a single conformation equals its contribution to the partition function, divided by the partition function. Creating single chains in our simulations essentially creates realizations of the ensemble represented by this partition function. A linear congruential random number generator was used for the simulations. A different integer seed between 0 and $2^{31}-1$ was used for each condition of chain length and temperature.

1.2.3 Chain size and shape parameters

An important chain size parameter is the squared end-to-end distance r^2, which was calculated as

$$r^2 = (r_x^2 + r_y^2 + r_z^2) \tag{1}$$

where r_x, r_y, r_z are the x, y and z coordinates of the end-to-end distance vector $\mathbf{r}$.

The hydrogen atoms of the chain start and end defined the end-to-end distance, with periodic boundary conditions taken into account to ensure the proper image of each atom position was employed. The squared radius of gyration (r_g^2) relates to the distance of each atom in the polymer chain from the center of mass,

$$r_g^2 = \sum_{j=1}^{N} m_j \left|\mathbf{r}_j - \mathbf{r}_{\text{com}}\right|^2 / \sum_{j=1}^{N} m_j \tag{2}$$

m_j is the mass of atom j, $\mathbf{r}_j = (x_j, y_j, z_j)^T$ is the position vector of atom j of a polymer chain, $\mathbf{r}_{\text{com}} = (x_{\text{com}}, y_{\text{com}}, z_{\text{com}})^T$ is the position vector of the center of mass of a polymer chain, and N is the total number of atoms in the chain. Proper periodic image calculations were included here as well.

Theodorou and Suter [36] used the eigenvalues ($\lambda_1,\ \lambda_2,\ \lambda_3$) of a radius of gyration matrix (S)

$$S = \begin{pmatrix} \overline{x^2} & \overline{xy} & \overline{xz} \\ \overline{xy} & \overline{y^2} & \overline{yz} \\ \overline{xz} & \overline{yz} & \overline{z^2} \end{pmatrix} \tag{3}$$

to quantify contributions directed along the three principal directions (eigenvec-

tors) of a chain conformation, where

$$\overline{xy} = \frac{1}{N}\sum_{j=1}^{N}\left(x_j - x_{\mathrm{com}}\right)\left(y_j - y_{\mathrm{com}}\right) \tag{4}$$

and other terms are defined analogously. The overbar indicates an average over all atoms in a single chain conformation. The radius of gyration matrix was transformed to a principal axis system, which diagonalised it such that its eigenvalues were in descending order ($\lambda_1 \geq \lambda_2 \geq \lambda_3$). Eigenvalue λ_1 corresponds to the principal direction with the longest dimension while λ_2 and λ_3 correspond to secondary directions. This approach effectively represents the size of a polymer chain using a rotational ellipsoid with a different size in each direction, rather than with a hollow sphere of radius r_g that has the same mass and moment of inertia as the polymer chain. The squared radius of gyration equals the sum of the three eigenvalues, [36]

$$r_g^2 = \lambda_1 + \lambda_2 + \lambda_3 \tag{5}$$

The number-weighted squared radius of Eq. (5) differed by less than 1% from the mass-weighted squared radius of Eq. (2). Computing the radius of gyration matrix, Eq. (3), also enabled quantifying chain shape. The chain shape parameters studied were b/r_g^2 (asphericity or deviation from spherical shape), c/r_g^2 (acylindricity or

deviation from cylindrical shape) and κ^2 (relative shape anisotropy), defined by [36]

$$b = \lambda_1 - \left(\frac{\lambda_2 + \lambda_3}{2} \right) \tag{6}$$

$$c = \lambda_2 - \lambda_3 \tag{7}$$

$$\kappa^2 = \left(\frac{b^2 + \frac{3}{4}c^2}{r_g^4} \right) \tag{8}$$

Asphericity b/r_g^2 equals zero when all dimensions are equal and goes to 1 when the principal direction is much larger, $\lambda_1 \gg \lambda_2, \lambda_3$. Acylindricity c/r_g^2 goes to zero when the secondary directions are equal lengths.

1.3 Results and Discussion

1.3.1 Chain size

The range of chain lengths allows for a limited test of the scaling of root-mean-squared end-to-end distance. Figure 2 depicts the simulation results for $\langle r^2 \rangle^{1/2}$ at each chain length, using the number of repeat units rather than molecular weight or number of backbone bonds. Dashed lines indicate the best fits using a scal-

ing exponent of 1/2, i.e. $\langle r^2 \rangle^{1/2} = (\text{const}) n^{0.5}$, that is expected for unperturbed chains. Dotted lines indicate the best fits for an exponent of 0.6, i.e. scaling in a good solvent. The simulation results match the unperturbed case for trans-1,4-polybutadiene. For cis-1,4-polybutadiene, regression using the prefactor and exponent as separate parameters leads to a best fit at an exponent slightly higher than 0.6 though with a similar correlation coefficient R^2. For both sets of simulation results, increases in size with chain length are much closer to the expectations for unperturbed chains than for chains in a good solvent. The slopes for the good solvent cases are too high compared to the simulation results. Thus we continue the analysis by considering the results to correspond to unperturbed chains.

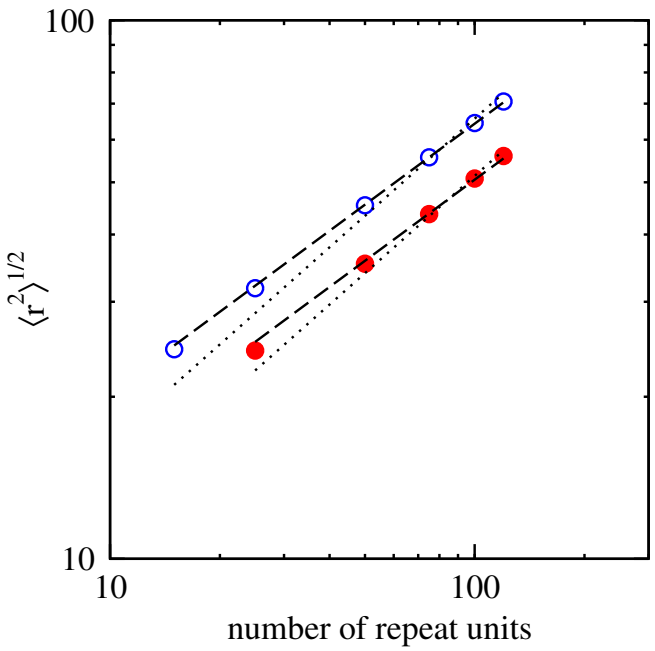

Figure 2: Scaling of root-mean-square end-to-end distance with chain length for cis- (filled) and trans-1,4-polybutadiene (open). Dashed and dotted lines indicate best fits using scaling exponents of 0.5 and 0.6, respectively.

Characteristic ratio (C_n) [8, 37] is defined as the ratio of mean squared end-to-end distance of a real chain under the theta condition to that of a freely jointed chain with the same bond lengths and number of bonds. This condition is relevant to an elastomer because conformations in the bulk polymer above the glass transition resemble those in a theta solvent [34]. This assumption has been made by others within simulating polybutadiene chains to interpret neutron scattering data [33] and it was found to be accurate in a simulated melt [13]. Because two

bond lengths arise in polybutadiene, they were incorporated separately as [10, 11]

$$C_n = \frac{\langle r^2 \rangle_0}{n_s l_s^2 + n_d l_d^2} \tag{9}$$

n_i is the number of backbone bonds of each type along a polymer chain, l_i is the bond length, and subscripts indicate single and double bonds. C_n quantifies chain expansion due to bond angle and torsion angle correlations. The subscript 0 of the mean squared end-to-end distance indicates unperturbed (theta) conditions.

Using the chains generated with the RIS procedure, we computed characteristic ratios of cis- and of trans-1,4-polybutadiene chains of different chain lengths at one temperature ($T = 343$ K) and of a single chain length ($n = 50$ units; $n_s = 149$, $n_d = 50$ bonds) at multiple temperatures. Figures 3 and 4 illustrate C_n results for different chain lengths and over different temperatures, respectively. Experimental values for cis-1,4-polybutadiene from intrinsic viscosity in theta solvents correspond to temperatures of 293.65 K [28]; 272.15 and 308.65 K [29]; and 283.45 K, 285.75 K, and 332.85 K [30]. Experimental results for trans-1,4-polybutadiene from intrinsic viscosity in a good solvent correspond to 328.15 K [10] and for a 36% cis, 57% trans, 7% 1,2-vinyl polybutadiene in a theta solvent correspond to 299.5 K [32]. Results from the RIS model correspond to 323.15 K [11] and 343.15 K

[9, 10, 12]. Molecular simulations provide results at 323 K [24] and 413 K [15, 23]. The temperature is not stated for calculations fit to neutron scattering of a mixed 37.1% cis, 55.9% trans, and 7% 1,2-vinyl polybutadiene [33].

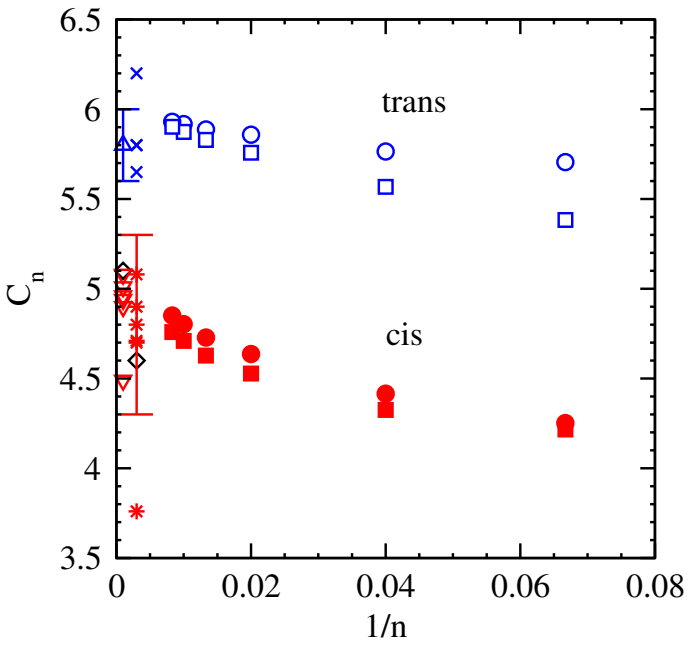

Figure 3: Characteristic ratio vs. inverse of repeat units n for cis- (filled) and trans-1,4-polybutadiene (open) using $\langle r^2 \rangle_0$ ($\circ$) and $6\langle r_g^2 \rangle_0$ ($\square$). Experimental results for cis-1,4-polybutadiene ($\triangledown$) [9, 28, 29, 30] , trans-1,4-polybutadiene ($\triangle$) [10], and mixed polybutadiene ($\diamond$) [32] are shown at $1/n = 0.001$. Prior model results for cis-1,4- ($*$) [9, 11, 12, 15, 23, 24], trans-1,4- ($\times$) [10, 11, 12, 24], and mixed polybutadiene ($\diamond$) [33] are shown at $1/n = 0.003$. These symbols are used throughout unless otherwise specified.

Figure 3 shows that calculated characteristic ratios are in good agreement with the experimental and prior computed characteristic ratios in the limit of infinite chain length for cis-1,4-polybutadiene chains. The only large simulation discrepancy is $C_\infty = 3.76$ from Kajiwara and Burchard [12]. They used a Monte Carlo

simulation that sampled 10^3 to 10^4 of the rotational isomeric states for chains of up to 100 repeat units. Though they used the states proposed by Mark [9, 10], their predicted characteristic ratio was about 25% lower than Mark's RIS result. Monte Carlo calculations [15] using a full potential at 413 K led to $C_\infty = 4.7$, with a slightly lower value for continuous unperturbed chains; the latter are isolated chains that are subject to the full torsional potential, rather than divided into discrete rotational isomeric states. Molecular dynamics simulations [23] using the same potential and temperature led to $C_\infty = 4.8$. These show that the RIS parameters of Mark lead to slightly more extended chains than a full potential energy function, and temperature effects are expected to expand the difference to some extent. The lower value $C_\infty = 4.6$ for a mixed polybutadiene [33] was attributed by Gkourmpis and Mitchell to how their simulations incorporated torsional correlations. The lowest experimental value, $C_\infty = 4.5$, corresponds to a measurement by Abe and Fujita [30] at 332.85 K, which we interpret using a viscosity constant that is consistent with the average characteristic ratio of 4.9 that Mark reports [9] on the basis of other experimental data [28, 29, 30]. This value is also an outlier in figure 4.

For trans-1,4-polybutadiene chains, the calculated characteristic ratios are

slightly higher than most prior computed values in the limit of infinite chain length. We note that Mark [10] and Kajiwara and Burchard [12] both obtained $C_\infty = 5.8$ for trans-1,4-polybutadiene, while Abe and Flory [11] obtained $C_\infty = 6.20$. Our results are between these prior RIS results.

The characteristic ratios increased with increasing chain length for both cis and trans chains. In both cases, chains of 120 repeat units were not yet at the long chain limit. This contrasts with an earlier demonstration that 30 to 40 repeat units were enough to reach the long chain limit in shorter Monte Carlo simulations [12]. The higher characteristic ratio for trans chains indicates a greater chain extension. This is potentially a consequence of the greater distance spanned between the carbon atoms bonded to the double bonded carbons, as noted by Mark [10] for a low energy state.

The characteristic ratio increased with temperature for both cis and trans chains, as shown in figure 4, and the increase was larger for trans than for cis polybutadiene chains. This indicates swelling of the average chain size upon heating. The trends are consistent with the prior modeling and experimental C_∞ results from the literature, particularly given that the $n = 50$ unit chain has a characteristic ratio somewhat below the long chain limit. The dependence on temperature

may be compared to results from force measurements on swollen networks. Mark [9] reports $d\ln\langle r^2\rangle_0/dT = 0.40\times10^{-3}\mathrm{K}^{-1}$ over 323 to 363 K for 1-4,cis-polybutadiene. Studies that included temperatures of 298 to 338 K [31] confirmed an average of $0.41\times10^{-3}\mathrm{K}^{-1}$; an earlier average [38] of $0.39\times10^{-3}\mathrm{K}^{-1}$ was also cited. Crespi and Flisi [39] report slopes $d\ln\langle r^2\rangle_0/dT$ for cis chains that range from $0.12\times10^{-3}\mathrm{K}^{-1}$ to $0.45\times10^{-3}\mathrm{K}^{-1}$ over 293 to 333 K. Slopes increased with increasing cross link density, with decreasing chain extension, and with decreasing temperature. Mark [10] reports $d\ln\langle r^2\rangle_0/dT = -0.65\times10^{-3}\mathrm{K}^{-1}$ for trans-1,4-polybutadiene but also notes experimental difficulties with the swollen network remaining stable, writing that "(these) results ... must therefore be considered only qualitative estimates." Followup work [31] refined this uncertain average to $-0.55\times10^{-3}\mathrm{K}^{-1}$. Gkourmpis and Mitchell [33] report a slight decrease in C_∞ with increasing temperature in their model calculations for a mixed polybutadiene. Our results may be compared by assuming n and l are independent of temperature, leading to

$$\frac{d\ln\langle r^2\rangle_0}{dT} = \frac{1}{C_\infty}\frac{dC_\infty}{dT}. \tag{10}$$

Fits over 273–343 K for the 50-unit chain lead to 0.48×10^{-3} and 1.6×10^{-3} K^{-1} for cis- and trans-, respectively. Agreement is good for cis-1,4-polybutadiene. Both

the sign and magnitude of $d\ln\langle r^2\rangle_0/dT$ determined here for trans-polybutadiene differ from the results from prior force measurements, which Mark cautioned should be used only qualitatively. The temperature dependence for trans- does appear consistent with the direct trend with temperature for the different C_∞ results that are available. These differences from earlier results are discussed further below.

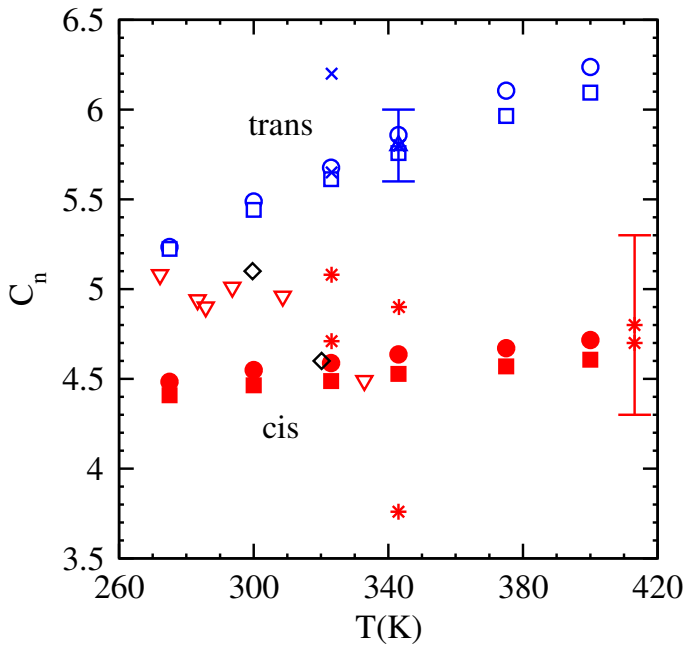

Figure 4: Characteristic ratio vs. temperature for cis- and trans-1,4-polybutadiene chains of 50 repeat units. Symbols match figure 2.

In the limit of long chains without long branches, the mean squared radius of gyration $\langle r_g^2\rangle_0$ should equal 1/6 of the mean squared end-to-end distance $\langle r^2\rangle_0$ [8]. Figure 3 shows the ratio $\langle r^2\rangle_0/\langle r_g^2\rangle_0$ was higher than 6 for shorter trans chains and decreased to 6 for longer chains. The ratio was slightly higher than 6 for cis

chains at all chain lengths. Figure 4 shows that the ratio $\langle r^2\rangle_0/\langle r_g^2\rangle_0$ was almost independent of temperature for cis chains, whereas for trans chains it increased with increase in temperature.

The probability density distribution of the squared end-to-end distance was calculated and compared with the probability density distribution for a Gaussian chain [8, 37],

$$P(r^2)dr = \left(\frac{3}{2\pi C_n n l^2}\right)^{\frac{3}{2}} \exp\left(\frac{-3r^2}{2C_n n l^2}\right) 2\pi r dr \tag{11}$$

The segments of each freely jointed chain in such an ensemble can be considered as performing a random walk in three dimensions with the only constraint being that each segment must be joined to its neighbors with a fixed bond length [8, 37].

Figure 5 compares the probability density distribution of squared end-to-end distance for cis and trans chains with the Gaussian model. Squared end-to-end distance for the cis chains ranged from 10 to 7,000 Å^2 and for the trans chains from 10 to 14,000 Å^2. Trans chains have a wider distribution than cis chains and consequently have higher characteristic ratios. For cis chains, excellent agreement between our simulation results and the Gaussian model was observed for chain sizes in the range of around 200 to 3500 Å^2. Our trans chain simulation results

showed agreement with the Gaussian model for a chain size range of around 200 to 8000 Å^2, and even beyond these ranges the differences were small. We classify these as medium sizes within the entire range of the chain size distribution. These medium size chains have the highest probability of occurence. While smaller chains have a comparable probability density, they span a much smaller range of squared end-to-end distance. The Gaussian model predicted higher probability than the simulation results for shorter chains (size range of around 10 to 200 Å^2 for cis and trans) as well as for longer chains (size range of around 3500 to 7000 Å^2 for cis and around 8000 to 14000 Å^2 for trans). Simulation results showed slightly higher probability than those predicted by the Gaussian model within parts of the medium size range. Cis chains showed a greater deviation from the Gaussian model compared to trans chains.

A similarity between conformations of RIS and Gaussian chains has been noted previously. Kajiwara and Burchard [12] calculated similar radii of gyration and hydrodynamic radii for RIS chains and Gaussian chains. Figure 5 shows that the similarities extend across the entire distribution of chain sizes.

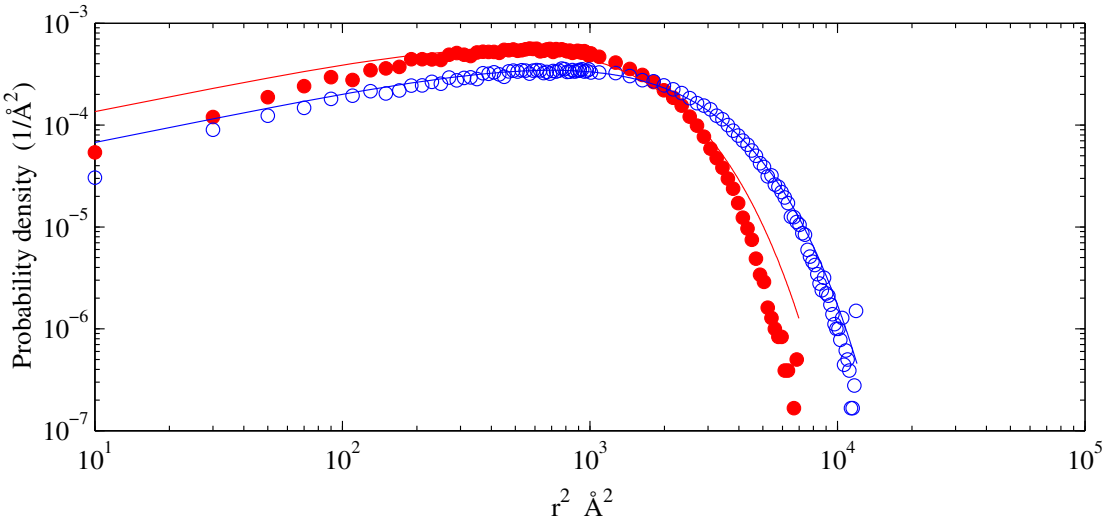

Figure 5: Probability density distribution of squared end-to-end distance for cis-(filled) and trans-(open) 1,4-polybutadiene chains of 50 repeat units at 343 K. Lines indicate a Gaussian distribution.

The temperature dependences of the probability density distributions of chain sizes for cis- and trans-1,4-polybutadiene are shown in figure 6. Squared end-to-end distance has a much wider distribution than the squared radius of gyration. Smaller size trans chains were slightly more probable at lower temperatures than at higher ones. Cis chains showed probabilities more independent of temperature.

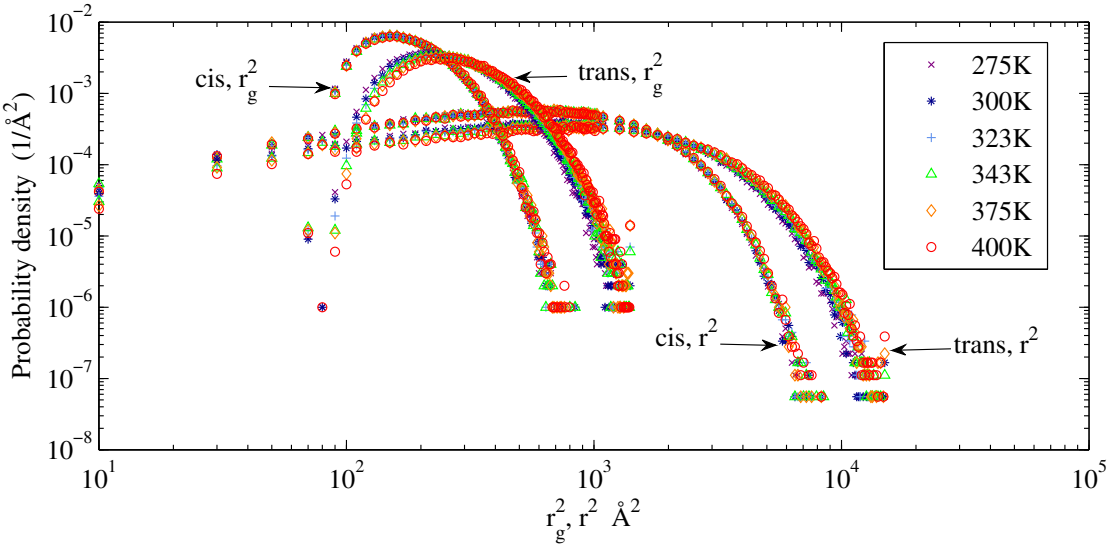

Figure 6: Probability density distribution of r^2 and r_g^2 for cis- and trans-1,4-polybutadiene chains of 50 repeat units at different temperatures.

This temperature dependency of the chain size distribution appears to conflict with the temperature dependence of characteristic ratio. The characteristic ratios increased with temperature, as shown in figure 4, though figure 6 suggests similar probabilities for the most probable chains (i.e. low and medium size chains) at different temperatures. There was a larger relative increase, though smaller absolute change, in the small probability density for larger chain sizes with temperature, as compared to a smaller relative decrease in probability density for smaller chain sizes. While only small absolute changes in probability densities with temperature were observed for all chain sizes, the characteristic ratio showed a steady increase in average size with temperature. This effect was more pronounced for trans chains

than for cis polybutadiene chains.

To examine this effect, characteristic ratios were calculated using only subsets of the chain size distribution, with results shown in figure 7. Chains with squared end-to-end distance $r^2 < 600$ Å^2 were considered as smaller chains, those with squared end-to-end distance in the range of 600 to 3000 Å^2 were considered as medium size chains, and those with $r^2 > 3000$ Å^2 were considered as larger chains. These squared distances correspond approximately to where the distributions from the RIS calculations and the Gaussian model cross each other in figure 5. A small decrease in characteristic ratio with increasing temperature was observed for smaller chains, while very slight rises in characteristic ratio were found for medium size chains. Characteristic ratios increased with increasing temperature for larger chains, and the increase was much more prominent for trans than for cis chains. The fraction of chains that were within each range changed little with temperature, as shown by the inset in figure 7. Increases in characteristic ratio with temperature (polymer chain swelling, figure 4) can thus be attributed to the size increases of the relatively few extended and taut conformations, rather than expansion uniformly across conformations of all sizes. Despite there only being a small change in low probability conformations, these resulted in an increase in average chain size. We

note that a sufficiently large sample size is required to obtain a sufficient number of these low-probability conformations that, by definition, occur rarely. The greater increase of characteristic ratio with temperature for larger chains, as shown in figures 4 and 7, indicates that this previously unreported *"taut conformation effect"* was more prominent for trans than for cis polybutadiene chains. This effect of rare extended chains is likely the cause of the difference in the temperature dependence of characteristic ratio in our results compared to those found in prior studies. Using a large enough sample set enabled larger numbers of rare extended conformations to be sampled.

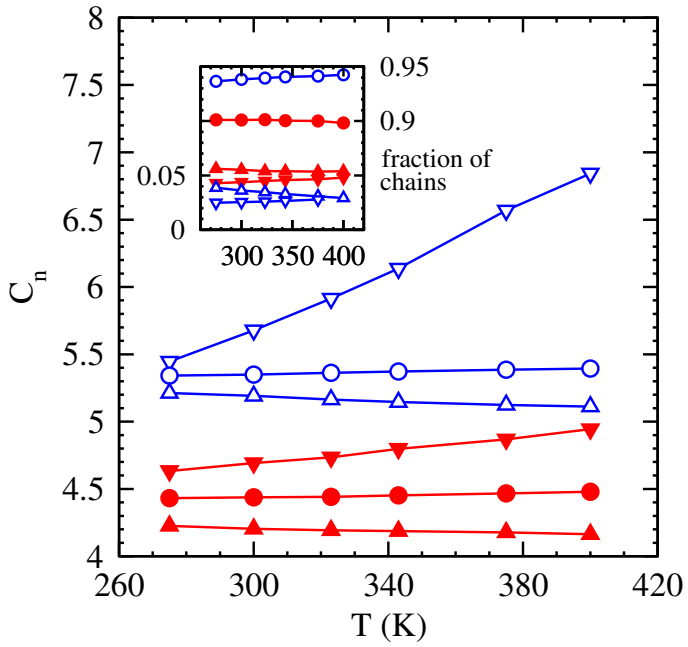

Figure 7: Characteristic ratio for larger (▽), medium (○), and smaller (△) subsets of the chain size distribution for cis- and trans-1,4-polybutadiene chains of 50 repeat units. The inset shows the number fraction of (from top) medium, smaller, and larger chains.

1.3.2 Chain shape

Ensemble averages of chain shape parameters were obtained in order to quantify shape variations among polybutadiene chains. Since each chain establishes its own principal axes, the analysis uses a different coordinate system for each chain. The results thus emphasize the deviations of each chain from a symmetric shape. Rotation differences between the principal axes and the original (x,y,z) coordinates are not important and were not taken into account when combining the results into averages and distributions.

The eigenvalues λ_1, λ_2, and λ_3 of the radius of gyration matrix indicate the extents of orthogonal principal axes that span the region occupied by a chain in primary and secondary directions. Ratios of eigenvalues thus indicate if chains are being stretched or compressed. Figures 8 and 9 show the eigenvalue ratios as functions of inverse of chain length and temperature, respectively. These calculations were carried out at 343 K and for 50 repeat units respectively.

Figure 8 shows that trans chains were more stretched than cis chains along the principal direction, though the distinction may vanish in the limit of long chains. For trans chains, the extent of stretching decreased slightly with increasing chain length. For cis chains, the extent of stretching was larger with increasing chain

length. The change in ratio between the two secondary directions followed the same trend as the principal direction but more subtly. These behaviors indicate that at the same chain length, trans chains were slightly less spherical than cis chains. Cis chains were slightly more elongated with increasing chain length, while trans chains were slightly less elongated. At long chain lengths, trans and cis chains have similar elongational deviations from a spherical shape. The changes in the ratio between the two secondary directions were small compared to the changes in average chain size $\langle r_g^2 \rangle_0$.

Figure 9 shows there was little or no variation in relative chain extent with temperature for cis chains. The principal direction ratio increased slightly with temperature for trans chains, while minor variations arose in ratio between the two secondary directions. This shows that as the temperature increased, trans chains were slightly more stretched along the principal direction and thus were slightly less spherical. Little or no variation in relative chain extent and thus in shape was found for cis chains as a function of temperature. Chain shape trends shown in figures 8 and 9 confirm that variations in the eigenvalue (λ_1) corresponding to the longest principal direction have the most significant effects on chain shapes.

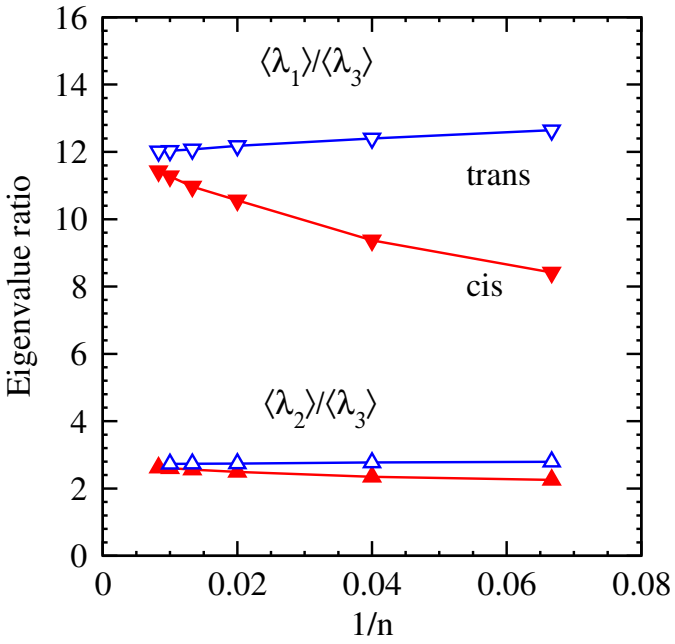

Figure 8: Averaged ratios of the largest and intermediate eigenvalues to the smallest eigenvalue at 343 K.

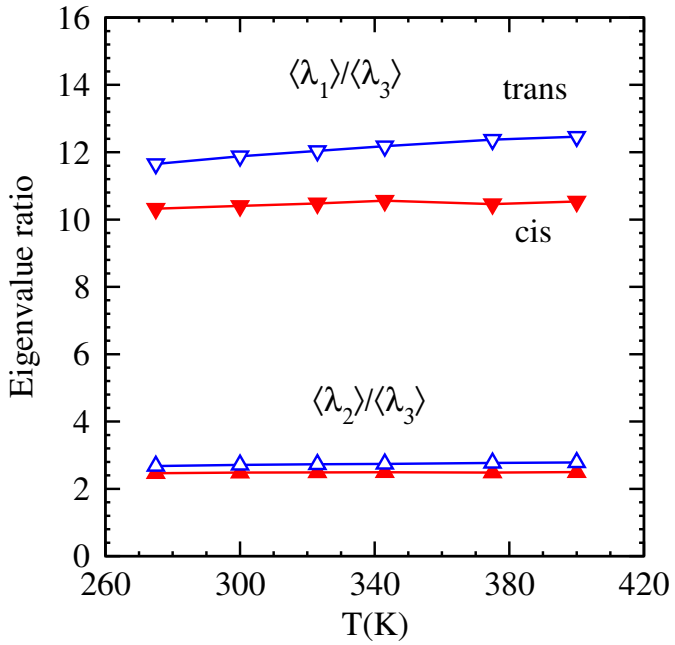

Figure 9: Averaged ratios of the largest and intermediate eigenvalues to the smallest eigenvalue for chains of 50 repeat units.

Figures 10 and 11 show variations in average shape parameters with inverse

of chain length and temperature respectively. An asphericity factor (b/r_g^2) of 0 suggests a spherical shape and 1 suggests a rod-like shape, while an acylindricity factor (c/r_g^2) of 0 suggests a round cross section and 0.5 suggests a more flat cross section normal to the longest axis. κ^2 of 0 suggests a rod-like shape whereas 1 suggests structures of tetrahedral or higher symmetry [36].

Figure 10 shows that both cis and trans chains show similar asphericity of 0.6 at longer chain lengths. An asphericity of 0.6 corresponds to a chain with a contribution to the squared radius of gyration that is around 5.5 times larger in the longest direction; it is also consistent with the 12:2.5:1 ratios shown in figures 8 and 9. Cis chains were more spherical at shorter chain lengths and gradually were slightly less spherical with increasing chain length. While trans chains were less spherical at all chain lengths, the difference decreased with increasing chain length. This change in shape was more subtle for trans chains than cis. This behavior followed the same trend shown in figure 8 for the eigenvalue ratios.

Figure 11 shows that cis chains exhibited little or no change in shape with temperature. Trans chains were slightly less spherical with increasing temperature. This behavior followed the same trend shown in figure 9.

The relative shape anisotropy followed the same trend as asphericity as func-

tions of both chain length and temperature. The acylindricity did not vary much with chain length or temperature for either cis or trans polybutadiene chains. Its value of 0.1 indicates chain fluctuations moderately larger in one minor direction compared to the other and thus corroborates the effect of small changes in ratio between the two secondary directions as compared to average chain size, as shown in figures 8 and 9.

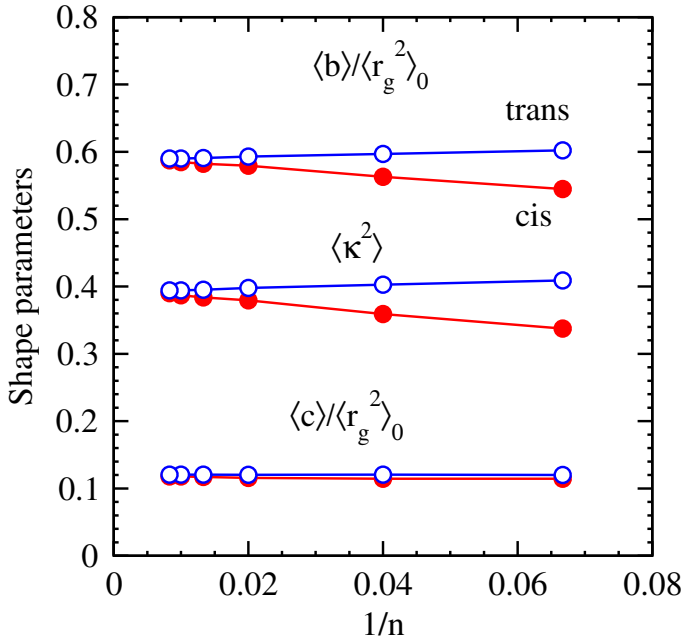

Figure 10: Average shape factors with inverse of repeat units at 343 K.

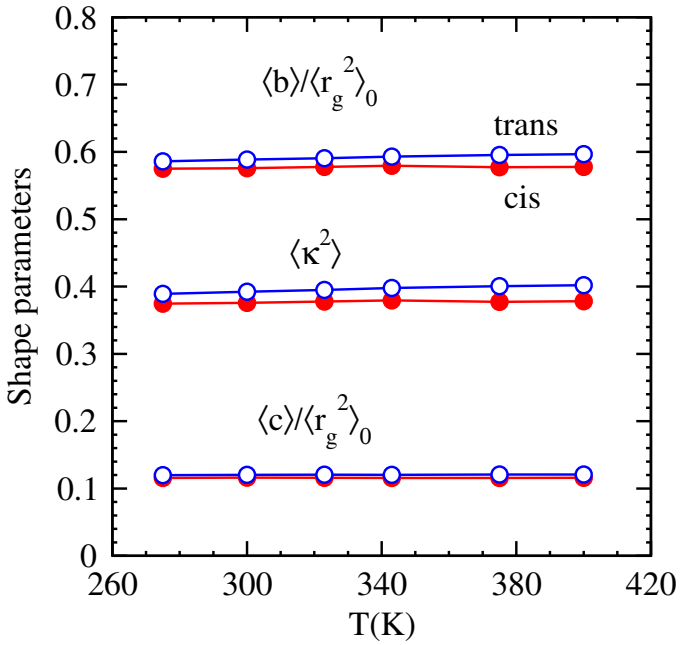

Figure 11: Average shape factors with temperature for chains of 50 repeat units.

1.3.3 Joint correlations in size and shape

Joint correlations between chain size and shape were studied to determine if their variations with chain length and temperature were independent or correlated properties. Cis and trans chains showed similar joint correlation behavior, with correlation and anti-correlation between chain size and shape occuring to a greater extent for trans chains as compared to cis chains.

Figures 12 and 13 show joint correlations for cis chains of 50 repeat units. Visualizations that animate rotations of these three-dimensional plots are available as supplementary material. Differences $\left[P(b/r_g^2, r_g^2) - P(b/r_g^2)P(r_g^2)\right]$ and $\left[P(c/r_g^2, r_g^2) - P(c/r_g^2)P(r_g^2)\right]$ of 0 indicate that size and shape are completely in-

dependent of each other, i.e. they act as mutually exclusive events. A positive difference indicates correlated events, while negative indicates anti-correlation.

For small rod-like chains, which arise less typically than average, figure 12 indicates some anti-correlation between size and shape. Small chains were nearer to spherical in shape, and high correlation between chain size and shape was observed for them. One physical interpretation is that for a chain of this length to have its ends near each other, its intermediate sections must expand in more htan one Cartesian coordinate direction. A hairpin turn that would enable conformations to emphasize a single direction is inconsistent with the allowed rotational isomeric states. For medium size chains, some correlation was found for chains that are near rod-like, while notable anti-correlation was found for more spherical chains. With the increased separation between chain ends at a fixed backbone length, the chain conformation apparently can emphasize a single direction more explicitly. Rod-like large chains showed correlation between chain size and shape, i.e. becoming more likely when a large distance between ends did not require a circuitous chain contour.

Figure 13 shows size-shape correlations for acylindricity in cis chains. Small chains showed good correlation while being somewhat round in cross section.

Medium size chains showed correlation for chains that were more flattened in cross section. For medium size chains with round cross sections, the relationship between size and shape became anti-correlated. Large chains showed minor correlation between chain size and shape with being nearly round in cross section. These correlations are consistent with the same explanations described regarding asphericity.

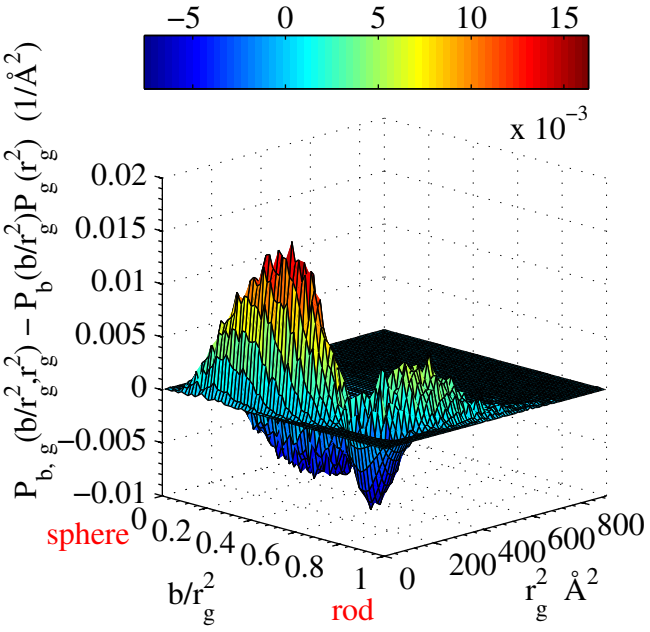

Figure 12: Joint correlations of probability density of chain size (P_g) and asphericity (P_b) for cis chains of 50 repeat units at 343 K.

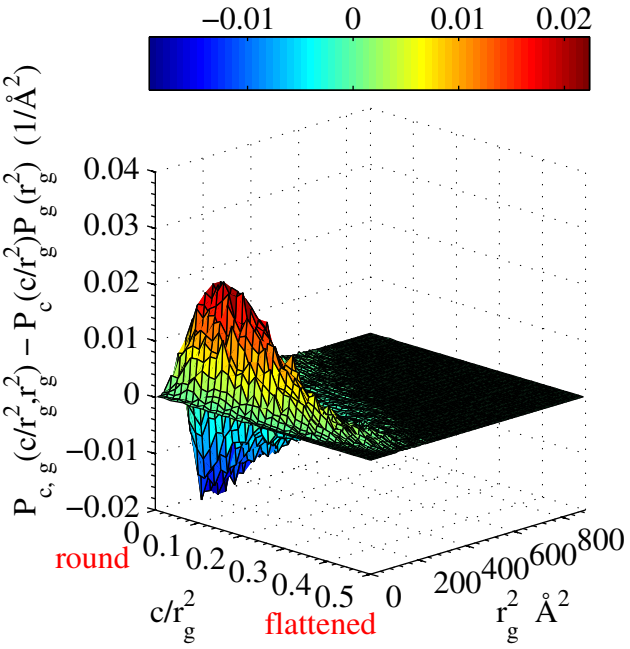

Figure 13: Joint correlations of probability density of chain size (P_g) and acylindricity (P_c) for cis chains of 50 repeat units at 343 K.

In total, different size and shape probability density distributions were found for cis and trans chains over different chain lengths and across a range of temperatures. Probability densities are related to the work required to alter chain size and shape, and thus different probability densities for cis- and trans-1,4-polybutadiene conformations indicate different extents of work that must be done in order to alter chain size and shape. Quantifying this deformation work is the subject of ongoing research.

1.4 Conclusions

Ensemble averages and probability density distributions of sizes and shapes of cis- and trans-1,4-polybutadiene chains have been quantified for isolated single chains under undeformed theta conditions using a Rotational Isomeric State approach. Such conformations are considered to be representative for a chain in its own melt.

Characteristic ratios were larger with increasing chain length for both cis and trans chains, and these were in good agreement with experimental and prior computed values (cis-1,4-polybutadiene), and slightly higher than prior computed values (trans-1,4-polybutadiene). Characteristic ratios were higher for trans chains than for cis chains and indicate greater chain extension, which could be due to a greater distance spanned between the carbon atoms bonded to the double bonded carbons.

A Gaussian model predicted higher probability than simulation results at shorter and longer chain sizes for both cis and trans chains. Simulation results predicted a higher probability than the Gaussian model at certain regions of medium size chains for cis and trans chains while at other regions of medium size chains, simulation and Gaussian results were in agreement.

Characteristic ratios increased with increasing temperature for both cis and trans chains, with trans chains showing greater temperature dependence. The dependence for cis chains matched prior findings, while for trans chains the $C_\infty(T)$ were consistent with direct reports of characteristic ratio but opposite in sign to the negative $d\ln\langle r^2\rangle_0/dT$ that have been reported from force measurements on networks. Despite the rise in characteristic ratio, only small absolute changes in chain size probability densities with increasing temperature were calculated. Smaller chain conformations showed a smaller relative decrease in probability density with increasing temperature, as compared to a larger relative increase for improbable larger chain conformations. In a subdivided chain distribution, smaller chains showed a small decrease in characteristic ratio with increasing temperature, medium size chains showed little or no variation in characteristic ratio, and larger chains showed more significant increases in characteristic ratio with increasing temperature. This accounted for an increase in average characteristic ratio of cis- and trans-polybutadiene chains with increasing temperature. This newly reported *"taut conformation effect"* was more pronounced for trans- than for cis-1,4-polybutadiene chains. It indicates that the increase in chain size originates from the fewer chains that are largest in size, rather than from increases in size

among chains across the size distribution.

With increasing chain length, trans chains were less elongated while cis chains were more stretched along the principal direction. At the same chain length, trans chains were slightly less spherical than cis chains. Cis chains were slightly less spherical with increasing chain length, while trans chains were slightly more spherical. At long chain lengths, trans and cis chains reach similar shapes. The extent of stretching and compression was greater along the principal direction than the secondary directions. With increasing temperature, trans chains were slightly stretched along the principal direction whereas cis chains showed little or no change in shape. Thus trans chains were slightly less spherical with increasing temperature, while little or no variation in shape was computed for cis chains. Variations of the largest eigenvalue λ_1 of the radius of gyration matrix have the most significant effects on chain shapes: most changes in shapes arose from changes along the longest principal direction.

At longer chain lengths, both cis and trans chains showed similar asphericity. Little or no variation was computed in acylindricity for either cis or trans polybutadiene chains. Relative shape anisotropy followed the same trend as asphericity as functions of both chain length and temperature for cis and trans polybutadiene

chains.

Joint correlation studies between chain size and shape showed that they are mutually dependent properties. For asphericity, rod-like small size and spherical medium size cis chains showed anti-correlation between chain size and shape. Spherical small size, near rod-like medium and large size chains showed correlation between chain size and shape. For acylindricity, medium size chains of flattened cross section, and small and large size chains of round cross section showed correlation between chain size and shape. Round cross section medium size chains showed anti-correlation between chain size and shape. Trans chains showed similar behavior as cis chains with correlation and anti-correlation between chain size and shape occuring to a greater extent.

Cis- and trans-1,4-polybutadiene show different size and shape probability density distributions, which imply different amounts of deformation work to alter chain shape and size. Quantifying this deformation work and its implications for mechanical properties, viscoelastic properties, and rolling resistance are the subject of ongoing work.

1.5 Supplementary Material

Visualizations that animate rotations of the three-dimensional plots of the size-shape correlations calculated for cis-1,4-polybutadiene, figures 12 and 13, are available as supplementary material which can be found online.

1.6 Acknowledgments

We thank the Ford Motor Company University Research Program for funding this research.

List of References

[1] C. M. Blow and C. Hepburn, *Rubber Technology and Manufacture*. Plastics and Rubber Institute, London, 1982.

[2] J. L. White, *Rubber Processing: Technology, Materials, and Principles*. Hanser, Munich, 1995.

[3] J. W. Brinke ten, V. M. Litvinov, J. E. G. J. Wijnhoven, and J. W. M. Noordermeer, "Interactions of stober silica with natural rubber under the influence of coupling agents, studied by ^{1}H NMR T_2 relaxation analysis," *Macromolecules*, vol. 35, no. 27, pp. 10 026–37, 2002.

[4] L. A. E. M. Reuvekamp, S. C. Debnath, J. W. Brinke Ten, J. P. Van Swaaij, and J. W. M. Noordermeer, "Effect of zinc oxide on the reaction of TESPT silane coupling agent with silica and rubber," *Rubber Chem Technol*, vol. 77, no. 1, pp. 34–49, 2004.

[5] C. M. Flanigan, L. Beyer, D. Klekamp, D. Rohweder, B. Stuck, and E. R. Terrill, "Comparative study of silica, carbon black and novel fillers in tread compounds," *Rubber World*, vol. 245, no. 5, pp. 18–31, 2012.

[6] C. W. Burkhart, "Structurally realistic modeling of elastomers," *Rubber Chem Technol*, vol. 71, no. 3, pp. 342–406, 1998.

[7] P. Flory, "Mean-square moments of chain molecules," *Proc Natl Acad Sci USA*, vol. 51, no. 6, pp. 1060–67, 1964.

[8] P. J. Flory, *Statistical Mechanics of Chain Molecules*. Wiley Interscience, 1969.

[9] J. E. Mark, "Random-coil configurations of cis-l,4-polybutadiene and cis-1,4-polyisoprene. Theoretical interpretation," *J Am Chem Soc*, vol. 88, no. 19, pp. 4354–9, 1966.

[10] J. E. Mark, "Interpretation of random-coil configurations of trans-1,4-polybutadiene and trans-1,4-polyisoprene," *J Am Chem Soc*, vol. 89, no. 26, pp. 6829–35, 1967.

[11] Y. Abe and P. J. Flory, "Configurational statistics of 1,4-polybutadiene chains," *Macromolecules*, vol. 4, no. 2, pp. 219–29, 1971.

[12] K. Kajiwara and W. Burchard, "Rotational isomeric state calculations of the dynamic structure factor and related properties of some linear chains. 1. The $\rho = \langle S^2 \rangle^{1/2} \langle R_H^{-1} \rangle$ parameter," *Macromolecules*, vol. 17, no. 12, pp. 2669–73, 1984.

[13] Y. Li and W. L. Mattice, "Atom-based modeling of amorphous 1,4-cis-polybutadiene," *Macromolecules*, vol. 25, no. 19, pp. 4942–47, 1992.

[14] E. Kim, S. Misra, and W. L. Mattice, "Atomistic models of amorphous polybutadienes. 2. Poly(1,4-trans-butadiene), poly(1,2-butadiene), and a random copolymer of 1,4-trans-butadiene, 1,4-cis-butadiene, and 1,2-butadiene," *Macromolecules*, vol. 26, no. 13, pp. 3424–31, 1993.

[15] P. Gestoso, E. Nicol, M. Doxastakis, and D. N. Theodorou, "Atomistic Monte Carlo simulation of polybutadiene isomers: cis-1,4-polybutadiene and 1,2-polybutadiene," *Macromolecules*, vol. 36, no. 18, pp. 6925–6938, 2003.

[16] E. Kim and W. L. Mattice, "Local chain dynamics of bulk amorphous polybutadienes: a molecular dynamics study," *J Chem Phys*, vol. 101, no. 7, pp. 6242–54, 1994.

[17] Y. Zhan and W. L. Mattice, "Molecular dynamics simulation of the collapse of poly(1,4-trans-butadiene) to globule and to a thin film," *Macromolecules*, vol. 27, no. 24, pp. 7056–62, 1994.

[18] R. H. Gee and R. H. Boyd, "Conformational dynamics and relaxation in bulk polybutadienes: a molecular dynamics simulation study," *J Chem Phys*, vol. 101, no. 9, pp. 8028–38, 1994.

[19] G. D. Smith, O. Borodin, D. Bedrov, W. Paul, X. Qiu, and M. D. Ediger, "^{13}C NMR spin-lattice relaxation and conformational dynamics in a 1,4-polybutadiene melt," *Macromolecules*, vol. 34, no. 15, pp. 5192–5199, 2001.

[20] G. D. Smith, O. Borodin, and W. Paul, "A molecular-dynamics simulation study of dielectric relaxation in a 1,4-polybutadiene melt," *J Chem Phys*, vol. 117, no. 22, pp. 10 350–10 359, 2002.

[21] O. Okada and H. Furuya, "Molecular dynamics simulation of cis-1,4-polybutadiene. 1. Comparison with experimental data for static and dynamic properties," *Polymer*, vol. 43, no. 3, pp. 971–976, 2001.

[22] O. Okada, H. Furuya, and T. Kanaya, "Molecular dynamics simulation of cis-1,4-polybutadiene. 2. Chain motion and origin of the fast process," *Polymer*, vol. 43, no. 3, pp. 977–982, 2001.

[23] G. Tsolou, V. G. Mavrantzas, and D. N. Theodorou, "Detailed atomistic molecular dynamics simulation of cis-1,4-poly(butadiene)," *Macromolecules*, vol. 38, no. 4, pp. 1478–1492, 2005.

[24] G. D. Smith and W. Paul, "United atom force field for molecular dynamics simulations of 1,4-polybutadiene based on quantum chemistry calculations on model molecules," *J Phys Chem A*, vol. 102, no. 7, pp. 1200–1208, 1998.

[25] C. Baysal, I. Bahar, B. Erman, and L. Monnerie, "Kinematics of polymer chains in dense medium. 4. Effect of backbone geometry and application to polybutadiene," *Macromolecules*, vol. 29, no. 8, pp. 2980–8, 1996.

[26] I. Bahar, "Local relaxation of polymers in dense media: Cooperative kinematics theory and applications," *Macrom Theory Simul*, vol. 6, no. 5, pp. 881–906, 1997.

[27] T. Haliloglu, I. Bahar, B. Erman, E.-G. Kim, and W. L. Mattice, "A dynamic rotational isomeric state approach for extension of the time scale of the local dynamics observed in fully atomistic molecular dynamics simulations: Application to polybutadiene," *J Chem Phys*, vol. 104, pp. 4828–4834, 1996.

[28] F. Danusso, G. Moraglio, and G. Gianotti, "cis-Tactic Polybutadiene: Solubility $[\eta] - M$ Relations in Different Solvents, and Molecular Conformation," *J Polym Sci*, vol. 51, pp. 475–485, 1961.

[29] G. Moraglio, "Cistactic polybutadiene: unperturbed molecular dimensions at various temperatures," *Eur Polym J*, vol. 1, no. 2, pp. 103–9, 1965.

[30] M. Abe and H. Fujita, "Binary mixtures of theta-solvents," *J Phys Chem*, vol. 69, no. 10, pp. 3263–7, 1965.

[31] R. H. Becker, C. U. Yu, and J. E. Mark, "Thermoelastic studies of diene polymers in elongation and compression," *Polym J*, vol. 7, no. 2, pp. 234–240, 1975.

[32] N. Hadjichristidis, Z. Xu, L. J. Fetters, and J. Roovers, "The characteristic ratios of stereoirregular polybutadiene and polyisoprene," *J Polym Sci Polym Phys Ed*, vol. 20, no. 4, pp. 743–50, 1982.

[33] T. Gkourmpis and G. R. Mitchell, "Three dimensional picture of the local structure of 1,4-polybutadiene from a complete atomistic model and neutron scattering data," *Macromolecules*, vol. 44, no. 8, pp. 3140–3148, 2011.

[34] P. J. Flory, *Principles of Polymer Chemistry.* Cornell University Press, 1953.

[35] M. P. Allen and D. J. Tildesley, *Computer Simulation of Liquids.* Oxford Univ. Press, 1987.

[36] D. N. Theodorou and U. W. Suter, "Shape of unperturbed linear polymers: polypropylene," *Macromolecules*, vol. 18, no. 6, pp. 1206–14, 1985.

[37] P. C. Hiemenz and T. P. Lodge, *Polymer Chemistry, 2nd Edition.* CRC Press, Taylor & Francis Group, 2007.

[38] J. E. Mark, "Thermoelastic properties of rubberlike networks and their thermodynamic and molecular interpretation," *Rubber Chem Technol*, vol. 46, no. 3, pp. 593–618, 1973.

[39] G. Crespi and U. Flisi, "Contribution of the internal energy to the retractive force of vulcanized cis-1,4 polybutadiene," *Makromol Chem*, vol. 60, pp. 191–201, 1963.

CHAPTER 2

"Simulating stress-strain behavior by using individual chains. 1. Uniaxial deformation of amorphous cis- and trans-1,4-polybutadiene"

by

Suvrajyoti Kar, Julie L Cuddigan, Michael L Greenfield *

Department of Chemical Engineering, University of Rhode Island, Kingston, RI - 02881, USA

is prepared for submission to Polymer

*Corresponding author email: greenfield@uri.edu

Abstract

This work focuses on developing a probability-based numerical method for quantifying mechanical properties of non-Gaussian polybutadiene chains subject to uniaxial deformation, with the intention of being able to incorporate polymer-polymer and polymer-filler interactions. In previous work, numerous non-Gaussian RIS cis- and trans-1,4-polybutadiene chains of different repeat unit sizes and at different temperatures were generated under unperturbed conditions. The numerical method arises from a probabilistic approach for evaluating the elastic free energy change of chain end-to-end vectors under deformation. The elastic free energy change, force, and stress computed using the numerical method were in excellent agreement with analytical solutions using a Gaussian chain model. Next it was applied to the available non-Gaussian RIS chains. Forces and stresses showed dependences on chain molecular weight and temperature, and increased with deformation. Compression forces were much larger than tension forces on chains. Fewer repeat unit size chains represent a much more tightly cross-linked network resulting in greater moduli than more repeat unit size chains. Young's moduli computed from the numerical model were in good agreement with experimental results.

Keywords: Uniaxial deformation, numerical method, Gaussian analytical, polybutadiene chains, stress-strain, moduli

2.1 Introduction

Polybutadiene is an important commercial polymer with pertinent applications in the automobile industry. It is such an essential ingredient in rubber tires that nearly 70% of polybutadiene manufactured worldwide is used in the production of vehicle tires. Additional uses include manufacture of golf balls, toughened plastics, shoe soles, gaskets, shock absorbers and others [1, 2].

As a tire rolls, the stresses on the tread exert strains through both elastic and viscous mechanisms. The latter results in energy dissipation leading to rolling resistance, which is the viscoelastic energy lost at low frequencies during flattening and re-rounding of tires. When a vehicle is in motion, the tire tread flattens against the road which results in the elastomer chains undergoing a change in their conformations [3, 4]. This leads to affine deformation of the elastomer system which changes the number of ways the elastomer chains can be arranged. The change in arrangement of elastomer chains affects the elastic free energy of the system, which is logarithmically related to the probability distribution of the chain end-to-end vectors [5]. Chains and particles in the undeformed portion of the tire tread relax.

The original distribution of the chains is restored by random fluctuations after deformation, and this change in elastic free energy requires work which is dissipated as heat leading to rolling resistance. Thus studying the chain conformations and their changes under deformation is of utmost importance to understanding the viscous mechanisms of this rubber system.

Prior experimental and theoretical work have been done to study changes in the molecular structure of rubber systems. NMR generally measures the average chain deformation and re-orientation on a local scale [6, 7, 8, 9] and SANS computes the average radius of gyration of chain conformations in a system [10]. Solid-state ^{13}C NMR experiments were performed by Kameda and Asakura [11] on natural rubber under uniaxial deformation to study changes in structural and dynamical behavior in the amorphous region of rubber. They observed the mobility of the amorphous chains increased with increasing deformation but decreased once deformation was stopped. Ott et al. [6] used Multiple Quantum NMR (MQ NMR) and SANS to analyze vulcanized cis-1,4-polyisoprene network structures under deformation. They compared their experimental results to numerical models [5, 12, 13, 14, 15] and found that the average local strains in stretched samples were significantly lower than those predicted by the phantom model while in good

agreement with the affine junction model. They inferred that excluded volume effects of nearby chains influenced the conformational space of the network.

Subhani et al. [16] performed uniaxial tension and compression tests on sheet-shaped rubber-like materials and developed a stored energy function to predict such experimental results. Their proposed model predicted tension behavior accurately for either uniaxial tension or compression.

Dubrović et al. [17] and Valić [18] studied molecular structure, dynamics, and segmental motion of rubber system molecules at lower deformation i.e. ratio $\lambda = L/L_0 = 1.5$. Dubrović et al. [17] studied the effect of uniaxial deformation on the microstructure of natural rubber during irradiation. They found that increasing the irradiation dose decreases the degree of swelling of natural rubber. A deformation of 1.5 introduced structural changes in the rubber matrix. Valić [18] studied orientational motion of natural rubber chain segments cross-linked by γ-irradiation under fixed uniaxial deformation of 1.5. Direction of applied force determined the dynamic behavior of chain segments and resulted in permanent spatial orientation of rubber chain segments in the direction of the force.

Starkova and Aniskevich [19] carried out uniaxial tension tests on silica-filled SBR rubber in order to determine the incompressibility limit of the rubber and

the corresponding Poisson's ratio. They found that the rubber system was incompressible up to a deformation of 4.5 and corresponded to a Poisson's ratio of 0.5. Beyond a deformation of 4.5 the Poisson's ratio decreased to 0.4.

Mark [20, 21] used the Rotational Isomeric State (RIS) approach proposed by Flory [22, 23] to study configurational statistics of single cis- and trans-1,4-polybutadiene chains under theta conditions. In the RIS approximation, torsions about single bonds are treated as existing in one or more discrete rotational states with each of these states chosen to coincide with a region of low potential energy. The RIS approach has been used as an effective tool to study single chain properties of polybutadiene by several researchers including Abe and Flory [24], Kajiwara and Burchard [25, 26], and also by us [27]. In our previous work [27], we studied size and shape properties of amorphous cis- and trans-1,4-polybutadiene systems. Single chains of polybutadiene under unperturbed conditions were generated, and single chain size analysis and shape analysis were performed. Characteristic ratios of both cis- and trans-1,4-polybutadiene chains increased on heating indicating chain swelling. Probability density distributions of the chains over a range of temperatures showed a previously unreported effect: increase in chain size on heating originated from the least likely, taut conformations rather than uniformly

across the size distribution. This was termed as the "*taut conformation effect*".

In this work, we propose a novel numerical method for simulating mechanical properties of elastomer chains subjected to uniaxial deformation. The numerical method arises from a probabilistic approach for evaluating the elastic free energy change of chain end-to-end vectors under deformation. From previous work [27], we have available distributions of end-to-end distances of cis- and trans-1,4-polybutadiene chains under unperturbed conditions that were generated using the RIS approach. Here we supplement those with numerical sets of end-to-end distances that follow a Gaussian distribution. These are used to confirm that the numerical deformation methodology implemented here obtains the known analytical stress-strain relationship for Gaussian chains. Computations were then performed to predict the stress-strain relationship of unoriented RIS chains subjected to uniaxial deformation by using changes in chain conformation statistics. This paper is part of an overall project aimed towards studying elastomer chain conformations and their role in computing rubber tire viscoelastic properties.

2.2 Methodology

The intent of the new methodology is to obtain mechanical properties from conformational statistics in a numerical approach that can incorporate directly

the effects of specific polymer-polymer and polymer-filler interactions, such as functionalized end-groups with silica filler interactions. The probability-based approach developed here enables sampling over many configurations without the cost of molecular dynamics simulations.

The approach arises from the elastic free energy change of single chains of elastomers under deformation in order to quantify their mechanical properties. Elastic free energy A_{el} of a single chain under deformation with an end-to-end vector $\vec{r}$ is related to the probability density distribution of the end-to-end vector of the chain [5, 23, 28]

$$A_{el} = c(T) - k_b T \ln P(\vec{r}) \tag{12}$$

where $P(\vec{r})$ is the probability density distribution of end-to-end vectors of a single chain, $c(T)$ is only a function of temperature T and k_b is the Boltzmann constant. The change in elastic free energy of a single chain from an undeformed to a deformed state is

$$\Delta A_{el} = A_{el} - A_{el,0} = -k_b T[\ln P(\vec{r}) - \ln P(\vec{r_0})] \tag{13}$$

The change in elastic free energy of an ensemble containing N chains was obtained by integrating over all chains. This was achieved by multiplying equation 13 by

the probability density distribution of $\vec{r}$ over all $\vec{r}$ and integrating over all possible end group positions,

$$\frac{\langle \Delta A_{el} \rangle}{k_b T} = \int P(\vec{r_0}) \ \ln P(\vec{r}_0) \ dr_0^3 - \int P(\vec{r}) \ \ln P(\vec{r}) \ dr^3 \tag{14}$$

In order to accurately compute the change in elastic free energy for chains having cross-links, it is necessary to distribute a front factor [29] or the ratio of mean-squared end-to-end distances in the cross-linked network relative to that of the undeformed network. The end-to-end vectors of the chains in the network are described through voxels, where each voxel represents a possible position of an end-to-end vector in three dimensional space. Numerical integration of equation 14 including this factor leads to

$$\frac{\langle \Delta A_{el} \rangle}{k_b T} = \sum_{\text{voxels}} P(\vec{r_0}) \ \ln P(\vec{r}_0) \ \frac{r_0^2}{\langle r^2 \rangle_0} \ (\Delta r_0)^3 - \sum_{\text{voxels}} P(\vec{r}) \ \ln P(\vec{r}) \ \frac{r^2}{\langle r^2 \rangle_0} \ (\Delta r)^3 \tag{15}$$

where $(\Delta r)^3 = (\Delta r_0)^3$ is the volume of a voxel, r_0^2 and r^2 represent undeformed and deformed chain end-to-end distances respectively, and $\langle r^2 \rangle_0$ is the average of the mean squared end-to-end distance of the undeformed chains. The $P(\vec{r})$ of chains

were computed based on their voxel location along the x, y, z coordinate directions

$$P(\vec{r}) = \frac{\text{number of chains in voxel}_{\text{xyz}} \text{ at } \vec{\text{r}}}{\text{volume of voxel}_{\text{xyz}} * \text{N}} \tag{16}$$

Deformation applied to elastomers induces strain on the systems, which leads to changes in elastic free energy. This induced strain leads to quantifiable forces and stresses. From thermodynamics, force is directly related to the change in elastic free energy with system dimension [29] and is given as

$$f_k = \left(\frac{\partial \lambda_k}{\partial L}\right)\left(\frac{\partial \langle \Delta A_{el} \rangle}{\partial \lambda_k}\right)_{T,V} \tag{17}$$

where deformation or stretch ratio $\lambda_k = r_k/r_{k,0}$ [30] applied in the kth direction leads to force f_k in the kth direction. r_k and $r_{k,0}$ are deformed and undeformed chain end-to-end vectors respectively and L is $V^{1/3}$ where V is the volume of a single chain. The tensile stress acting on the system due to deformation is obtained by dividing the force with the cross-sectional area (A_m) whose unit vector is aligned with the applied force

$$\sigma_{mk} = \left(\frac{1}{LA_m}\right)\left(\frac{\partial \langle \Delta A_{el} \rangle}{\partial \lambda_k}\right)_{T,V} \tag{18}$$

The choice of cross-sectional area, as actual or initial, results in either true or

engineering stress [29].

Uniaxial deformation was applied to chain ensembles such that extension was along the x direction and compression was along the y and z directions. Affine deformation was assumed, i.e. deformation applied macroscopically is transferred microscopically and uniformly to every chain making up the ensemble [29, 31]. Since polybutadiene is an elastomer, it was assumed to be incompressible with a Poisson's ratio (ν) of 0.5 [19, 30]. No change in volume of the system was expected as a result of deformation thus $\lambda_x \lambda_y \lambda_z = 1$. The deformations applied along the y and z directions are compressions such that $\lambda_y = \lambda_z = 1/\sqrt{\lambda_x}$.

In this work true stress has been computed and cross-sectional area is represented by L^2/λ_k. Thus equation 18 can be written as

$$\sigma_{mk} = \left(\frac{\lambda_k}{V}\right)\left(\frac{\partial\langle\Delta A_{el}\rangle}{\partial\lambda_k}\right)_{T,V} \tag{19}$$

The volume of a single chain (V) is a function of its molecular weight and temperature, and was calculated using polybutadiene densities. Densities of cis- and trans-1,4-polybutadiene at different temperatures were obtained from prior experimental and theoretical results [32, 33, 34].

Tension force in the x direction can be obtained numerically from equations

15 and 17 as

$$\frac{f_x}{k_bT} = \frac{1}{L}\left(\frac{\partial\left(\sum\limits_{\text{voxels}} P(\vec{r_0})\ \ln P(\vec{r_0})\ \frac{r_0^2}{\langle r^2\rangle_0}\ (\Delta r_0)^3 - \sum\limits_{\text{voxels}} P(\vec{r})\ \ln P(\vec{r})\ \frac{r^2}{\langle r^2\rangle_0}\ (\Delta r)^3\right)}{\partial\lambda}\right)_{T,V} \tag{20}$$

where λ is changing in all three directions i.e. extension along the x direction and compression along the y and z directions. For compression, $\partial\left(\frac{1}{\sqrt{\lambda}}\right) = -\frac{1}{2\lambda^{3/2}}\partial\lambda$ thus

$$\frac{f_{y,z}}{k_bT} = -\frac{2\lambda^{3/2}}{L}\left(\frac{\partial\left(\sum\limits_{\text{voxels}} P(\vec{r_0})\ \ln P(\vec{r_0})\ \frac{r_0^2}{\langle r^2\rangle_0}\ (\Delta r_0)^3 - \sum\limits_{\text{voxels}} P(\vec{r})\ \ln P(\vec{r})\ \frac{r^2}{\langle r^2\rangle_0}\ (\Delta r)^3\right)}{\partial\lambda}\right)_{T,V} \tag{21}$$

where $f_{y,z}$ are compression forces in the y and z directions respectively.

Numerical equations for tensile and compressive stresses are obtained by dividing tension and compression forces with their respective cross-sectional areas, which are $L_yL_z = L^2/\lambda$ for tension and $L_xL_y = L_xL_z = L^2\sqrt{\lambda}$ for compression

$$\frac{\sigma_{xx}}{k_bT} = \frac{\lambda}{V}\left(\frac{\partial\left(\sum\limits_{\text{voxels}} P(\vec{r_0})\ \ln P(\vec{r_0})\ \frac{r_0^2}{\langle r^2\rangle_0}\ (\Delta r_0)^3 - \sum\limits_{\text{voxels}} P(\vec{r})\ \ln P(\vec{r})\ \frac{r^2}{\langle r^2\rangle_0}\ (\Delta r)^3\right)}{\partial\lambda}\right)_{T,V} \tag{22}$$

$$\frac{\sigma_{yy,zz}}{k_bT} = -\frac{2\lambda}{V}\left(\frac{\partial\left(\sum\limits_{\text{voxels}} P(\vec{r}_0)\ \ln P(\vec{r}_0)\ \frac{r_0^2}{\langle r^2\rangle_0}\ (\Delta r_0)^3 - \sum\limits_{\text{voxels}} P(\vec{r})\ \ln P(\vec{r})\ \frac{r^2}{\langle r^2\rangle_0}\ (\Delta r)^3\right)}{\partial\lambda}\right)_{T,V} \tag{23}$$

Unperturbed RIS chain end-to-end distances (r_0) from previous work [27] were used as inputs for computing end-to-end vectors of chains before and after deformation. In order to evaluate equations 20 to 23, the end-to-end vectors had to be distributed over a three dimensional space. The chain conformations were randomly oriented over the $(+x, +y, +z)$ octant of a sphere prior to imposing deformation. Distributing the chains over a single octant of a sphere assumes that the same distribution occurs along the remaining sections of the sphere, and it provides better statistics while requiring less computation time.

Deformation on the chains is implemented by applying the deformation ratio, representative of either extension (λ) or compression ($1/\sqrt{\lambda}$), to each of the vector components in their respective x, y, and z directions. First we considered randomly distributed unperturbed end-to-end vectors of the chains in spherical coordinates,

$$(r_{x,0}\ , r_{y,0}\ , r_{z,0}) = r_0(\sin\theta\cos\phi\ , \sin\theta\sin\phi\ , \cos\theta) \tag{24}$$

Each elevation or latitudinal angle $\theta\ \epsilon\ [0,\pi/2]$ was chosen uniformly from a sinu-

soidal distribution between [0,1] and longitudinal angle ϕ was chosen uniformly within [0,π/2). Probability density distributions for the unperturbed end-to-end vectors were obtained by averaging over all $\vec{r_0}$. After deformation, the end-to-end vectors of the chains were represented by

$$(r_x\ , r_y\ , r_z) = r_0(\lambda_x \sin\theta\cos\phi\ , \frac{1}{\sqrt{\lambda_x}}\sin\theta\sin\phi\ , \frac{1}{\sqrt{\lambda_x}}\cos\theta) \tag{25}$$

Probability density distributions for the deformed end-to-end vectors were obtained by averaging over the number of chains ending in the region around each $\vec{r}$.

In order to verify the accuracy of the proposed numerical method, it was applied to Gaussian chains and the results were compared with analytical solutions. The probability density distribution for the end-to-end vector $\vec{r_0}$ of a Gaussian chain is given as [23]

$$P(\vec{r_0}) = \left(\frac{3}{2\pi C_n\left(n_s l_s^2 + n_d l_d^2\right)}\right)^{\frac{3}{2}} \exp\left(\frac{-3r_0^2}{2C_n\left(n_s l_s^2 + n_d l_d^2\right)}\right) \tag{26}$$

where r_0 is the end-to-end distance of a chain, C_n is the characteristic ratio [22], n_i is the number of backbone bonds of each type along a polymer chain, l_i is the bond length, and subscripts s and d indicate single and double bonds where l_s = 1.53 Å and l_d = 1.10 Å for polybutadiene [20]. Gaussian chains were generated by

repeatedly determining the distance r_0 that satisfies

$$\xi = \left(\frac{3}{2\pi C_n \left(n_s l_s^2 + n_d l_d^2\right)}\right)^{\frac{3}{2}} \int_0^{r_0} \exp\left(\frac{-3r_0^2}{2C_n \left(n_s l_s^2 + n_d l_d^2\right)}\right) 4\pi r_0^2 dr_0 \tag{27}$$

where ξ was chosen uniformly within [0,1). A linear congruential random number generator was used to generate each ξ with a different seed used in each system to ensure independent statistics.

The change in elastic free energy for an ensemble of N Gaussian chains is obtained by substituting equation 26 in equation 13 and averaging over N chains [5]

$$\frac{\langle \Delta A_{el} \rangle}{k_b T} = \frac{3}{2} N \left(\frac{\langle r^2 \rangle}{\langle r^2 \rangle_0} - 1\right) \tag{28}$$

The mean squared end-to-end distances can be represented in terms of end-to-end vectors as

$$\langle r^2 \rangle_0 = \langle r_x^2 \rangle_0 + \langle r_y^2 \rangle_0 + \langle r_z^2 \rangle_0 \tag{29}$$

$$\langle r^2 \rangle = \langle r_x^2 \rangle + \langle r_y^2 \rangle + \langle r_z^2 \rangle \tag{30}$$

Assuming the elastomer system to be isotropic in a state of rest [5]

$$\langle r_x^2 \rangle_0 = \langle r_y^2 \rangle_0 = \langle r_z^2 \rangle_0 = \frac{\langle r^2 \rangle_0}{3} \tag{31}$$

The average mean squared end-to-end distances can be written in terms of deformation ratio as

$$\langle r_i^2 \rangle = \langle r_i^2 \rangle_0 \lambda_i^2 \tag{32}$$

where $i = x, y, z$. The free energy change for Gaussian chains can be written in terms of deformation ratios [5] by substituting equations 29, 30, 31, and 32 in equation 28

$$\frac{\langle \Delta A_{el} \rangle}{k_b T} = \frac{1}{2} N \left(\lambda_x^2 + \lambda_y^2 + \lambda_z^2 - 3 \right) \tag{33}$$

Under uniaxial deformation in the x direction, equation 33 can be written as [30]

$$\frac{\langle \Delta A_{el} \rangle}{k_b T} = \frac{1}{2} N \left(\lambda^2 + \frac{2}{\lambda} - 3 \right) \tag{34}$$

and compared with results obtained from using equation 15 for Gaussian chains to determine accuracy of the numerical method for elastic free energy change computations.

Analytical tension (f_x) and compression forces ($f_{y,z}$) on the Gaussian chain ensembles were obtained from equations 17 and 33

$$\frac{f_x}{k_b T} = \frac{N}{L} \left(\lambda - \frac{1}{\lambda^2} \right) \tag{35}$$

$$\frac{f_{y,z}}{k_bT} = \frac{2N}{L}\left(\frac{1}{\sqrt{\lambda}} - \lambda^{5/2}\right) \tag{36}$$

and compared with equations 20 and 21 respectively to verify the numerical method accuracy for force computations.

Analytic tensile (σ_{xx}) and compressive stresses ($\sigma_{yy,zz}$) were obtained for the Gaussian chain model by dividing the tension and compression forces by their respective cross-sectional areas, leading to

$$\frac{\sigma_{xx}}{k_bT} = \frac{N}{V}\left(\lambda^2 - \frac{1}{\lambda}\right) \tag{37}$$

$$\frac{\sigma_{yy,zz}}{k_bT} = \frac{2N}{V}\left(\frac{1}{\lambda} - \lambda^2\right) \tag{38}$$

and compared with equations 22 and 23 respectively for numerical method accuracy determination for stresses.

From our previous work [27], distributions of amorphous, single RIS chains of cis- and trans-1,4-polybutadiene for different molecular weights (x = 15, 25, 50, 75, 100, and 120 repeat units) at a temperature of 343 K, as well as at different temperatures (T = 275, 300, 323, 343, 375, and 400 K) for a single repeat unit size of 50, were available for analysis. Ensembles of Gaussian chains were generated under the same conditions as the RIS chains. Each ensemble consisted of 10^5 single

RIS and Gaussian chains. Following the numerical and analytical comparisons of Gaussian chains, the numerical method was extended to studying stress-strain behavior of non-Gaussian RIS chains. Slopes of the linear regime of the stress-strain plots were used to compute Young's moduli (E) [29, 30]. The magnitude of the deformations imposed here ($\lambda = 1$ to 3.5) emphasized the need for utilizing finite strain (ϵ) which can be related to engineering strain (ϵ_e) as [35]

$$\epsilon = \frac{1}{2}\epsilon_e^2 + \epsilon_e \tag{39}$$

For tension, engineering strain (ϵ_e) is related to deformation or stretch ratio (λ) as [30]

$$\epsilon_e = \lambda - 1 \tag{40}$$

thus finite strain (ϵ) for tension in terms of λ is [36]

$$\epsilon = \frac{1}{2}\left(\lambda^2 - 1\right). \tag{41}$$

2.3 Results and Discussion

A significant step towards determining the accuracy of the numerical method was comparing our numerical results with Gaussian analytical equations. In order to bring about such comparisons, Gaussian chains were generated using equation

27. Figure 14 shows good agreement in the probability density distribution of generated Gaussian chains with the Gaussian analytical probability density distribution.

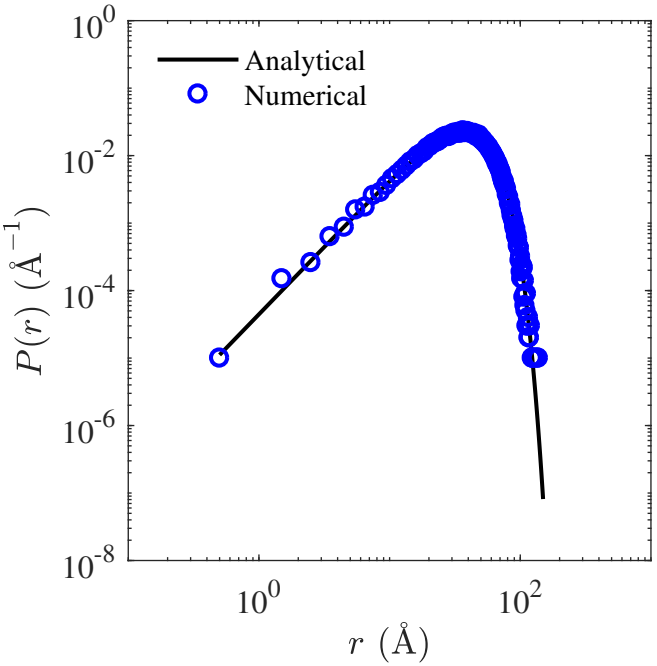

Figure 14: Generation of Gaussian chains of trans-1,4-polybutadiene of 50 repeat units at 343 K.

These chains were then uniaxially extended along the x direction and compressed along the y and z directions. End-to-end vectors of the chains under undeformed and deformed conditions were obtained. Chain deformation resulted in a change in their probability density distributions and elastic free energy which allowed for determining forces and stresses. Figure 15 shows excellent agreement between numerical results and analytical equations for elastic free energy change,

force and stress for trans-1,4-polybutadiene chains of 50 repeat units at 343 K. Similar agreement was also observed for compression forces and stresses of cis- and trans-1,4-polybutadiene chains of all repeat unit sizes and at all temperatures. Comparative analysis of numerical results and analytical solutions of Gaussian chains indicated that the numerical method determines stress-strain behavior accurately for a given model of elastic free energy.

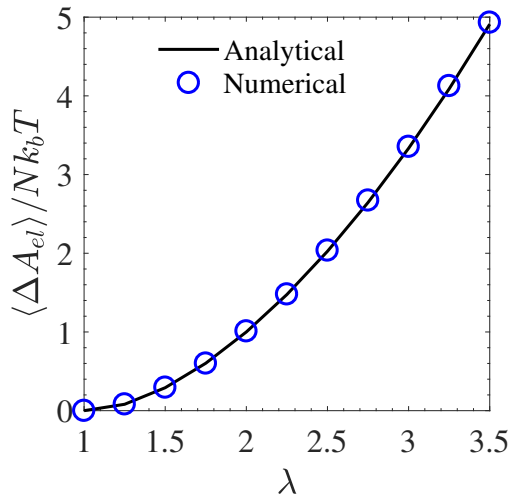

(a) Elastic free energy change

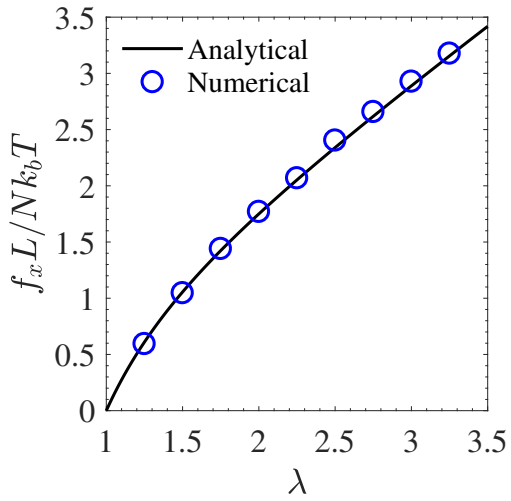

(b) Tension force

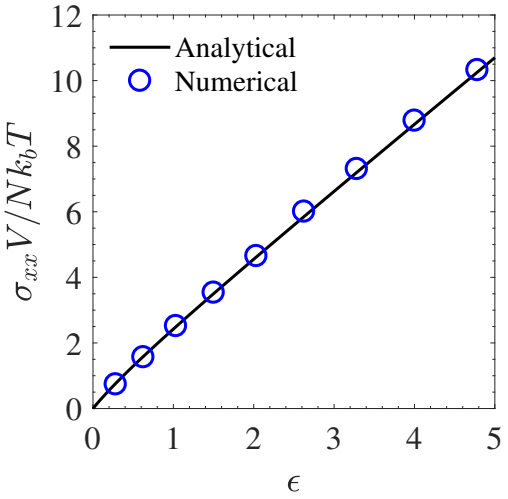

(c) Tensile stress

Figure 15: Analytical and numerical comparisons for trans-1,4-polybutadiene chains of 50 repeat units at 343 K.

Next the simulation method was applied to RIS chains of cis- and trans-1,4-polybutadiene of different repeat unit sizes at 343 K. Figure 16 shows probability density distributions of end-to-end vectors of trans-1,4-polybutadiene chains of 50 and 120 repeat units under uniaxial tension (figure 16(a),(b)) and compression

(figure 16(c),(d)). The distribution of r_x is initially narrow under undeformed conditions and gradually widens with increasing deformation. This indicates that the highly probable shorter conformations become less probable upon stretching while longer conformations become increasingly present. Inversely, r_y or r_z distributions contract with increasing deformation indicating more probable shorter conformations and less probable longer conformations on compression. Chains of 120 repeat units showed lesser probabilities than 50 repeat unit chains since they spanned greater lengths.

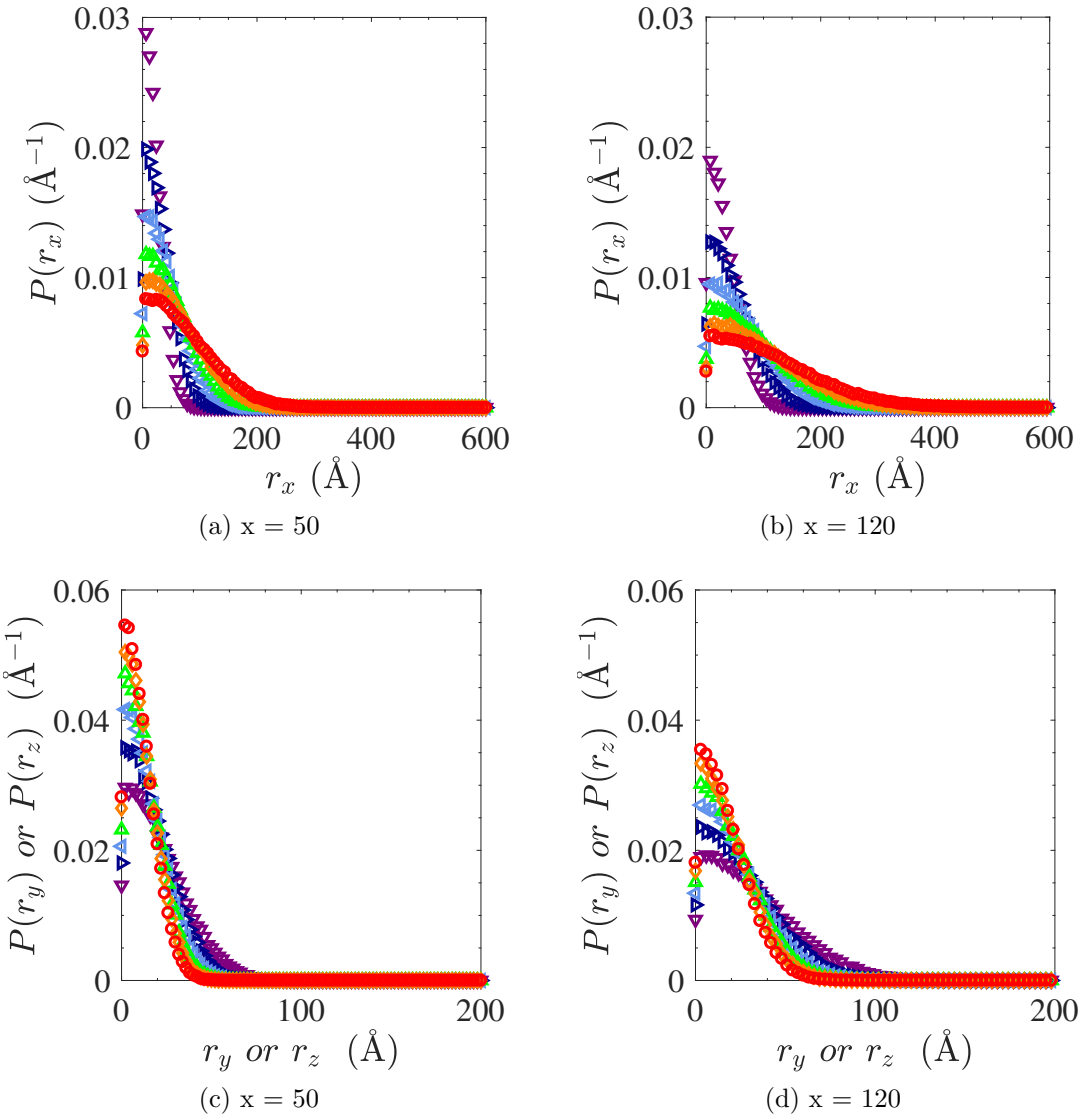

(a) x = 50 (b) x = 120

(c) x = 50 (d) x = 120

Figure 16: Probability density distributions of end-to-end vectors for trans-1,4-polybutadiene chains of 50 and 120 repeat units at 343 K. Deformation ratios (λ): 1 ($\triangledown$ violet), 1.5 ($\triangleright$ indigo), 2 ($\triangleleft$ blue), 2.5 ($\triangle$ green), 3 ($\diamond$ orange), and 3.5 ($\circ$ red).

Figure 17 shows that tension and compression forces for chains at the same temperature increased with increasing deformation. The overlap of the normalized forces indicates that chains of different repeat unit sizes are impacted by molecular weight and volume. Much larger forces were required to shrink the system than

elongate it indicated by the larger magnitudes of compressive forces as shown in figure 17(b). This corroborates behavior observed experimentally [37].

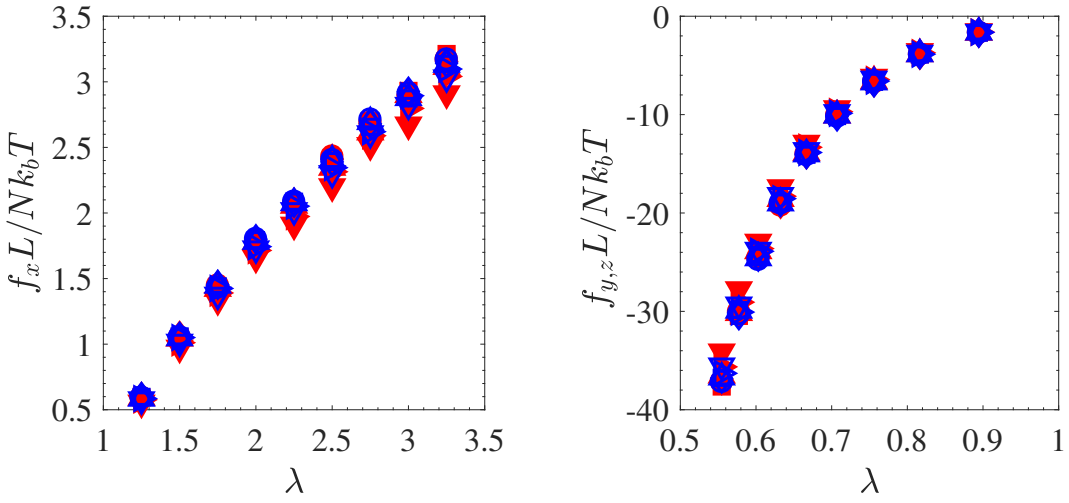

(a) Tension (b) Compression

Figure 17: Forces vs. λ for cis- and trans-1,4-polybutadiene chains of all sizes at 343 K. Filled red symbols for cis and open blue for trans. x = 15 ($\triangledown$), 25 ($\triangleright$), 50 ($\triangle$), 75 ($\square$), 100 ($\diamond$), and 120 ($\circ$).

Similar to the force behavior, tensile stresses acting on the chains increased with increasing deformation (or strain), as shown in figure 18. The normalized tensile stresses on the chains show that across different sizes, stresses are impacted by molecular weight and volume of the chains.

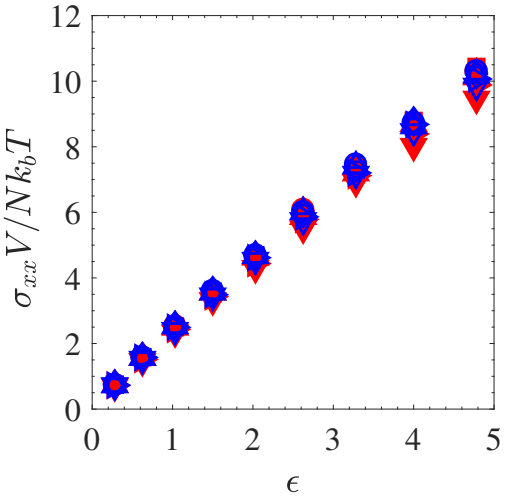

Figure 18: Tensile stresses vs. strain for cis- and trans-1,4-polybutadiene chains of all sizes at 343 K. Symbols follow convention of figure 17.

Figure 19 shows increasing tension and compression forces with deformation for chains at varying temperatures. The behavior of the normalized curves are identical to those of figure 17. This indicates that the only difference across chains of the same molecular weight is the choice of temperature.

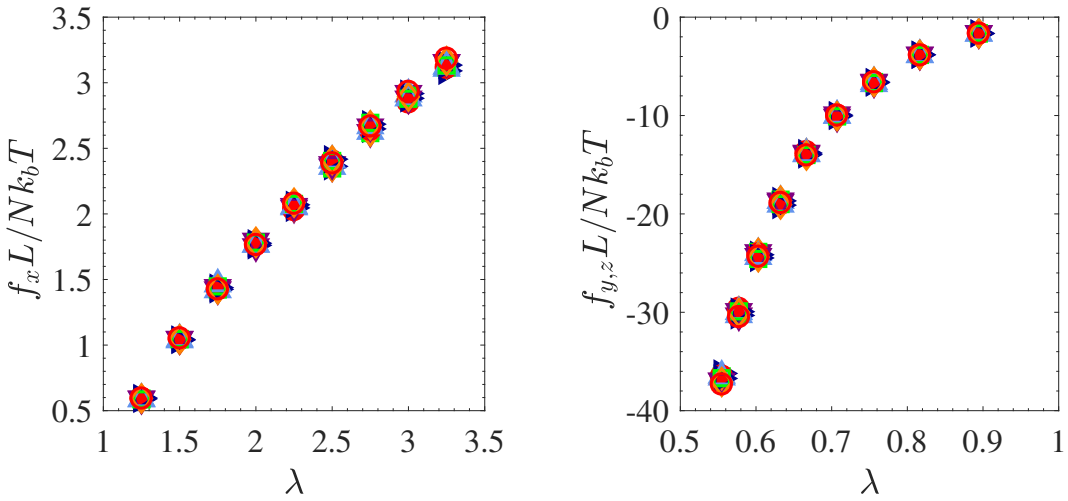

(a) Tension (b) Compression

Figure 19: Forces vs. λ for cis- and trans-1,4-polybutadiene chains of 50 repeat units. Filled symbols for cis and open for trans. T = 275 K ($\triangledown$ violet), 300 K ($\triangleright$ indigo), 323 K ($\triangle$ blue), 343 K ($\square$ green), 375 K ($\diamond$ orange), and 400 K ($\circ$ red).

The tensile stresses increased with deformation (or strain) as shown in figure 20. The normalized tensile stresses on chains of the same repeat unit size were consistent across all temperatures. Similar to force, the overlap emphasizes that non-normalized tensile stresses are impacted by temperature.

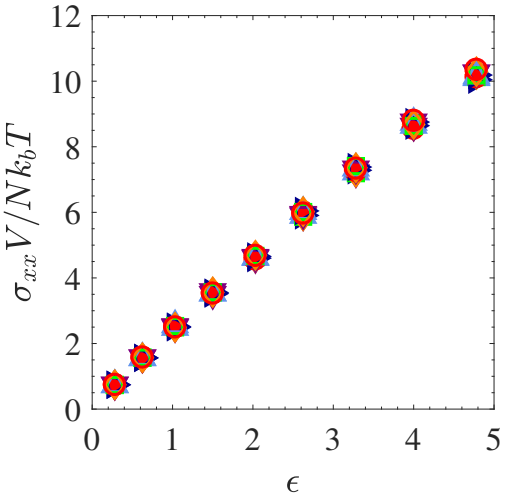

Figure 20: Tensile stresses vs. strain for cis- and trans-1,4-polybutadiene chains of 50 repeat units. Symbols and colors follow convention of figure 19.

Computations of Young's moduli from the slope of the linear regime of the stress-strain plots for cis- and trans-1,4-polybutadiene chains of different repeat units and temperatures are shown in figure 21. Moduli significantly decreased with increasing repeat unit size and marginally increased with increasing temperature. The fewer repeat unit size chains correspond to lower molecular weight between cross-links causing a more tightly cross-linked chain network. This resulted in greater moduli as compared to chains of more repeat units. A slight linear increase in moduli with temperature of chains of the same repeat unit size was observed. This indicated that stiffness of the chains increased up on heating. These moduli were in good agreement with experimental results [38, 39]. Textbooks on rubber elasticity [5, 40] and polymer engineering [30] have reported Young's modulus of

polybutadiene to be ∼1 to 3 MPa and our numerical results fall within that range.

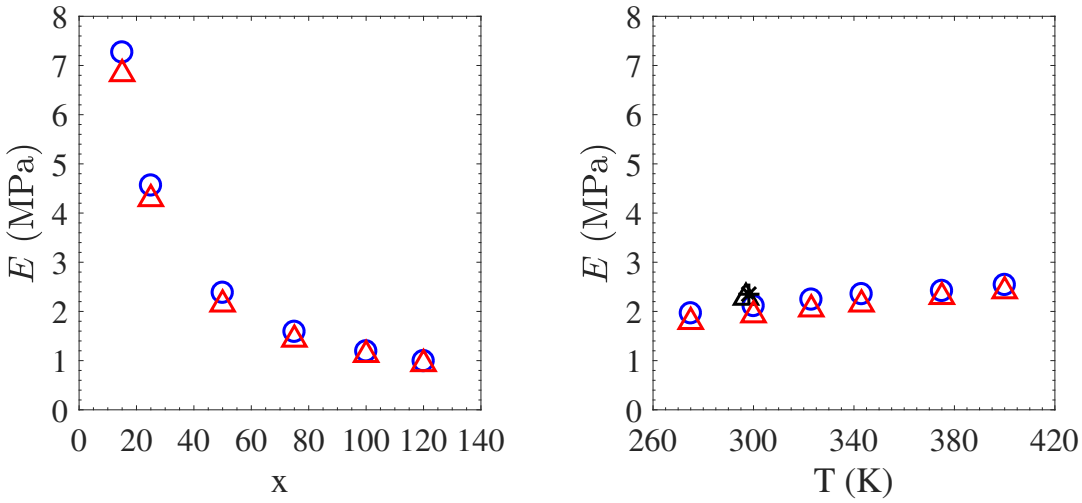

(a) All chain lengths at T = 343 K

(b) All temperatures for x = 50

Figure 21: Tensile or Young's moduli of cis- and trans-1,4-polybutadiene chains of different repeat unit sizes and temperatures. Numerical model results: trans (○ blue), cis (△ red). Experimental results: At T = 297 K (△ black) [38] and T = 298.15 K (∗ black) [39].

2.4 Conclusions

The aim of this work was to develop a probability-based numerical tool to accurately predict mechanical properties of polybutadiene chains of different repeat unit sizes and temperatures under deformation. This task began with generating Gaussian chains which were randomly distributed over the $(+x, +y, +z)$ octant of a sphere and extended along the x direction while being compressed along the y and z directions. Probability density distributions of the chain end-to-end vectors changed due to deformation, which resulted in changes in the elastic free energy

of the chain ensembles. The numerical method derived for computing the elastic free energy change of chain ensembles ultimately led to numerical evaluations of force and stress. These results were in great agreement with analytical solutions thus the simulation method was applied to calculate mechanical properties of RIS chains.

Ensembles of cis- and trans-1,4-polybutadiene chains generated under unperturbed conditions using Flory's RIS method in our previous work [27] were uniaxially extended. Elastic free energy change, force, and stress equations were calculated using the newly developed method. Forces (tension and compression) and tensile stresses increased with deformation and the normalized results emphasized the significance of chain volume and temperature. Variation in stresses and forces were minimal between cis and trans chains.

The slope of the stress-strain curves in the linear regime provided Young's moduli of chain ensembles of different repeat unit sizes and temperatures. Significant variation was observed in moduli with chain repeat unit size while only minor variations were observed with temperature. Fewer repeat unit size chains corresponded to a much more tightly cross-linked network than more repeat unit size chains, and resulted in greater moduli. Numerically computed moduli were in

good agreement with available experimental results.

2.5 Acknowledgments

We thank the Ford Motor Company University Research Program for funding this research.

List of References

[1] C. M. Blow and C. Hepburn, *Rubber Technology and Manufacture*. Plastics and Rubber Institute, London, 1982.

[2] J. L. White, *Rubber Processing: Technology, Materials, and Principles*. Hanser, Munich, 1995.

[3] J. W. ten Brinke, V. M. Litvinov, J. E. G. J. Wijnhoven, and J. W. M. Noordermeer, "Interactions of stober silica with natural rubber under the influence of coupling agents, studied by ^{1}H NMR T_2 relaxation analysis," *Macromolecules*, vol. 35, no. 27, pp. 10 026–37, 2002.

[4] L. A. E. M. Reuvekamp, S. C. Debnath, J. W. Brinke Ten, J. P. Van Swaaij, and J. W. M. Noordermeer, "Effect of zinc oxide on the reaction of TESPT silane coupling agent with silica and rubber," *Rubber Chem Technol*, vol. 77, no. 1, pp. 34–49, 2004.

[5] J. E. Mark and B. Erman, *Rubberlike Elasticity: A Molecular Primer*. Wiley Interscience, 1988.

[6] M. Ott, R. Pérez-Aparicio, H. Schneider, P. Sotta, and K. Saalwächter, "Microscopic study of chain deformation and orientation in uniaxially strained

polymer networks: NMR results versus different network models," *Macromolecules*, vol. 47, no. 21, pp. 7597–7611, 2014.

[7] S. Schlögl, M. L. Trutschel, W. Chasśe, G. Riess, and K. Saalwächter, "Entanglement effects in elastomers: Macroscopic vs microscopic properties," *Macromolecules*, vol. 48, no. 8, p. 2855, 2014.

[8] J. Cohen Addad, B. P. Thanh, and H. Montes, "Evidence for a linear NMR-Elasticity interrelationship in polymeric gels," *Macromolecules*, vol. 30, no. 15, pp. 4374–4380, 1997.

[9] A. Vieyres, R. Pérez Aparicio, P. A. Albouy, O. Sanseau, K. Saalwächter, D. R. Long, and P. Sotta, "Sulfur-cured natural rubber elastomer networks: correlating cross-link density, chain orientation, and mechanical response by combined techniques," *Macromolecules*, vol. 46, no. 3, pp. 889–899, 2013.

[10] F. Bates, R. Cohen, and C. Berney, "Small-angle neutron scattering determination of macrolattice structure in a polystyrene-polybutadiene diblock copolymer," *Macromolecules*, vol. 15, no. 2, pp. 589–592, 1982.

[11] T. Kameda and T. Asakura, "Structure and dynamics in the amorphous region of natural rubber observed under uniaxial deformation monitored with solid-state ^{13}C NMR," *Polymer*, vol. 44, no. 24, pp. 7539–7544, 2003.

[12] H. M. James and E. Guth, "Theory of the elasticity of rubber," *J Appl Phys*, vol. 15, no. 4, pp. 294–303, 1944.

[13] M. Rubinstein and S. Panyukov, "Nonaffine deformation and elasticity of polymer networks," *Macromolecules*, vol. 30, no. 25, pp. 8036–8044, 1997.

[14] G. Heinrich, E. Straube, and G. Helmis, "Rubber elasticity of polymer networks: Theories," *Adv Polym Sci*, vol. 85, pp. 33–87, 1988.

[15] M. Wagner, "Analysis of small-angle neutron scattering data on poly (dimethylsiloxane) network unfolding," *Macromolecules*, vol. 27, no. 18, pp. 5223–5226, 1994.

[16] P. M. Subhani and R. K. Kumar, "A new stored energy function for rubber like materials for low strains," *Mech Adv Mater Struct*, vol. 16, no. 5, pp. 402–416, 2009.

[17] I. Dubrović, D. Klepac, S. Valić, and G. Žauhar, "Study of natural rubber crosslinked in the state of uniaxial deformation," *Radiat Phys Chem*, vol. 77, no. 6, pp. 811–817, 2008.

[18] S. Valić, "Orientational motions of chain segments in natural rubber crosslinked under uniaxial deformation," *Radiat Phys Chem*, vol. 97, pp. 393–397, 2014.

[19] O. Starkova and A. Aniskevich, "Poisson's ratio and the incompressibility relation for various strain measures with the example of a silica-filled SBR rubber in uniaxial tension tests," *Polym Test*, vol. 29, no. 3, pp. 310–318, 2010.

[20] J. E. Mark, "Random-coil configurations of cis-l,4-polybutadiene and cis-1,4-polyisoprene. Theoretical interpretation," *J Am Chem Soc*, vol. 88, no. 19, pp. 4354–9, 1966.

[21] J. E. Mark, "Interpretation of random-coil configurations of trans-1,4-polybutadiene and trans-1,4-polyisoprene," *J Am Chem Soc*, vol. 89, no. 26, pp. 6829–35, 1967.

[22] P. J. Flory, *Principles of Polymer Chemistry*. Cornell University Press, 1953.

[23] P. J. Flory, *Statistical Mechanics of Chain Molecules*. Wiley Interscience, 1969.

[24] Y. Abe and P. J. Flory, "Configurational statistics of 1,4-polybutadiene chains," *Macromolecules*, vol. 4, no. 2, pp. 219–29, 1971.

[25] K. Kajiwara and W. Burchard, "Rotational isomeric state calculations of the dynamic structure factor and related properties of some linear chains. 1. The $\rho = \langle S^2 \rangle^{1/2} \langle R_H^{-1} \rangle$ parameter," *Macromolecules*, vol. 17, no. 12, pp. 2669–73, 1984.

[26] K. Kajiwara and W. Burchard, "Rotational isomeric state calculations of the dynamic structure factor and related properties of some linear chains. 2. First cumulant of the dynamic structure factor," *Macromolecules*, vol. 17, no. 12, pp. 2674–8, 1984.

[27] S. Kar and M. L. Greenfield, "Sizes and shapes of simulated amorphous cis- and trans-1,4-polybutadiene," *Polymer*, vol. 62, pp. 129–138, 2015.

[28] J. E. Mark, R. Abou-Hussein, T. Z. Sen, and A. Kloczkowski, "Some simulations on filler reinforcement in elastomers," *Polymer*, vol. 46, no. 21, pp. 8894–8904, 2005.

[29] P. C. Hiemenz and T. P. Lodge, *Polymer Chemistry, 2nd Edition*. CRC Press, Taylor & Francis Group, 2007.

[30] N. G. McCrum, C. P. Buckley, and C. B. Bucknall, *Principles of Polymer Engineering, 2nd Edition*. Oxford Univ Press, 1997.

[31] M. Rubinstein and R. H. Colby, *Polymer physics*. Oxford University Press New York, 2003.

[32] G. Tsolou, V. G. Mavrantzas, and D. N. Theodorou, "Detailed atomistic molecular dynamics simulation of cis-1,4-poly(butadiene)," *Macromolecules*, vol. 38, no. 4, pp. 1478–1492, 2005.

[33] R. H. Gee and R. H. Boyd, "Conformational dynamics and relaxation in bulk polybutadienes: A molecular dynamics simulation study," *J Chem Phys*, vol. 101, no. 9, pp. 8028–38, 1994.

[34] D. Paul and A. DiBenedetto, "Diffusion in amorphous polymers," *J Polym Sci: Part C*, no. 10, pp. 17–44, 1965.

[35] A. R. A. Ragab and S. E. A. Bayoumi, *Engineering solid mechanics: fundamentals and applications*. CRC Press, 1998.

[36] I. M. Ward and J. Sweeney, *Mechanical properties of solid polymers*. John Wiley & Sons, 2012.

[37] L. Treloar, "Stress-strain data for vulcanised rubber under various types of deformation," *Trans Faraday Soc*, vol. 40, pp. 59–70, 1944.

[38] F. Q. Pancheri and L. Dorfmann, "Strain-controlled biaxial tension of natural rubber: New experimental data," *Rubber Chem Technol*, vol. 87, no. 1, pp. 120–138, 2014.

[39] M. Fujikawa, N. Maeda, J. Yamabe, Y. Kodama, and M. Koishi, "Determining stress-strain in rubber with in-plane biaxial tensile tester," *Exp Mech*, vol. 54, no. 9, pp. 1639–1649, 2014.

[40] L. R. G. Treloar, *The physics of rubber elasticity*. Oxford University Press, USA, 1975.

CHAPTER 3

"Simulating stress-strain behavior by using individual chains. 2. Biaxial deformation and shear of amorphous cis- and trans-1,4-polybutadiene"

by

Suvrajyoti Kar, Julie L Cuddigan, Michael L Greenfield *

Department of Chemical Engineering, University of Rhode Island, Kingston, RI - 02881, USA

is prepared for submission to Polymer

*Corresponding author email: greenfield@uri.edu

Abstract

This work continues developing a configuration-based approach to predict mechanical properties of non-ideal polymer chains subject to deformation. In the previous work on uniaxial deformation of polybutadiene (part 1), a probability-based simulation method for computing stress from changes in chain elastic free energy under deformation was developed. Here, this method was extended to predicting stress-strain behavior under equibiaxial deformation and shear. Mechanical properties showed the expected dependence on chain volume and temperature. Tensile stresses were similar in magnitude for equibiaxial and uniaxial extensions and were greater than shear stresses. Moduli computed using the numerical method were in good agreement with experimental results available from literature.

Keywords: Biaxial deformation, shear, numerical method, Gaussian analytical, polybutadiene chains, mechanical properties

3.1 Introduction

Our research is directed towards evaluating elastomer chain conformations and their role in affecting viscoelastic and mechanical properties of rubber tires. During vehicle motion, tires are subjected to various forms of external forces that lead to deformation of the tire tread. Under uniaxial deformation, elastomers are stretched

along a single direction and compressed along the other orthogonal directions [1, 2]. For biaxial deformation, elastomers are stretched along two orthogonal directions while being compressed along the third direction [1, 2]. Shear considers chains to be subjected to a sliding motion resulting in their lateral displacement [1].

Several research groups proposed models for computing mechanical properties of rubber and performed experiments to determine their efficacy. Pancheri and Dorfmann [3] conducted uniaxial, equibiaxial and shear testing on filled and unfilled rubber samples to verify their stress model based on Ogden's [4] and Valanis-Landel hypothesis [5] of energy density. They found good agreement in their model and experimental results. Hariharaputhiran and Saravanan [6] proposed novel experimental methods and stored energy functions based on the methodology of Rivlin and Saunders [7] for uniaxial and equibiaxial deformation of vulcanized rubber. They concluded that their proposed model had limited predictive capability for uniaxial but showed greater accuracy for equibiaxial tests. The slip-link model proposed by Ball et al. [8] and extended by Edwards and Vilgis [9] formed the basis of energy equations proposed by Meissner et al. [10] to predict stress-strain behavior of cross-linked rubber-like networks. Their model and experimental data were in decent agreement with a predicted difference of around 10%.

In order to develop a better understanding of the impact of microscopic changes on macroscopic elastomer properties, this work focuses on the development of novel numerical methods for evaluating changes in elastomer chain conformations under deformation. From previous work [11], we have available distributions of end-to-end distances of cis- and trans-1,4-polybutadiene chains under unperturbed conditions that were generated using the RIS approach. These chains were uniaxially deformed to understand molecular level changes in their mechanical properties. Novel numerical methods were developed to quantitatively and qualitatively analyze the impact of the external stresses on the chains in a multipart series submitted simultaneously (part 1). This paper continues that analysis in order to extend the application of these new methods to biaxial and shear conditions.

3.2 Methodology

Part 1 focused on uniaxial deformation of polybutadiene chains. There, we developed a probability-based numerical method for computing the change in elastic free energy and stress-strain behavior of chains. In this work, we extend that methodology to study mechanical properties of chains subject to equibiaxial deformation and shear. Prior to being applied to non-Gaussian RIS chains, the

accuracy of the method for these new deformation directions was tested against known analytical equations by using simulated Gaussian chains.

The probability-based numerical method being described here for the change in elastic free energy of an ensemble of N chains due to deformation is given as (part 1)

$$\frac{\langle \Delta A_{el} \rangle}{k_b T} = \sum_{\text{voxels}} P(\vec{r_0}) \ \ln P(\vec{r_0}) \ \frac{r_0^2}{\langle r^2 \rangle_0} \ (\Delta r_0)^3 - \sum_{\text{voxels}} P(\vec{r}) \ \ln P(\vec{r}) \ \frac{r^2}{\langle r^2 \rangle_0} \ (\Delta r)^3 \quad (42)$$

where $(\Delta r)^3 = (\Delta r_0)^3$ is the volume of a voxel, r_0^2 and r^2 represent undeformed and deformed chain end-to-end distances respectively, and $\langle r^2 \rangle_0$ is the average of the mean squared end-to-end distance of the undeformed chains. Each voxel represents a possible position of an end-to-end vector in three dimensional space. The $P(\vec{r})$ of chains were computed based on their voxel location along the x, y, z coordinate directions

$$P(\vec{r}) = \frac{\text{number of chains in voxel}_{\text{xyz}} \text{ at } \vec{\text{r}}}{\text{volume of voxel}_{\text{xyz}} * \text{N}} \quad (43)$$

From thermodynamics, force is directly related to the change in elastic free energy with system dimension [12] as a result of deformation and is given as

$$f_k = \left(\frac{\partial \lambda_k}{\partial L} \right) \left(\frac{\partial \langle \Delta A_{el} \rangle}{\partial \lambda_k} \right)_{T,V} \quad (44)$$

where deformation or stretch ratio $\lambda_k = r_k/r_{k,0}$ [1] applied in the kth direction leads to force f_k in the kth direction. r_k and $r_{k,0}$ are deformed and undeformed chain end-to-end vectors respectively and L is $V^{1/3}$ where V is the volume of a single chain. Stresses acting on the system due to deformation are obtained by dividing the forces with the appropriate cross-sectional areas (A_m)

$$\sigma_{mk} = \left(\frac{1}{LA_m}\right)\left(\frac{\partial\langle\Delta A_{el}\rangle}{\partial\lambda_k}\right)_{T,V} \tag{45}$$

Biaxial deformation involves deforming the chains in tension along the x and y directions with compression along the z direction. For shear, we assume chains to be sheared along the x and z directions and unchanged along the y direction. Affine deformation was assumed [12, 13] and since polybutadiene is an elastomer, it was assumed to be incompressible with a Poisson's ratio (ν) of 0.5 [1, 14]. No change in volume was expected as a result of deformation thus $\lambda_x\lambda_y\lambda_z = 1$. For biaxial deformation, the tension along x and y directions were represented by deformation ratios λ_x and λ_y respectively. Compression occurs along the z direction such that $\lambda_z = 1/\lambda_x\lambda_y$. Deformation ratio for shear along the x direction is λ_x or λ and along the z direction is $1/\lambda$, with no change in the y direction i.e. $\lambda_y = 1$.

For tensile stresses, the cross-sectional areas of interest are those whose unit

vector is aligned with the applied force, and for shear stresses the cross-sectional areas are normal to the applied force. The cross-sectional areas for biaxial tension

$$(L_y L_z)_{\text{biaxial}} = \frac{L^2}{\lambda_x} \tag{46}$$

$$(L_x L_z)_{\text{biaxial}} = \frac{L^2}{\lambda_y} \tag{47}$$

compression

$$(L_x L_y)_{\text{biaxial}} = L^2 \lambda_x \lambda_y \tag{48}$$

and shear

$$(L_x L_z)_{\text{shear}} = L^2 \tag{49}$$

For biaxial tension, substituting area from equation 46 or 47 into 45 leads to

$$\sigma_{mk} = \left(\frac{\lambda_k}{V}\right)\left(\frac{\partial \langle \Delta A_{el} \rangle}{\partial \lambda_k}\right)_{T,V} \tag{50}$$

Similarly, substituting equation 49 into equation 45 for shear leads to

$$\sigma_{mk} = \left(\frac{1}{V}\right)\left(\frac{\partial \langle \Delta A_{el} \rangle}{\partial \lambda_k}\right)_{T,V} \tag{51}$$

The volume of a single chain (V) is a function of its molecular weight and temperature, and was calculated using polybutadiene densities. Densities of cis- and

trans-1,4-polybutadiene at different temperatures were obtained from prior experimental and theoretical results [15, 16, 17].

Forces can be obtained numerically by applying equation 44 to equation 42 for biaxial tension

$$\frac{f_x}{k_bT}_{\text{biaxial}} = \frac{1}{L}\left(\frac{\partial\left(\sum_{\text{voxels}} P(\vec{r_0})\ \ln P(\vec{r_0})\ \frac{r_0^2}{\langle r^2\rangle_0}\ (\Delta r_0)^3 - \sum_{\text{voxels}} P(\vec{r})\ \ln P(\vec{r})\ \frac{r^2}{\langle r^2\rangle_0}\ (\Delta r)^3\right)}{\partial\lambda_x}\right)_{T,V} \tag{52}$$

$$\frac{f_y}{k_bT}_{\text{biaxial}} = \frac{1}{L}\left(\frac{\partial\left(\sum_{\text{voxels}} P(\vec{r_0})\ \ln P(\vec{r_0})\ \frac{r_0^2}{\langle r^2\rangle_0}\ (\Delta r_0)^3 - \sum_{\text{voxels}} P(\vec{r})\ \ln P(\vec{r})\ \frac{r^2}{\langle r^2\rangle_0}\ (\Delta r)^3\right)}{\partial\lambda_y}\right)_{T,V} \tag{53}$$

compression

$$\frac{f_z}{k_bT}_{\text{biaxial}} = \frac{1}{L}\left(\frac{\partial\left(\sum_{\text{voxels}} P(\vec{r_0})\ \ln P(\vec{r_0})\ \frac{r_0^2}{\langle r^2\rangle_0}\ (\Delta r_0)^3 - \sum_{\text{voxels}} P(\vec{r})\ \ln P(\vec{r})\ \frac{r^2}{\langle r^2\rangle_0}\ (\Delta r)^3\right)}{\partial\left(1/\lambda_x\lambda_y\right)}\right)_{T,V} \tag{54}$$

and shear

$$\frac{f_x}{k_b T}_{\text{shear}} = \frac{1}{L}\left(\frac{\partial\left(\sum_{\text{voxels}} P(\vec{r_0})\ \ln P(\vec{r_0})\ \frac{r_0^2}{\langle r^2\rangle_0}\ (\Delta r_0)^3 - \sum_{\text{voxels}} P(\vec{r})\ \ln P(\vec{r})\ \frac{r^2}{\langle r^2\rangle_0}\ (\Delta r)^3\right)}{\partial\lambda}\right)_{T,V}. \tag{55}$$

Shear force in the z direction can be given as

$$\frac{f_z}{k_b T}_{\text{shear}} = -\frac{\lambda^2}{L}\left(\frac{\partial\left(\sum_{\text{voxels}} P(\vec{r_0})\ \ln P(\vec{r_0})\ \frac{r_0^2}{\langle r^2\rangle_0}\ (\Delta r_0)^3 - \sum_{\text{voxels}} P(\vec{r})\ \ln P(\vec{r})\ \frac{r^2}{\langle r^2\rangle_0}\ (\Delta r)^3\right)}{\partial\lambda}\right)_{T,V} \tag{56}$$

Stresses were numerically obtained by substituting equation 42 in equations 50 and 51 respectively for biaxial tension

$$\frac{\sigma_{xx}}{k_b T}_{\text{biaxial}} = \frac{\lambda_x}{V}\left(\frac{\partial\left(\sum_{\text{voxels}} P(\vec{r_0})\ \ln P(\vec{r_0})\ \frac{r_0^2}{\langle r^2\rangle_0}\ (\Delta r_0)^3 - \sum_{\text{voxels}} P(\vec{r})\ \ln P(\vec{r})\ \frac{r^2}{\langle r^2\rangle_0}\ (\Delta r)^3\right)}{\partial\lambda_x}\right)_{T,V} \tag{57}$$

$$\frac{\sigma_{yy}}{k_b T}_{\text{biaxial}} = \frac{\lambda_y}{V}\left(\frac{\partial\left(\sum_{\text{voxels}} P(\vec{r_0})\ \ln P(\vec{r_0})\ \frac{r_0^2}{\langle r^2\rangle_0}\ (\Delta r_0)^3 - \sum_{\text{voxels}} P(\vec{r})\ \ln P(\vec{r})\ \frac{r^2}{\langle r^2\rangle_0}\ (\Delta r)^3\right)}{\partial\lambda_y}\right)_{T,V} \tag{58}$$

compression

$$\frac{\sigma_{zz}}{k_bT}_{\text{biaxial}} = \frac{1}{V\lambda_x\lambda_y}\left(\frac{\partial\left(\sum\limits_{\text{voxels}} P(\vec{r_0})\ \ln P(\vec{r_0})\ \frac{r_0^2}{\langle r^2\rangle_0}\ (\Delta r_0)^3 - \sum\limits_{\text{voxels}} P(\vec{r})\ \ln P(\vec{r})\ \frac{r^2}{\langle r^2\rangle_0}\ (\Delta r)^3\right)}{\partial\left(1/\lambda_x\lambda_y\right)}\right)_{T,V} \tag{59}$$

and shear

$$\frac{\sigma_{yx}}{k_bT}_{\text{shear}} = \frac{1}{V}\left(\frac{\partial\left(\sum\limits_{\text{voxels}} P(\vec{r_0})\ \ln P(\vec{r_0})\ \frac{r_0^2}{\langle r^2\rangle_0}\ (\Delta r_0)^3 - \sum\limits_{\text{voxels}} P(\vec{r})\ \ln P(\vec{r})\ \frac{r^2}{\langle r^2\rangle_0}\ (\Delta r)^3\right)}{\partial\lambda}\right)_{T,V}. \tag{60}$$

The numerical method was tested by applying it to a distribution of Gaussian chains, for which analytical force and stress equations are available. Gaussian chains available from previous work on uniaxial deformation were oriented randomly over the $(+x, +y, +z)$ octant of a sphere using combinations of θ and ϕ (part 1). The end-to-end vectors of the chains $(r_{x,0}, r_{y,0}, r_{z,0})$ in spherical coordinates under undeformed conditions were

$$(r_{x,0}\ , r_{y,0}\ , r_{z,0}) = r_0(\sin\theta\cos\phi\ , \sin\theta\sin\phi\ , \cos\theta) \tag{61}$$

and after deformation

$$(r_x\ ,r_y\ ,r_z)_{\text{biaxial}} = r_0(\lambda_x \sin\theta\cos\phi\ ,\lambda_y \sin\theta\sin\phi\ ,\frac{1}{\lambda_x\lambda_y}\cos\theta) \tag{62}$$

$$(r_x\ ,r_y\ ,r_z)_{\text{shear}} = r_0(\lambda \sin\theta\cos\phi\ ,\sin\theta\sin\phi\ ,\frac{1}{\lambda}\cos\theta) \tag{63}$$

The change in elastic free energy of an ensemble of N Gaussian chains is written analytically as [2]

$$\frac{\langle \Delta A_{el}\rangle}{k_b T} = \frac{1}{2}N\left(\lambda_x^2+\lambda_y^2+\lambda_z^2-3\right) \tag{64}$$

Under biaxial deformation and shear, equation 64 can be written as

$$\frac{\langle \Delta A_{el}\rangle}{k_b T}_{\text{biaxial}} = \frac{1}{2}N\left(\lambda_x^2+\lambda_y^2+\frac{1}{\lambda_x^2\lambda_y^2}-3\right) \tag{65}$$

$$\frac{\langle \Delta A_{el}\rangle}{k_b T}_{\text{shear}} = \frac{1}{2}N\left(\lambda^2+\frac{1}{\lambda^2}-2\right) \tag{66}$$

and compared with results obtained from using equation 42 for Gaussian chains to determine accuracy of the numerical method for elastic free energy change computations.

Analytical forces on the Gaussian chain ensembles were obtained from equa-

tions 44 and 65 for biaxial tension

$$\frac{f_x}{k_bT}_{\text{biaxial}} = \frac{N}{L}\left(\lambda_x - \frac{1}{\lambda_x^3\lambda_y^2}\right) \tag{67}$$

$$\frac{f_y}{k_bT}_{\text{biaxial}} = \frac{N}{L}\left(\lambda_y - \frac{1}{\lambda_x^2\lambda_y^3}\right) \tag{68}$$

and compression

$$\frac{f_z}{k_bT}_{\text{biaxial}} = \frac{N}{L}\left(\frac{1}{\lambda_x\lambda_y} - \lambda_x^3\lambda_y - \lambda_y^3\lambda_x\right). \tag{69}$$

Similarly, analytical shear force on Gaussian ensembles in the x and z directions can be obtained from equations 44 and 66 as

$$\frac{f_x}{k_bT}_{\text{shear}} = \frac{N}{L}\left(\lambda - \frac{1}{\lambda^3}\right) \tag{70}$$

$$\frac{f_z}{k_bT}_{\text{shear}} = \frac{N}{L}\left(\frac{1}{\lambda} - \lambda^3\right) \tag{71}$$

The analytical force equations were compared with their numerical counterparts (equations 52, 53, 54, 55, and 56) to verify the accuracy of the force calculations within the numerical method.

Analytic stresses on Gaussian chain ensembles were obtained by dividing forces

with the respective cross-sectional areas. This led to equations for biaxial tension

$$\frac{\sigma_{xx}}{k_bT}_{\text{biaxial}} = \frac{N}{V}\left(\lambda_x^2 - \frac{1}{\lambda_x^2\lambda_y^2}\right) \tag{72}$$

$$\frac{\sigma_{yy}}{k_bT}_{\text{biaxial}} = \frac{N}{V}\left(\lambda_y^2 - \frac{1}{\lambda_x^2\lambda_y^2}\right) \tag{73}$$

compression

$$\frac{\sigma_{zz}}{k_bT}_{\text{biaxial}} = \frac{N}{V}\left(\frac{1}{\lambda_x^2\lambda_y^2} - \lambda_x^2 - \lambda_y^2\right) \tag{74}$$

and shear

$$\frac{\sigma_{yx}}{k_bT}_{\text{shear}} = \frac{N}{V}\left(\lambda - \frac{1}{\lambda^3}\right). \tag{75}$$

These results were compared with equations 57, 58, 59 and 60 for determination of numerical accuracy of stresses.

This work focuses on extending the application of the numerical method for evaluating elastomer mechanical properties developed in our prior work (part 1) to equibiaxial and shear conditions. Various ensembles of 10^5 RIS and Gaussian single chains were available from previous work for different molecular weights (x = 15, 25, 50, 75, 100, and 120 repeat units) at a temperature of 343 K, as well as at different temperatures (T = 275, 300, 323, 343, 375, and 400 K) for a single repeat unit size of 50 [11]. Following the numerical and analytical comparisons

of Gaussian chains, the numerical method was extended to studying stress-strain behavior of non-Gaussian RIS chains.

Slopes of the linear regime of the respective stress-strain plots were used to compute Young's modulus (E) and shear modulus (G) [1, 12]. The magnitude of the deformations imposed here ($\lambda = 1$ to 3.5) emphasized the need for utilizing finite strain (ϵ,γ) which can be related to engineering strain (ϵ_e,γ_e) as [18]

$$\epsilon = \frac{1}{2}\epsilon_e^2 + \epsilon_e \tag{76}$$

For tension, engineering strain (ϵ_e) is related to deformation or stretch ratio (λ) as [1]

$$\epsilon_e = \lambda - 1 \tag{77}$$

thus finite strain (ϵ) for tension in terms of λ is [19]

$$\epsilon = \frac{1}{2}\left(\lambda^2 - 1\right). \tag{78}$$

For shear, engineering strain (γ_e) is related to λ as [1]

$$\gamma_e = \lambda - \frac{1}{\lambda} \tag{79}$$

thus finite shear strain (γ) in terms of λ is

$$\gamma = \frac{1}{2}\left(\lambda - \frac{1}{\lambda}\right)^2 + \left(\lambda - \frac{1}{\lambda}\right). \tag{80}$$

Shear and Young's modulus can be related as [1, 12]

$$G = \frac{E}{2(1+\nu)} \tag{81}$$

For elastomer systems of $\nu = 0.5$, equation 81 can be simplified to $G = E/3$.

3.3 Results and Discussion

In order to test the accuracy of the numerical method, comparisons were done with analytical solutions for Gaussian chains under equibiaxial tension and shear. Figure 22 shows excellent agreement between numerical results and analytical solutions for elastic free energy change, forces and stresses. The plots are for trans-1,4-polybutadiene chains of 50 repeat units at 343 K and were shown to emphasize the accuracy of the numerical method.

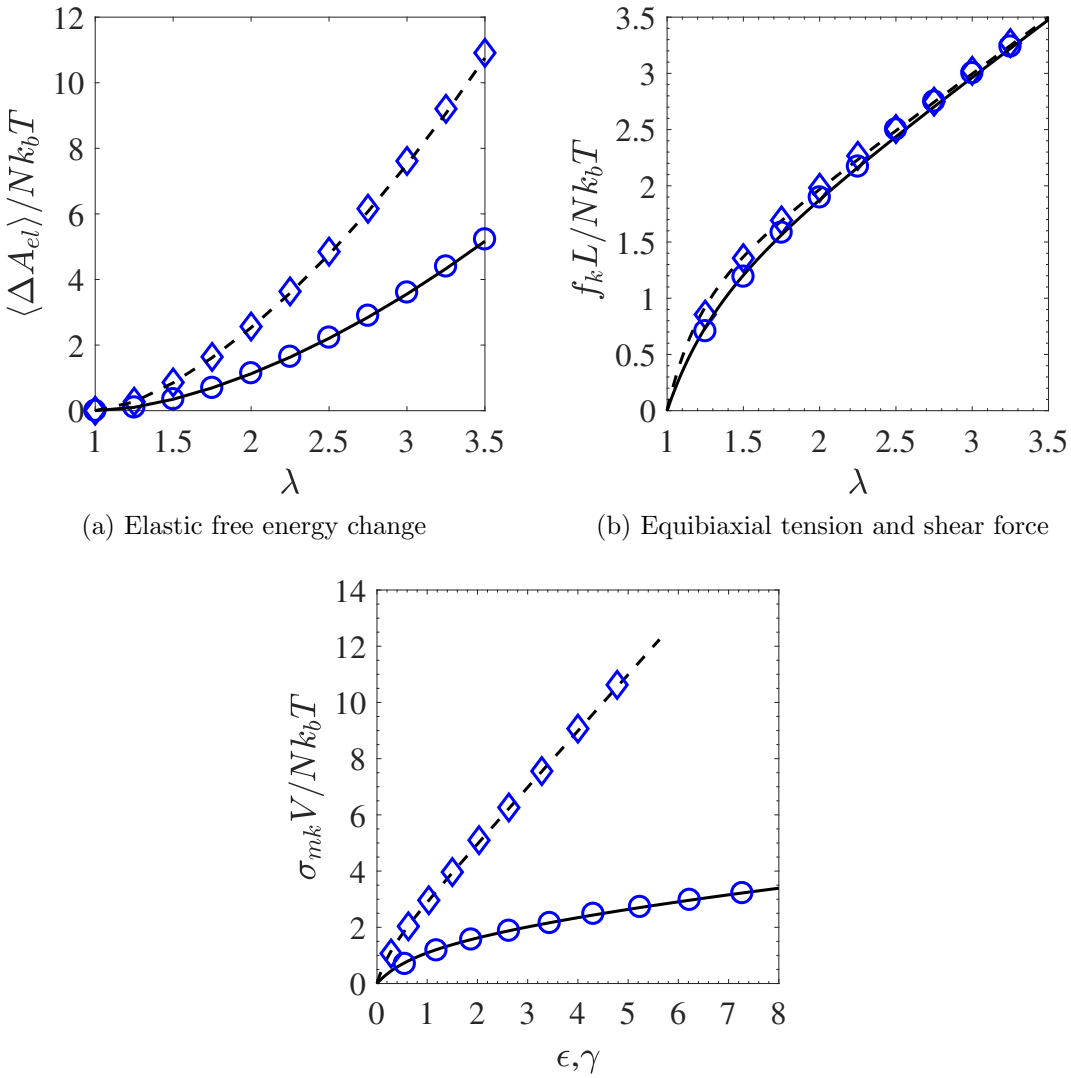

(a) Elastic free energy change

(b) Equibiaxial tension and shear force

(c) Equibiaxial tensile and shear stress

Figure 22: Analytical and numerical comparisons for trans-1,4-polybutadiene chains of 50 repeat units at 343 K. Equibiaxial (f_x or f_y, σ_{xx} or σ_{yy}): numerical ($\diamond$ blue), and analytical (dashed line). Shear (f_x, σ_{yx}): numerical ($\circ$ blue), and analytical (solid line).

With the numerical accuracy of the simulation method confirmed, it was applied to RIS chains. Figure 23 shows probability density distributions of end-to-end vectors of trans-1,4-polybutadiene chains of 50 repeat units under equibiax-

ial extension (figure 23 (a),(c)) and shear (figure 23(b),(d)). Distributions of r_x for equibiaxial and shear were similar because the chains were stretched by the same magnitude along the same direction. This distribution was initially narrow under undeformed conditions and gradually widened with increasing deformation. This indicated that highly probable shorter conformations became less probable upon stretching while longer conformations became increasingly present. Inversely, r_z distributions contract with increasing deformation indicating more probable shorter conformations and less probable longer conformations on compression. This effect was much more prominent for equibiaxial compression.

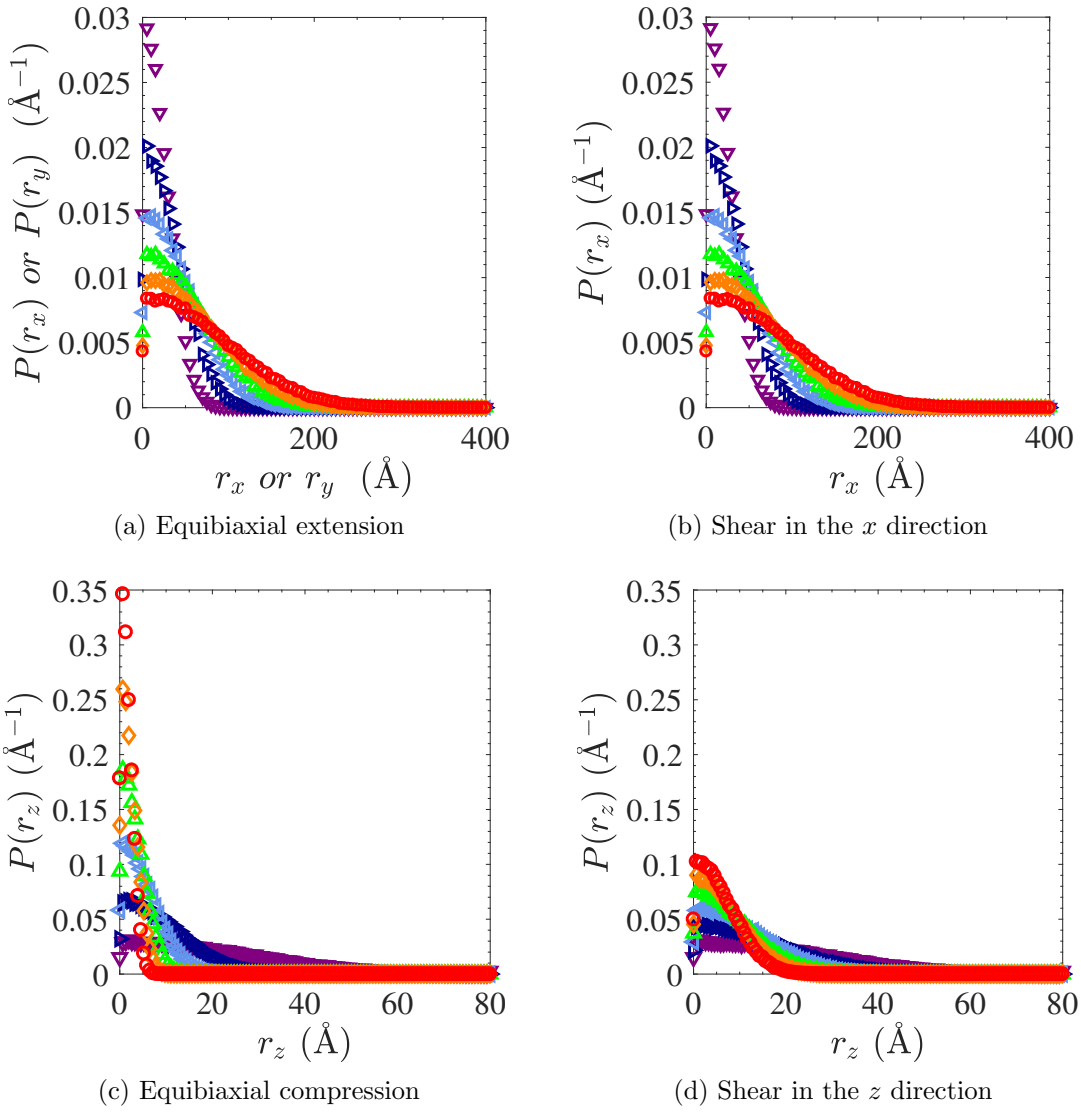

(a) Equibiaxial extension

(b) Shear in the x direction

(c) Equibiaxial compression

(d) Shear in the z direction

Figure 23: Probability density distributions of end-to-end vectors for trans-1,4-polybutadiene chains of 50 repeat units at 343 K under equibiaxial deformation and shear. Deformation ratios (λ): 1 ($\triangledown$ violet), 1.5 ($\triangleright$ indigo), 2 ($\triangleleft$ blue), 2.5 ($\triangle$ green), 3 ($\diamond$ orange), and 3.5 ($\circ$ red).

Mechanical properties are compared across equibiaxial and shear on trans chains of 15 and 120 repeat units at 343 K in figures 24 and 25. Uniaxial results available from previous work (part 1) were also used for comparison. Tension,

compression and shear forces increased with deformation as seen in figure 24. The tension force under equibiaxial and uniaxial deformation, and shear in the x direction were equivalent. Compression forces under equibiaxial deformation were much larger than uniaxial deformation, and shear force in the z direction, due to its compensation for multiaxial extensions. Figure 25 shows that equibiaxial stresses per direction of extension and uniaxial stresses are similar, and both are much greater than shear. The overlap of normalized forces and stresses across different sizes at the same temperature indicates that their non-normalized counterparts are impacted by the molecular weight and the volume of chains.

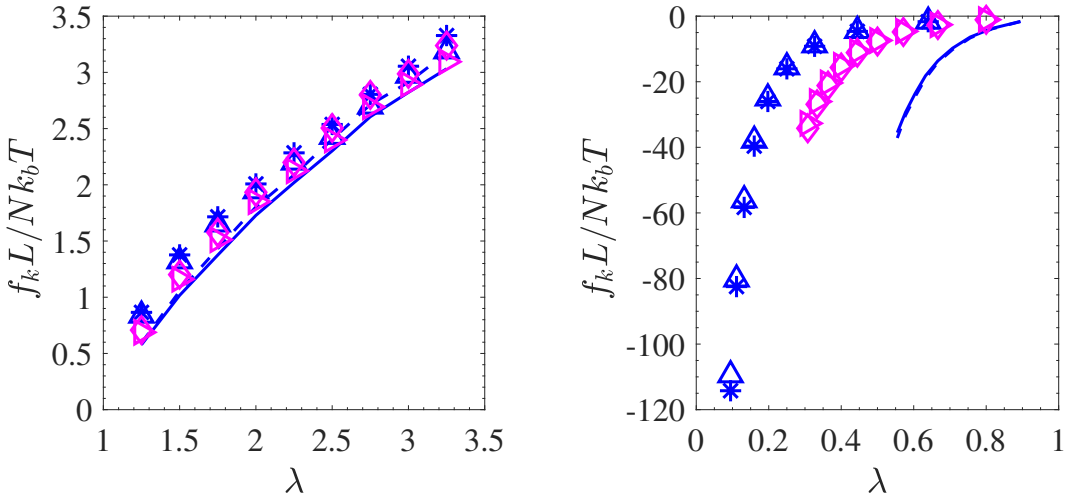

(a) Tension force and shear force in x direction

(b) Compression force and shear force in z direction

Figure 24: Forces on trans-1,4-polybutadiene chains at 343 K subjected to equibiaxial deformation and shear. Equibiaxial (tension force f_x or f_y, compression force f_z): x = 15 ($\triangle$ blue) and 120 ($*$ blue); shear (in x direction f_x, in z direction f_z): x = 15 ($\triangleright$ magenta) and 120 ($\diamond$ magenta). Uniaxial results (tension force f_x, compression force f_y or f_z) (part 1) are provided for comparison: x = 15 (solid line) and x = 120 (dashed line).

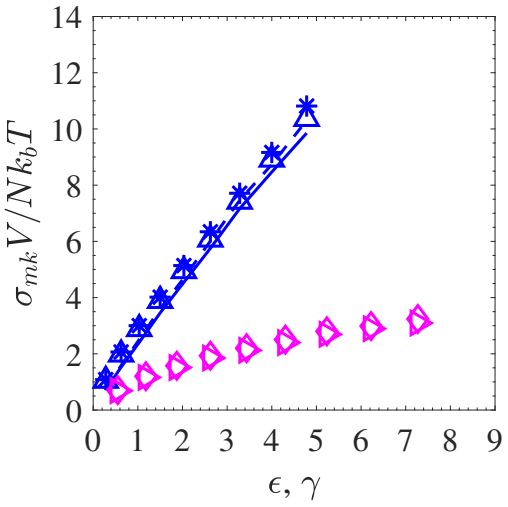

Figure 25: Tensile and shear stress on trans-1,4-polybutadiene chains at 343 K subjected to equibiaxial, uniaxial deformation and shear. Equibiaxial : σ_{xx} or σ_{yy}, shear: σ_{yx}, and uniaxial: σ_{xx}. Symbols and colors follow convention of figure 24.

Figures 26 and 27 compare trans-1,4-polybutadiene chains of 50 repeat units

at 275 K and 400 K, and show collapsing of the normalized forces and stresses at different temperatures on chains of the same volume. This indicates that the non-normalized properties are impacted by temperature. Force and stress plots for trans-1,4-polybutadiene chains for all repeat unit sizes and over all temperatures under equibiaxial deformation and shear have been included in appendix B.

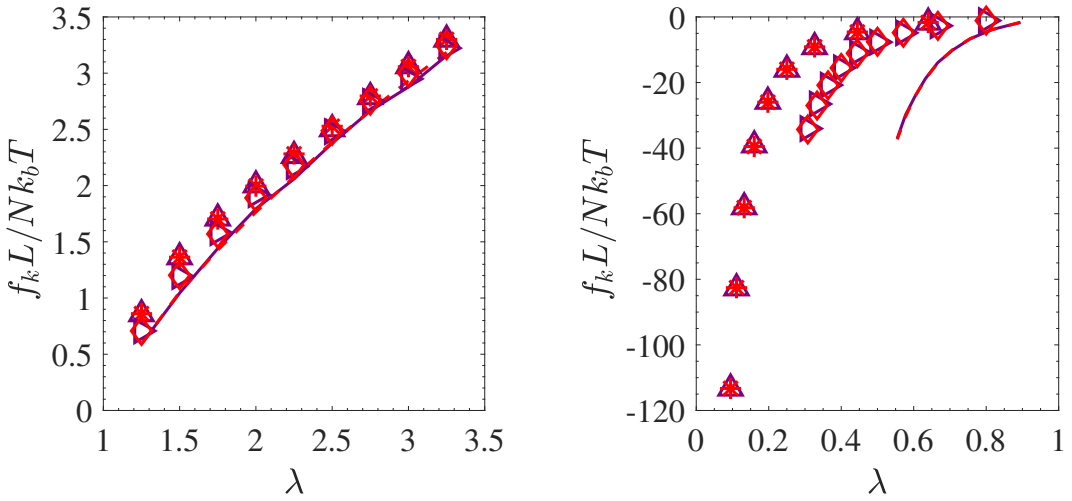

(a) Tension force and shear force in the x direction

(b) Compression force and shear force in the z direction

Figure 26: Force comparison on trans-1,4-polybutadiene chains of x = 50 subjected to equibiaxial deformation and shear. Equibiaxial (tension force f_x or f_y, compression force f_z): $T = 275$ K ($\triangle$ violet) and 400 K ($*$ red) and shear (in x direction force f_x, in z direction force f_z): $T = 275$ K ($\triangleright$ violet) and 400 K ($\diamond$ red). Uniaxial results (tension force f_x, compression force f_y or f_z) (part 1) are provided for comparison: $T = 275$ K (solid line) and 400 K (dashed line).

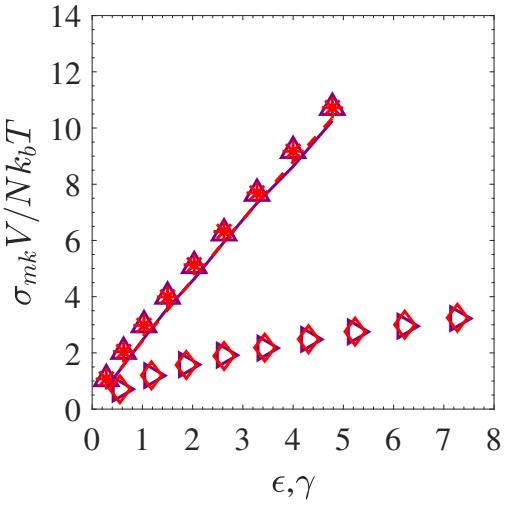

Figure 27: Tensile and shear stress on trans-1,4-polybutadiene chains of 50 repeat units subjected to equibiaxial, uniaxial deformation and shear. Equibiaxial : σ_{xx} or σ_{yy}, shear: σ_{yx}, and uniaxial: σ_{xx}. Symbols and colors follow convention of figure 26.

Moduli were computed from linear regions of stress-strain curves for RIS chains of all sizes and temperatures and are shown in figure 28. Tensile or Young's moduli (E) were computed for equibiaxial and uniaxial extensions while shear moduli (G) were computed for shear. Similar Young's moduli were observed for tensile extensions for all chain repeat unit sizes and temperatures. Shear moduli were $\sim$1/3 of Young's moduli, which matches elastomer predictions [1, 12]. Chains of fewer repeat units correspond to smaller molecular weights between cross-links, which leads to a more tightly cross-linked chain network and thus higher stiffness than chains of more repeat units. There was a slight linear increase in moduli with temperature for chains of the same repeat unit size. Young's and shear moduli

computed using our numerical method were in good agreement with experimental results [3, 20, 21].

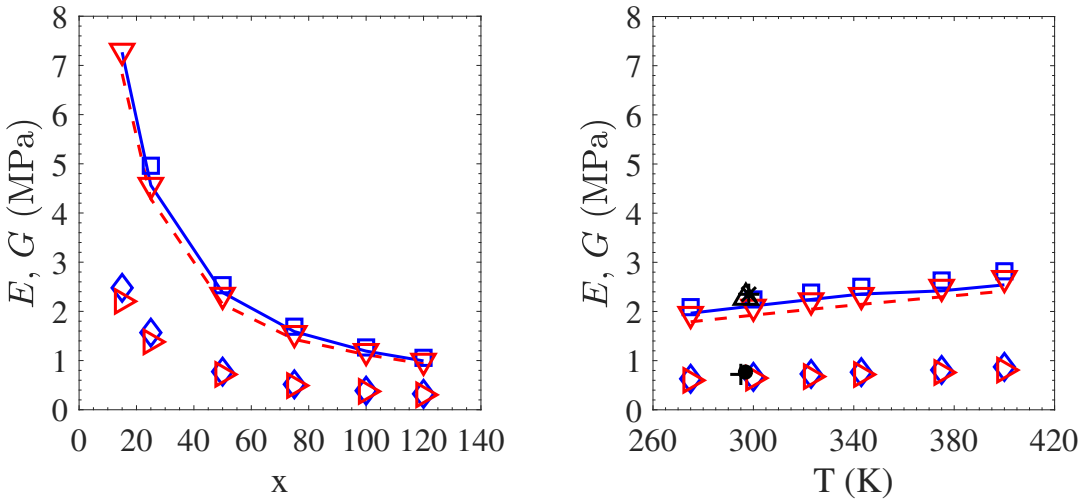

(a) All size at T = 343 K

(b) All T at x = 50

Figure 28: Moduli of cis- and trans-1,4-polybutadiene chains of different sizes and over different temperatures under uniaxial and equibiaxial deformation, and shear. Numerical model results - uniaxial Young's moduli: trans (solid line blue), cis (dashed line red) (part 1), equibiaxial Young's moduli: trans (□ blue), cis (▽ red), shear moduli: trans (◇ blue), cis (▷ red). Experimental results: At T = 295 K (+ black) [21], T = 297 K (△, filled ○ black) [3], and T = 298.15 K (∗ black) [20]

3.4 Conclusions

The aim of this work was to apply our new probability-based numerical method toward computing changes in elastic free energy and mechanical properties of elastomer systems under equibiaxial deformation and shear. Excellent agreement was observed between the numerical method applied to Gaussian chains and analytical functions, hence proving its correct implementation. This method

was then applied to RIS generated cis- and trans-1,4-polybutadiene chains to predict their stress-strain behavior. Studies were done on chains of varying repeat unit size and temperature, and were compared with previous findings under uniaxial deformation (part 1). Elastic free energy change, force and stress increased with deformation for all three types of deformation. The tension force under equibiaxial and uniaxial deformation, and shear in the x direction were equivalent. Compression forces were much larger than extension or shear forces. Force, stress, and ultimately moduli showed dependence on volume or temperature for chains of the same temperature or repeat unit size respectively. Similar tensile stresses were observed for chains under uniaxial and equibiaxial extension per direction of stretching, and were greater than shear stresses. Fewer repeat unit chains correspond to a much more tightly cross-linked network than more repeat unit chains, resulting in greater moduli. Good agreement in moduli was found between our numerical method and experimental results, with shear moduli being $\sim 1/3$ of Young's moduli. Our numerical method in combination with the RIS method [22] has the potential to incorporate specific polymer-polymer and polymer-filler interactions, that cannot be accommodated easily for analytical models of chain configuration.

3.5 Acknowledgments

We thank the Ford Motor Company University Research Program for funding this research.

List of References

[1] N. G. McCrum, C. P. Buckley, and C. B. Bucknall, *Principles of Polymer Engineering, 2nd Edition*. Oxford Univ Press, 1997.

[2] J. E. Mark and B. Erman, *Rubberlike Elasticity: A Molecular Primer*. Wiley Interscience, 1988.

[3] F. Q. Pancheri and L. Dorfmann, "Strain-controlled biaxial tension of natural rubber: New experimental data," *Rubber Chem Technol*, vol. 87, no. 1, pp. 120–138, 2014.

[4] R. W. Ogden, "Large deformation isotropic elasticity - On the correlation of theory and experiment for incompressible rubberlike solids," *Proc R Soc Lond A*, vol. 326, no. 1567, pp. 565–584, 1972.

[5] K. C. Valanis and R. F. Landel, "The strain-energy function of a hyperelastic material in terms of the extension ratios," *J Appl Phys*, vol. 38, no. 7, pp. 2997–3002, 1967.

[6] H. Hariharaputhiran and U. Saravanan, "A new set of biaxial and uniaxial experiments on vulcanized rubber and attempts at modeling it using classical hyperelastic models," *Mech Mater*, vol. 92, pp. 211–222, 2016.

[7] R. S. Rivlin and D. Saunders, "Large elastic deformations of isotropic materials. VII. Experiments on the deformation of rubber," *Phil Trans R Soc Lond A*, vol. 243, no. 865, pp. 251–288, 1951.

[8] R. C. Ball, M. Doi, S. F. Edwards, and M. Warner, "Elasticity of entangled networks," *Polymer*, vol. 22, no. 8, pp. 1010–1018, 1981.

[9] S. Edwards and T. Vilgis, "The effect of entanglements in rubber elasticity," *Polymer*, vol. 27, no. 4, pp. 483–492, 1986.

[10] B. Meissner and L. Matjka, "Comparison of recent rubber-elasticity theories with biaxial stress-strain data: The slip-link theory of Edwards and Vilgis," *Polymer*, vol. 43, no. 13, pp. 3803–3809, 2002.

[11] S. Kar and M. L. Greenfield, "Sizes and shapes of simulated amorphous cis- and trans-1,4-polybutadiene," *Polymer*, vol. 62, pp. 129–138, 2015.

[12] P. C. Hiemenz and T. P. Lodge, *Polymer Chemistry, 2nd Edition*. CRC Press, Taylor & Francis Group, 2007.

[13] M. Rubinstein and R. H. Colby, *Polymer physics*. Oxford University Press New York, 2003.

[14] O. Starkova and A. Aniskevich, "Poisson's ratio and the incompressibility relation for various strain measures with the example of a silica-filled SBR rubber in uniaxial tension tests," *Polym Test*, vol. 29, no. 3, pp. 310–318, 2010.

[15] G. Tsolou, V. G. Mavrantzas, and D. N. Theodorou, "Detailed atomistic molecular dynamics simulation of cis-1,4-poly(butadiene)," *Macromolecules*, vol. 38, no. 4, pp. 1478–1492, 2005.

[16] R. H. Gee and R. H. Boyd, "Conformational dynamics and relaxation in bulk polybutadienes: A molecular dynamics simulation study," *J Chem Phys*, vol. 101, no. 9, pp. 8028–38, 1994.

[17] D. Paul and A. DiBenedetto, "Diffusion in amorphous polymers," *J Polym Sci: Part C*, no. 10, pp. 17–44, 1965.

[18] A. R. A. Ragab and S. E. A. Bayoumi, *Engineering solid mechanics: fundamentals and applications*. CRC Press, 1998.

[19] I. M. Ward and J. Sweeney, *Mechanical properties of solid polymers*. John Wiley & Sons, 2012.

[20] M. Fujikawa, N. Maeda, J. Yamabe, Y. Kodama, and M. Koishi, "Determining stress-strain in rubber with in-plane biaxial tensile tester," *Exp Mech*, vol. 54, no. 9, pp. 1639–1649, 2014.

[21] U. D. Cakmak and Z. Major, "Experimental thermomechanical analysis of elastomers under uni- and biaxial tensile stress state," *Exp Mech*, vol. 54, no. 4, pp. 653–663, 2013.

[22] P. J. Flory, *Statistical Mechanics of Chain Molecules*. Wiley Interscience, 1969.

CHAPTER 4

"Size Distribution Analysis of Simulated Amorphous Vinyl Polymer Chains: Polypropylene and Polystyrene"

by

Suvrajyoti Kar, Julie L Cuddigan, Michael L Greenfield *

Department of Chemical Engineering, University of Rhode Island, Kingston, RI - 02881, USA

is prepared for submission to Polymer

*Corresponding author email: greenfield@uri.edu

Abstract

Random conformations of amorphous, atactic polypropylene and polystyrene single chains were generated using Flory's Rotational Isomeric State approach with discrete rotational states defined by Suter, Yoon, Sundararajan, and Flory. These conformations were analyzed to determine chain behavior at different chain lengths and over a range of temperatures. Intra-chain and inter-chain interactions occur in our systems as indicated by the relationship shown between root- mean-squared end-to-end distance and number of repeat units. Computed characteristic ratios decreased with increasing temperature indicating chain shrinkage upon heating. This behavior is defined by negative temperature coefficients computed in this work, as well as prior experimental and theoretical work. Small absolute changes in chain size probability density distributions were observed with temperature. The least probable longer chains showed a large relative decrease in probability density with increasing temperature compared to shorter chains, which showed a small relative increase in probability density. The probability densities of intermediate size chains were unaffected by temperature variation. Chain subsets corroborate the significant impact of long or taut chain conformations on average chain size with change in temperature.

Keywords: Rotational Isomeric State, chain conformations, size distribution, vinyl polymers, squared end-to-end distance, taut conformations

4.1 Introduction

Polypropylene is a thermoplastic polymer that is used in a wide variety of applications including packaging, automotive components, laboratory equipment, loudspeakers, and textiles [1]. It has a high melting point which makes it a popular choice for manufacturing microwavable food containers. Polystyrene is another popular thermoplastic polymer and is manufactured worldwide for use in protective packaging, container lids, bottles, trays, and disposable cutlery. The versatility of polypropylene and polystyrene have encouraged researchers to study their properties for decades. One particular area of interest has been studying polymer properties at the microscopic level to understand their impact on the macroscopic scale. Analyzing polymer chain conformations lead to qualitative and quantitative understanding of physical and mechanical properties of polymers. Single chain conformations impact overall chain statistics and understanding their effect across overall distributions motivates this work.

Polypropylene and polystyrene are vinyl polymers and are polymerized from propylene and styrene respectively [2]. Their repeat unit structure can be writ-

ten as -$(CH_2CHR)_X$- where x is the number of repeat units and -R is -CH_3 for polypropylene and -C_6H_5 for polystyrene. The stereochemical relationship of consecutive -R groups along the polymer backbone determines the tacticity of the polymer. Isotactic and syndiotactic chains are stereoregular which tend to crystallize easily in bulk systems while stereoirregular atactic chains do not crystallize as easily, hence we have focused our studies on atactic chains in amorphous state.

Polymer chain conformations enable the computation of chain size properties such as characteristic ratio (C_n) [3, 4] and its temperature coefficient [3]. Characteristic ratio can be defined as the ratio of mean-squared end-to-end distance of a real chain under theta conditions to that of a freely jointed chain with the same number of bonds and bond length. Temperature coefficient shows variation in chain size with temperature and can be computed from characteristic ratio.

The most common and cost effective method for experimentally determining average polymer chain sizes is through intrinsic viscosity experiments. Various molecular weight fractions of a polymer are dissolved in theta solvents and analyzed to determine intrinsic viscocity, which ultimately lead to mean-squared end-to-end distances of unperturbed chains [3, 5]. Kinsinger and Hughes [6, 7], Inagaki et al. [8], Nakjima and Saijyo [9], and Heatley et al. [10] performed such experiments

on polypropylene under theta conditions. Using their data, Suter and Flory [11] computed characteristic ratios and temperature coefficients. Similarly, Krigbaum and Flory [12], Orofino and Mickey [13], and Altares et al. [14] carried out such experiments for polystyrene and reported intrinsic viscosities and mean-squared end-to-end distances. Flory [3] computed characteristic ratio from those data.

Orofino et al. [15] analyzed a sample of cross-linked bulk polystyrene over 393.15-448.15 K. At each temperature, the sample was stretched to a desired elongation and allowed to relax until the applied tension appeared constant. Mean-squared end-to-end distance and temperature coefficient were calculated from tension. Additionally, they performed intrinsic viscosity experiments on polystyrene in different theta solvents, at different temperatures and reported a similar temperature coefficient. Cotton et al. [16] performed neutron scattering experiments on amorphous polystyrene in a bulk system and determined mean-squared radius of gyration. Measurements were made for eight monodisperse polystyrene samples over a wide range of molecular weights. They compared the conformations in bulk to those in a theta solvent, and inferred that the chain dimensions in bulk were the same as those in a theta solvent. They also reported negative temperature coefficient for polystyrene.

Theoretical methods enable generating polymer chain conformations and studying their properties. The Rotational Isomeric State approach (RIS) proposed by Flory [3] has been a powerful theoretical tool for such investigations. The RIS method is efficient for sampling single-chain conformations, as each chain realization in RIS provides an independent sample. While the standard molecular dynamics and Monte Carlo methods provide sequences of related states, the small changes that occur in each step lead to correlations that must be relaxed to sample an equilibrium distribution. The RIS method offers an advantage of generating a much larger number of uncorrelated random chain conformations in a computationally cheap manner [17]. In the RIS approximation, torsions about backbone bonds are treated as existing in discrete rotational states, with each possible state chosen to coincide with a region of low potential energy. States differ in relative energy and thus in Boltzmann-weighted probability. Discrete states are defined only around bonds that allow torsion, such as single bonds [17].

Flory, Mark, and Abe [18], Abe [19], Boyd and Breitling [20], Suter and Flory [11], and Asakura et al. [21] used RIS approximation to generate unperturbed, random polypropylene chains, compute the chain size properties, and compare intramolecular energies among different rotational isomeric states per repeat unit of

polypropylene. The characteristic ratios and temperature coefficients computed using the RIS approach were in decent agreement with the experimental calculations [6, 7, 8, 9, 10]. Fujiwara et al. [22], Flory et al. [3], Yoon et al. [23], and Rapold et al. [24] used RIS method to compute polystyrene chain properties under unperturbed conditions. They all obtained characteristic ratios which are within approximation of experimental findings [12, 13, 14]. Yoon et al. [23] and Rapold et al. [24] reported negative temperature coefficients for polystyrene.

In our previous computational work on polybutadiene, we found that temperature dependence of average chain size can largely be attributed to large relative changes in low probability density for larger chains. We termed this the "*taut conformation effect*" [17]. This work studies the impact of such taut conformations on average sizes of polypropylene and polystyrene chains. Size properties of random chain conformations of polypropylene and polystyrene were studied by calculating the distribution of single chain conformations [17]. We assumed that multiple random conformations of a single chain in a theta solvent will have the same statistics as multiple chains generated in the bulk under the same conditions. Thus using a single chain in each computation is justified [5] and computationally cheaper. Chain size properties were computed based on ensemble averages of single

chain conformations at different chain lengths and over a range of temperatures.

4.2 Methodology

The simulations consist of generating random conformations of atactic, amorphous polypropylene and polystyrene single chains. Relative probabilities of local chain geometry guide the choice of torsion angles for each chain. Temperature ranges for polypropylene and polystyrene were selected to ensure the chains were in an amorphous state above the glass transition (T_g) [1], which is ∼258 K for atactic polypropylene [25] and ∼372 K for atactic polystyrene [26]. 100,000 chains were generated for a single chain length (degree of polymerization x = 50, 120) at temperatures T = 275, 300, 323, 343, 375, 400, and 413 K for polypropylene, and T = 375, 400, 413, 430, 450, 475, and 500 K for polystyrene. 100,000 single chains of polypropylene and polystyrene were generated at x = 15, 25, 50, 75, 100, 120, and 250 repeat units at 300 K for polypropylene and 400 K for polystyrene. At each temperature and chain length, ensemble averages of chain size parameters were computed using an equal weighting for each chain.

4.2.1 Chain Geometry and Internal Energy

Details of chain start location, simulation box dimensions and total energy of each system are discussed in our previous work [17]. Bond lengths and bond angle supplements used in our computations are shown in tables 3, 4, and 5. They were obtained from Suter and Flory [11] for polypropylene, and Yoon, Sundararajan and Flory [23] for polystyrene. These are shown in tables .

Table 3: Bond length geometries [11, 23]

Bond	Length (Å)
C–C	1.53
C–CH_3	1.51
C–C_6H_5	1.51
C–H	1.09

Table 4: Bond angle geometries for polypropylene [11]

Angle	Supplement
$\angle$ CH_2–$CHCH_3$–CH_2 (θ'')	68°
$\angle$ $CHCH_3$–CH_2–$CHCH_3$ (θ')	68°
$\angle$ CH_2–$CHCH_3$–H (θ''_H)	62.833°
$\angle$ $CHCH_3$–CH_2–H (θ'_H)	71°
$\angle$ CH_2–$CHCH_3$–CH_3 (θ'_R)	70°

Table 5: Bond angle geometries for polystyrene [23]

Angle	Supplement
$\angle$ CH_2–CHC_6H_5–CH_2 (θ'')	68°
$\angle$ CHC_6H_5–CH_2–CHC_6H_5 (θ')	66°
$\angle$ CH_2—CHC_6H_5–H (θ''_H)	73.194°
$\angle$ CHC_6H_5–CH_2–H (θ'_H)	71°
$\angle$ CH_2–CHC_6H_5–C_6H_5 (θ'_R)	68°

The torsional angle states around C-C single bonds were based on regions of low potential energy. Suter and Flory [11] used five discrete rotational isomeric states for each torsional bond of polypropylene while Yoon, Sundararajan and Flory [23] chose two for polystyrene. The isomeric states for polypropylene correspond to $\phi = -115°$, $15°$, $50°$, $70°$, $105°$ [11], and $\phi = 10°$ and $110°$ for polystyrene [23].

4.2.2 Chain Generation

Transformation matrices convert bond vectors from one reference system to another [3] and were used to determine atom positions within each single chain from internal coordinates. Two transformation matrices were used per repeat unit of polypropylene and polystyrene: one for the -CHR group and other for the -CH_2 group [11, 23].

Each polymer chain was built in an atom-by-atom manner. Torsion was considered only around the C-C chain backbone bonds, thus only two torsional angles per repeat unit (ϕ_i, ϕ_{i+1}) were used, as defined in figures 29 and 30. Torsion angle ϕ_i about bond i directly affects positions of the pendant hydrogen atoms H_i and $H_{i'}$, and backbone carbon atom C_{i+1}. Torsion angle ϕ_{i+1} about bond $i+1$ directly affects positions of the pendant hydrogen atom H_{i+1}, backbone carbon atom C_{i+2},

and the pendant R group ($i + 1^{\star}$) atoms.

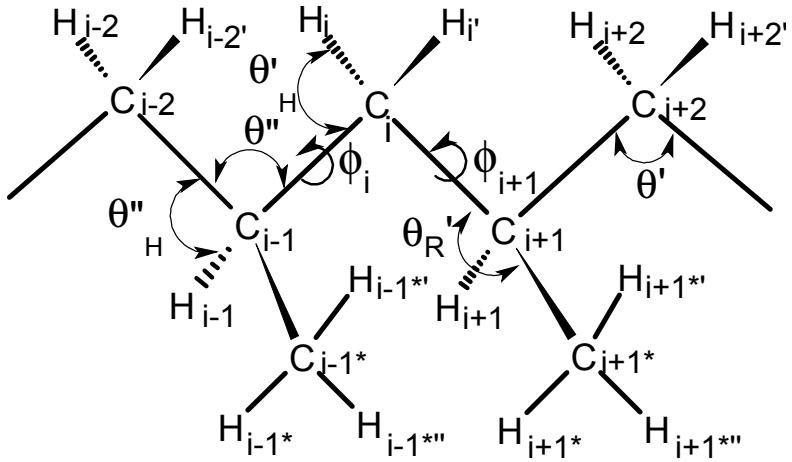

Figure 29: Polypropylene structure showing bonds, bond angles and torsion angles. Atoms from C_i to C_{i+1} and their pendant atoms comprise a single repeat unit. Numbering employs Flory's convention [3].

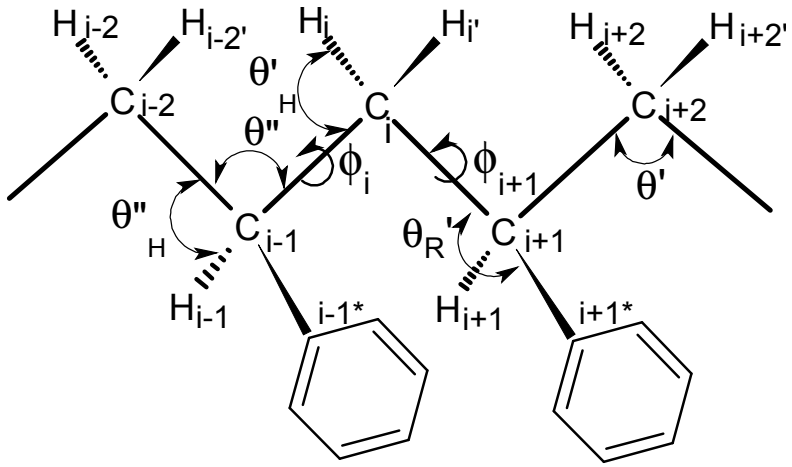

Figure 30: Polystyrene structure showing bonds, bond angles and torsion angles. Follows the same numbering convention as polypropylene.

The rotational isomeric states (i.e. torsion angles) for each repeat unit were selected randomly based on probabilities that account for relative energies of adding two consecutive torsion angles. These relative energies are statistical weights which

are stored in statistical weight matrices [3]. Such weights were suggested by Suter and Flory [11] for polypropylene and Yoon, Sundararajan and Flory [23] for polystyrene. Chains were generated based on Boltzmann-weighted probabilities that account for relative energies of adding two consecutive torsion angles. The probabilities were computed on the basis of a partition function [3] which incorporates each possible combination of rotational isomeric states of a chain. The pairwise probability of a single conformation equals its contribution to the partition function, divided by the partition function. Single chains in our simulations create realizations of the ensemble represented by this partition function. A linear congruential random number generator was used for the simulations and a different integer seed between 0 and $2^{31} - 1$ was used for each condition of chain length and temperature [17].

4.2.3 Chain Size Parameters

Squared end-to-end distance r^2 is an important chain size parameter and was calculated as

$$r^2 = (r_x^2 + r_y^2 + r_z^2) \tag{82}$$

where r_x, r_y, r_z are the x, y and z coordinates of the end-to-end distance vector $\mathbf{r}$. The vinyl polymer chains generated here are of the form CH_3-(CHR-CH_2)$_{x-1}$-CHR-CH_3 where the chain start and end carbon atoms define the end-to-end distance. Periodic boundary conditions [27] were taken into account to ensure the proper image of each atom position was employed.

The squared radius of gyration (r_g^2) relates to the distance of each atom in the polymer chain from the center of mass,

$$r_g^2 = \frac{1}{N}\sum_{j=1}^{N} |\mathbf{r}_j - \mathbf{r}_{\text{com}}|^2 \tag{83}$$

where $\mathbf{r}_j = (x_j, y_j, z_j)^T$ is the position vector of atom j of a polymer chain, $\mathbf{r}_{\text{com}} = (x_{\text{com}}, y_{\text{com}}, z_{\text{com}})^T$ is the position vector of the center of mass of a polymer chain, and N is the total number of atoms in the chain. Proper periodic image calculations were included here as well.

Theodorou and Suter [28] used the eigenvalues (λ_1, λ_2, λ_3) of a radius of gyration matrix (S)

$$S = \begin{pmatrix} \overline{x^2} & \overline{xy} & \overline{xz} \\ \overline{xy} & \overline{y^2} & \overline{yz} \\ \overline{xz} & \overline{yz} & \overline{z^2} \end{pmatrix} \tag{84}$$

to quantify contributions directed along the three principal directions (eigenvectors) of a chain conformation, where

$$\overline{xy} = \frac{1}{N}\sum_{j=1}^{N}\left(x_j - x_{\mathrm{com}}\right)\left(y_j - y_{\mathrm{com}}\right) \tag{85}$$

and other terms are defined analogously. The overbar indicates an average over all atoms in a single chain conformation. The radius of gyration matrix was diagonalized and its eigenvalues were sorted in descending order ($\lambda_1 \geq \lambda_2 \geq \lambda_3$). λ_1 corresponds to the principal direction with the longest dimension and λ_2, λ_3 correspond to secondary directions. This approach effectively represents the size of a polymer chain using a rotational ellipsoid with a different size in each direction, rather than with a hollow sphere of radius r_g that has the same mass and moment of inertia as the polymer chain [17]. The squared radius of gyration equals the sum of the three eigenvalues [28],

$$r_g^2 = \lambda_1 + \lambda_2 + \lambda_3 \tag{86}$$

The squared radii of gyration obtained from the eigenvalues (eq. 86) are equivalent to those from the number-weighted equation (eq. 83). Chain size parameters

were quantified to analyze chain behavior at different lengths and over a range of temperatures.

4.3 Results and Discussion

A balance between intra-chain and inter-chain interactions can be inferred from the relationship between end-to-end distance and chain length. The root-mean-squared end-to-end distance increases with the number of repeat units as $\langle r^2 \rangle^{1/2} = (\text{const})\text{x}^{\nu}$, where ν is the scaling exponent [4]. Figure 31 shows that a scaling exponent of 0.553 best describes the simulated polypropylene data while for polystyrene it is 0.569. In both cases, ν is in between that of a theta solvent ($\nu = 0.5$) and a good solvent ($\nu = 0.6$) [4]. This indicates that a balance exists between intra-chain and inter-chain interactions in the simulated vinyl polymers.

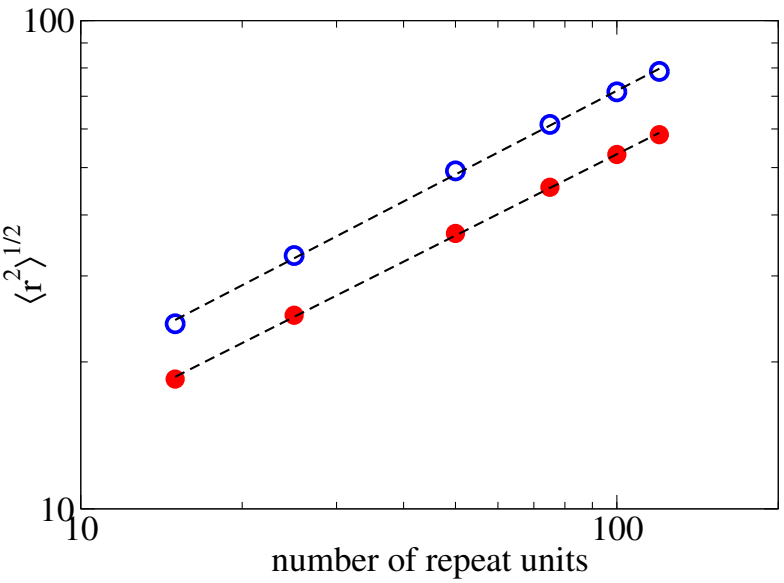

Figure 31: Scaling of root-mean-squared end-to-end distance with chain length for polystyrene (blue-unfilled) at 400 K and polypropylene (red-filled) at 300 K. These symbols are used throughout unless otherwise specified. Dashed lines indicate best fits using scaling exponents of 0.569 and 0.553 for polystyrene and polypropylene, respectively.

Characteristic ratio (C_n) [3, 4] can be written as

$$C_n = \frac{\langle r^2 \rangle}{nl^2} \tag{87}$$

where n is the number of backbone bonds along a polymer chain and l is the bond length of C-C. For vinyl polymer chains, there are two C-C bonds per repeat unit thus $n = 2x$. Figures 32 and 33 show characteristic ratio as a function of temperature.

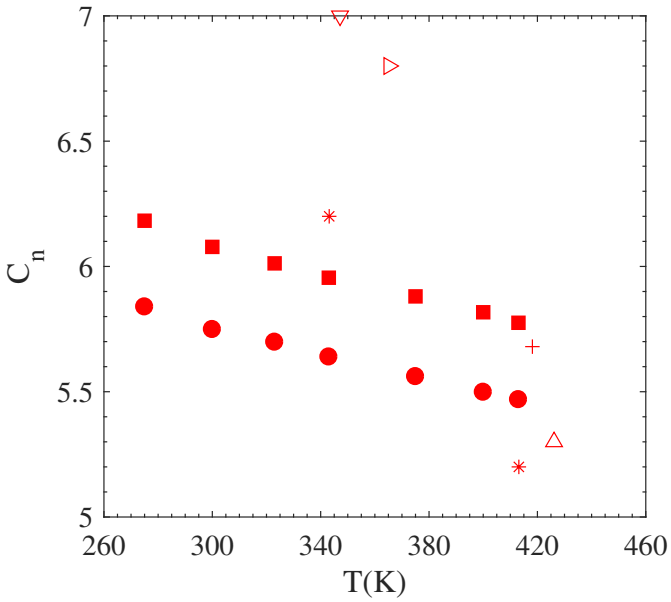

Figure 32: Characteristic ratio vs. temperature for polypropylene. Filled circles are for x = 50, filled squares are for x = 120. Prior model results (∗) [11] at 343.15 K (x = 100), (∗) [11] at 413.15 K (x = 100), (+) [20] at 418.15 K (x = 18). Experimental results (▽) [7] at 347.15 K ($K = 18.2 \times 10^{-4}$), (▷) 365.15 K ($K = 17.2 \times 10^{-4}$), and (△) 426.15 K ($K = 12.0 \times 10^{-4}$). K is a Mark-Houwink parameter with units (deciliter g^{-1}) (g mol wt)$^{-0.5}$ [3].

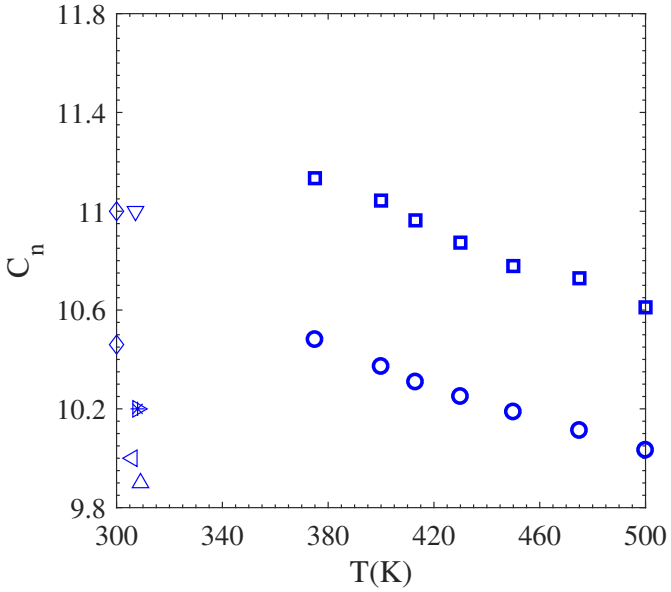

Figure 33: Characteristic ratio vs. temperature for polystyrene. Circles are for x = 50 and squares are for x = 120. Prior model results ($\diamond$) [23, 24] at 300 K (x >200). Experimental results (left-pointing triangle) [13] at 305.95 K ($K = 7.8 \times 10^{-4}$), ($\triangledown$) [29] at 307.15 K ($K = 8.2 \times 10^{-4}$), ($\triangleright$) [12] at 307.95 K ($K = 8.2 \times 10^{-4}$), ($*$) [14] at 307.95 K ($K = 8.4 \times 10^{-4}$), and ($\triangle$) [13] at 309.05 K ($K = 7.7 \times 10^{-4}$).

Characteristic ratios of both polypropylene and polystyrene chains decrease with increasing temperature which indicates chain shrinking on heating. Higher C_n are observed for 120 repeat units than 50 repeat units at the same temperature. Experimental data for polypropylene from intrinsic viscosity experiments in theta solvents correspond to temperatures of 307.15 K, 347.15 K, 365.15 K, and 426.15 K. Our simulation results are in decent agreement with prior model results but some disagreement is observed between our results and experimental intrinsic viscosity results. This could be the result of our chains not being in unperturbed or theta conditions as opposed to the experiments. Experimental [12, 13, 14] and theoretical

[23, 24, 29] characteristic ratios were obtained for polystyrene at temperatures (∼300 K) below its glass transition temperature. The decreasing behavior seen in figs. 32 and 33 are indicative of negative temperature coefficients for both polypropylene and polystyrene.

Temperature coefficient ($d\ln\langle r^2\rangle/dT$) gives a qualitative and quantitative measure of chain size dependence on temperature. Our results may be compared to theoretical and experimental data by assuming n and l to be independent of temperature [17]

$$\frac{d\ln\langle r^2\rangle}{dT} = \frac{1}{C_n}\frac{dC_n}{dT}. \tag{88}$$

Temperature coefficients from prior experimental and theoretical work, and present work are included in table 6. For polystyrene we found $d\ln\langle r^2\rangle/dT$ to be -0.34×10^{-3} for x = 50 and -0.39×10^{-3} for x = 120. For polypropylene, our $d\ln\langle r^2\rangle/dT$ was -0.47×10^{-3} for x = 50 and 120. Our results are in decent agreement with theoretical estimates. Orofino et al. [15] found a positive temperature coefficient for polystyrene and mentioned that their "result contrasts with some previous estimates found in literature... possible sources of disparity with earlier work". Flory et al. [18] acknowledged that discrepancies may arise between experimental and theoretical temperature coefficients due to the sheer difficulty in

obtaining theta conditions. Mark [30] mentioned about experimental difficulties with stability of swollen networks which impacts temperature coefficient calculations. It is possible that analogous difficulties could impact shrunken networks as well.

Table 6: Temperature coefficients

Polymer	Reference	Temperature coefficient (K^{-1})	T(K)
Polypropylene	Experimental [7]	-0.1×10^{-3}	307.15-426.15
Polypropylene	Theoretical [20]	-0.75×10^{-3}	
Polypropylene	Theoretical [11]	-0.6×10^{-3}	300-500
Polypropylene	Present work	-0.47×10^{-3}	275-413
Polystyrene	Experimental [15]	$+0.4 \times 10^{-3}$	279.75-331.75
Polystyrene	Experimental [31]	-0.1×10^{-3}	
Polystyrene	Experimental [16]	-0.1×10^{-3}	
Polystyrene	Theoretical [23]	-0.7×10^{-3}	
Polystyrene	Theoretical [24]	-1.6×10^{-3}	300-500
Polystyrene	Present work	-0.34×10^{-3}	375-500
Polystyrene	Present work	-0.39×10^{-3}	375-500

The temperature dependences of the probability density distributions of chain sizes for polypropylene and polystyrene can be seen in figures 34 and 35. The probability densities of 120 repeat units have wider distributions than 50 repeat units for both polypropylene and polystyrene chains. This results in larger mean-squared end-to-end distances and thus larger characteristic ratios for 120 repeat units, which is consistent with the findings shown in figs. 32 and 33.

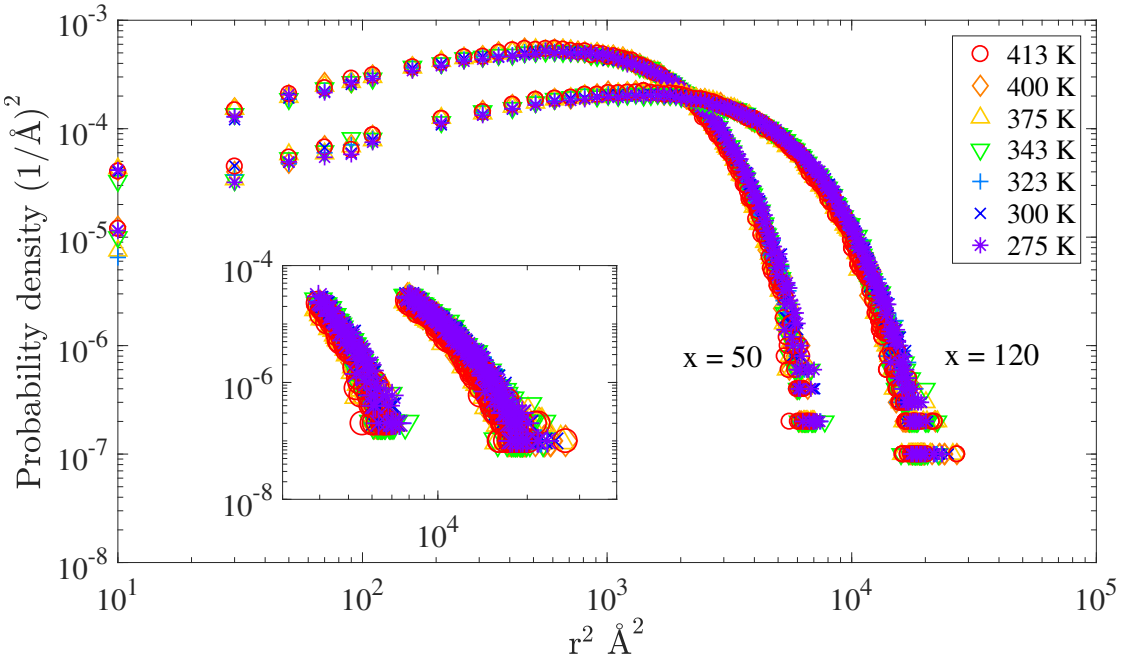

Figure 34: Probability density distributions of squared end-to-end distances for polypropylene chains of 50 and 120 repeat units at different temperatures. Inset shows expanded sections of long chains emphasizing taut conformation effect.

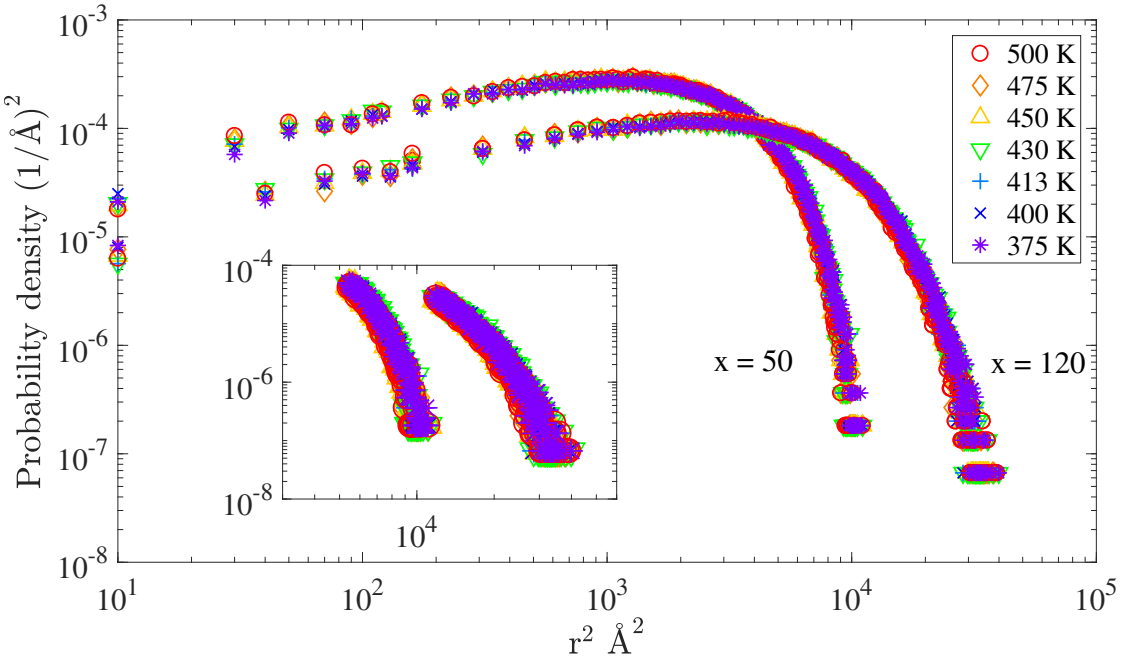

Figure 35: Probability density distributions of squared end-to-end distances for polystyrene chains of 50 and 120 repeat units at different temperatures. Inset shows expanded sections of long chains emphasizing taut conformation effect.

The highest probability density is observed for medium size chains, while shorter and longer size chains are less probable. The medium size chains are twice as likely to occur as shorter chains and 100 times more likely than longer chains. Probability density of the medium size chains appear to be unaffected by changes in temperature, indicated by the complete overlap of the distribution across all temperatures. Small absolute changes in chain size probability densities occur with temperature. For shorter chains, the probability densities slightly increase with increasing temperature. It appears that both medium and shorter chains are the most probable overall and would in turn have the most influence on the characteristic ratio. However, figs. 32 and 33 indicate that characteristic ratio decreases with increasing temperature. It can be seen that the probability density of the longer size chains decrease with increasing temperature. Despite their much lower probability density, the longer chains show a dominant influence on the dependence of characteristic ratio on temperature. A larger relative decrease in probability density for the longer chains is observed as compared to the smaller relative increase of the probability density of the shorter chains.

To further investigate the influence of longer chains on the characteristic ratio, each distribution from figures 34 and 35 were divided into chain subsets, details of

which are given in table 7.

Table 7: Chain subsets for polypropylene and polystyrene

Polymer	x	short (Å^2)	medium (Å^2)	long (Å^2)
Polypropylene	50	<600	600-2400	>2400
Polypropylene	120	<1500	1500-6000	>6000
Polystyrene	50	<1000	1000-4000	>4000
Polystyrene	120	<2500	2500-10000	>10000

The fractions of each subset in the overall distribution are shown in figures 36 and 37. Maximum fraction of chains in the subsets are of medium size while longer size chains are minimum. Chain fraction for medium size chains remains steady with temperature while shorter chains increase and longer chains decrease with increasing temperature. The relative presence of each subset was similar for both repeat units based on the ranges considered.

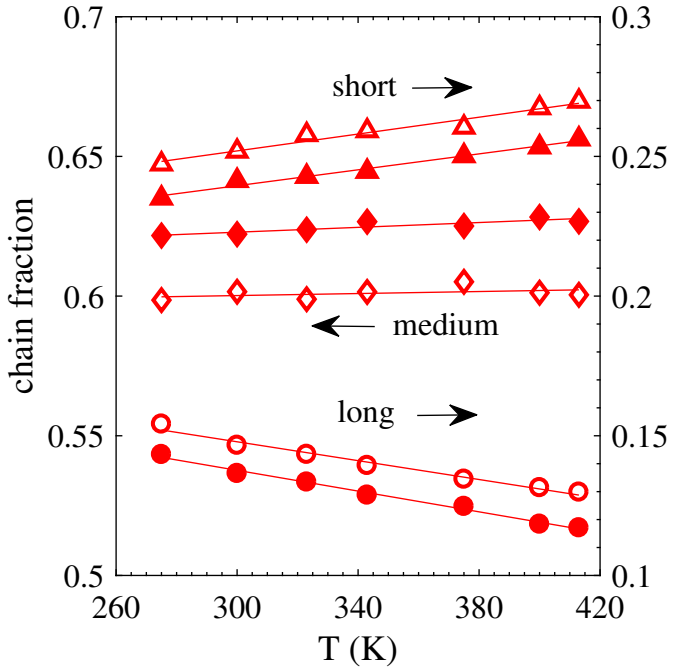

Figure 36: Chain fraction of subset of polypropylene chains at different temperatures. Filled symbols are for x = 50 and unfilled ones are for x = 120.

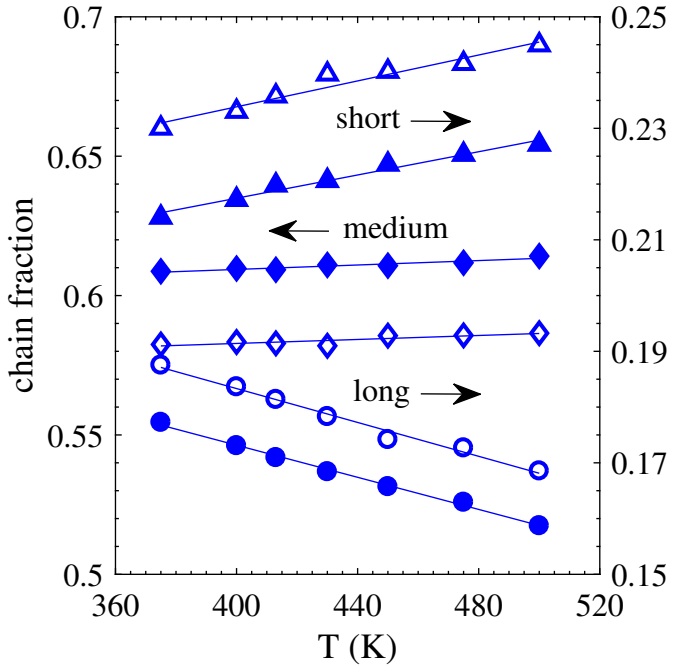

Figure 37: Chain fraction of subset of polystyrene chains at different temperatures. Symbols follow the same convention as figure 36.

Characteristic ratios were calculated for each of the chain subsets at the different temperatures and weighted by the fraction of those chains present in the distributions,

$$C_n = \frac{1}{nl^2}\frac{1}{N}\left(\sum_{short} r_i^2 + \sum_{med} r_i^2 + \sum_{long} r_i^2\right) \tag{89}$$

where N is the total number of chains in an ensemble. These weighted characteristic ratios for each subset are shown in figures 38 and 39, and the overall characteristic ratios (as shown in figs. 32 and 33) can be obtained by summing over each temperature per chain length. Figures 38 and 39 indicate that longer chains are the only fraction of the chain population that contributes to a decrease in characteristic ratio with temperature. This distinction shows that these very few, extended chains are responsible for the reduction in characteristic ratio, rather than the reduction occurring uniformly over all size ranges. This corroborates the hypothesis that the less probable longer, taut conformations are having a significant impact on the average chain size with temperature, as was observed for cis-1,4 and trans-1,4 polybutadiene chains [17].

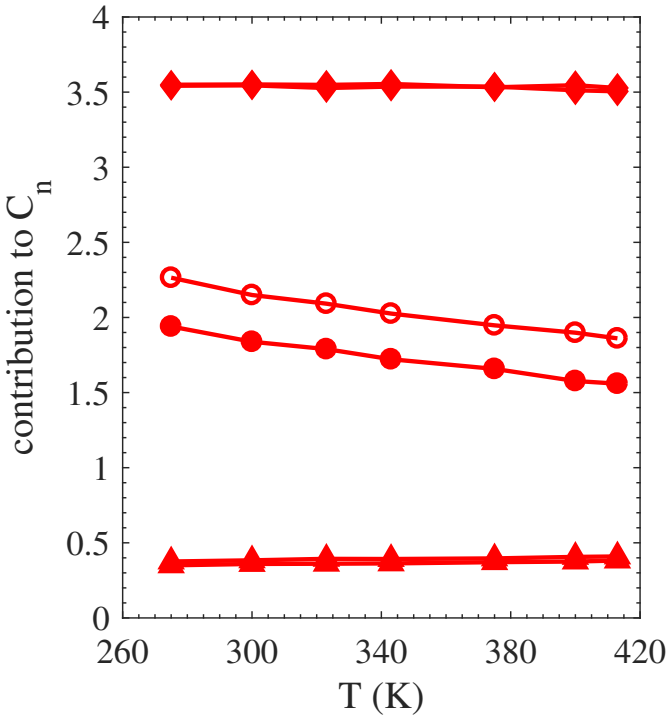

Figure 38: Weighted characteristic ratio of subset of polypropylene chains at different temperatures. Symbols follow the same convention as figure 36.

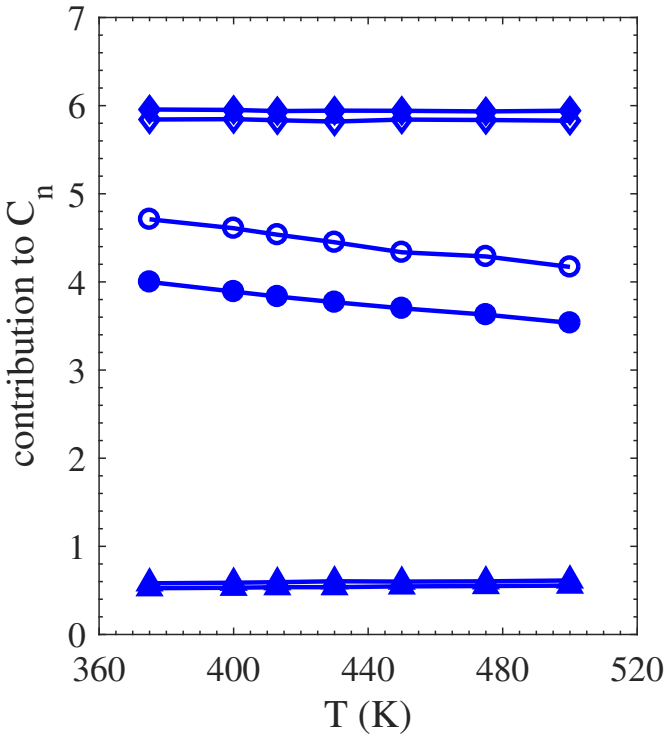

Figure 39: Weighted characteristic ratio of subset of polystyrene chains at different temperatures. Symbols follow the same convention as figure 36.

Dependence of characteristic ratio on chain length at a single temperature showed an increase with chain length for both polypropylene and polystyrene, as seen in figure 40. Polystyrene chains have a much higher C_n than polypropylene chains with the same number of repeat units. This shows that polystyrene chains have much greater mean-squared end-to-end distances than polypropylene chains of the same chain length. Polystyrene chains also have a steeper slope than polypropylene chains showing larger changes in C_n with chain length. The RIS model was used by Suter and Flory [11] (x = 100) at 343.15 K and 413.15 K, and

Boyd and Breitling [20] (x = 18) at 418.15 K for polypropylene. Yoon et al. [23] and Rapold et al. [24] used RIS models at 300 K for polystyrene and considered chains of 200 repeat units or more. Our simulation results are in decent agreement with prior RIS results.

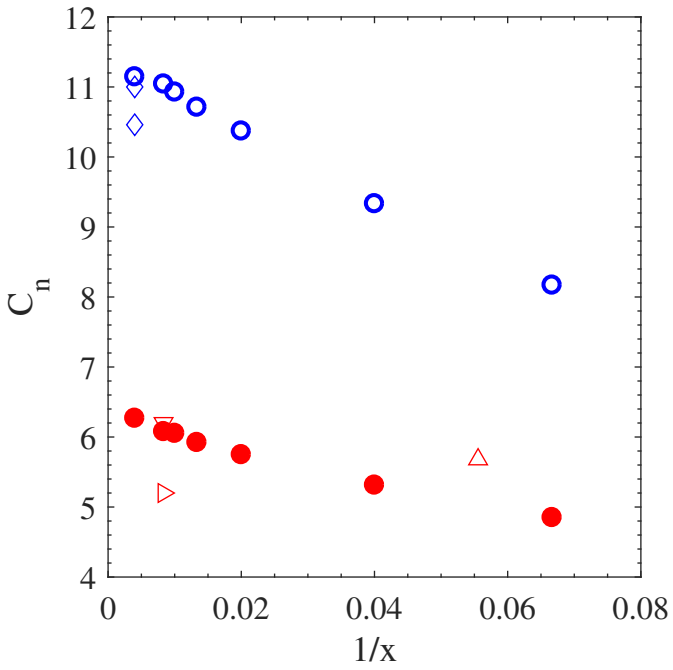

Figure 40: Characteristic ratio vs. inverse of repeat unit x for polystyrene and polypropylene chains at 400 K and 300 K respectively. Prior model results for polypropylene (▽) [11] at 343.15 K, (▷) [11] at 413.15 K, (△) [20] at 418.15 K, and polystyrene (◇) [23, 24] at 300 K.

The mean-squared radius of gyration $\langle r_g^2 \rangle_0$ should equal 1/6 of the mean-squared end-to-end distance $\langle r^2 \rangle_0$ under unperturbed conditions and in the limit of long chains without long branches [32]. Figure 41 shows a ratio further above 6 for polystyrene than for polypropylene for the same chain length. It was also

observed that $\langle r^2 \rangle / \langle r_g^2 \rangle$ decreased with increasing chain length but did not reach 6 indicating that the chains of 250 repeat units were not yet at the long chain limit.

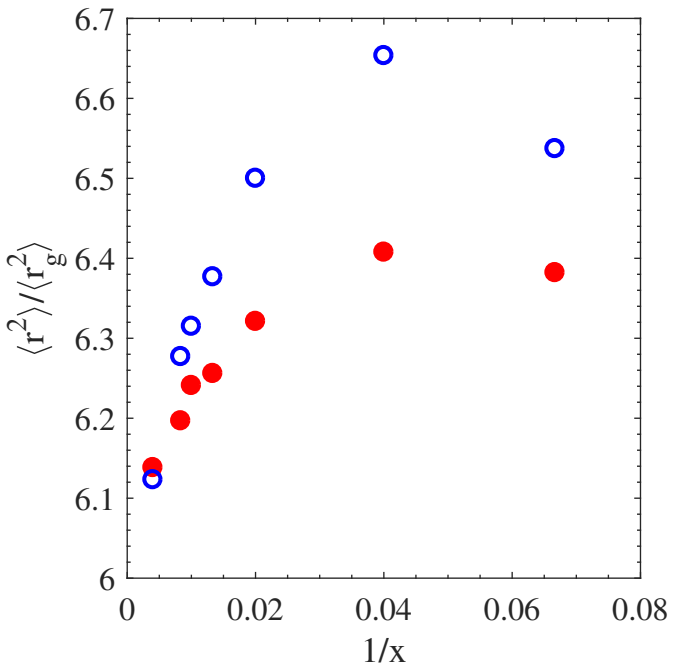

Figure 41: Ratio of squared end-to-end distance to squared radius of gyration ($\langle r^2 \rangle / \langle r_g^2 \rangle$) vs. inverse of repeat unit x for polystyrene and polypropylene chains at 400 K and 300 K respectively.

4.4 Conclusions

Rotational Isomeric State approach was used to generate random conformations of single chains of amorphous, atactic polypropylene and polystyrene at different chain lengths and over a range of temperatures. Ensemble averages and probability density distributions of these chains were quantified to study size properties. Scaling exponents of polypropylene and polystyrene chains are indicative of intra-chain and inter-chain interactions occurring in the systems.

Characteristic ratios decreased with increasing temperature for both polypropylene and polystyrene chains indicating chain shrinking with heating. Temperature coefficients obtained for both polymers were consistent with prior experimental and theoretical work. Probability density distributions of squared end-to-end distances at different temperatures indicated that although medium size chains were the most probable, their distributions hardly changed with temperature. The slightly less probable short size chains showed an increase in probability density with increasing temperature. Neither of these size ranges indicated a decrease in chain size with increasing temperature. The much less probable long chains showed a decrease in distribution with increasing temperature, however the relative decrease in probability density of longer chains with temperature was greater than the relative increase in probability density of shorter chains. Chain subsets showed that the characteristic ratio of the most probable medium size chains remained unaffected with increasing temperature while short chains showed a marginal increase. The least probable, largest size chains or taut conformations were the only chain subset to show a decrease in characteristic ratio with increasing temperature, hence accounting for the overall decrease in average chain size. Thus, these taut conformations have a significant impact on the average chain size and

contribute to chain shrinking with heating. Characteristic ratios for both vinyl polymer chains increased with increasing chain length, with polystyrene chains showing greater C_n than polypropylene chains of the same length. Our results are in decent agreement with prior model characteristic ratios.

List of References

[1] N. G. McCrum, C. P. Buckley, and C. B. Bucknall, *Principles of Polymer Engineering, 2nd Edition*. Oxford Univ Press, 1997.

[2] P. C. Hiemenz and T. P. Lodge, *Polymer Chemistry, 2nd Edition*. CRC Press, Taylor & Francis Group, 2007.

[3] P. J. Flory, *Statistical Mechanics of Chain Molecules*. Wiley Interscience, 1969.

[4] M. Rubinstein and R. H. Colby, *Polymer physics*. Oxford University Press New York, 2003.

[5] P. J. Flory, *Principles of Polymer Chemistry*. Cornell University Press, 1953.

[6] J. Kinsinger and R. Hughes, "Intrinsic viscosity-molecular weight relationships for isotactic and atactic polypropylene," *J Phys Chem*, vol. 63, no. 12, pp. 2002–2007, 1959.

[7] J. B. Kinsinger and R. Hughes, "The unperturbed dimensions of atactic and isotactic polypropylene," *J Phys Chem*, vol. 67, no. 9, pp. 1922–1923, 1963.

[8] H. Inagaki, T. Miyamoto, and S. Ohta, "The unperturbed dimensions of polypropylene and polyethylene," *J Phys Chem*, vol. 70, no. 11, pp. 3420–3431, 1966.

[9] A. Nakajima and A. Saijyo, "Unperturbed chain dimensions of isotactic polypropylene in theta solvents," *J Polym Sci Part B: Polym Phys*, vol. 6, no. 4, pp. 735–744, 1968.

[10] F. Heatley, R. Salovey, and F. Bovey, "Polymer Nuclear Magnetic Resonance Spectroscopy. XVIII. The Nuclear Magnetic Resonance Spectrum, Dimensions, and Steric Interactions of Isotactic Polypropylene," *Macromolecules*, vol. 2, no. 6, pp. 619–623, 1969.

[11] U. W. Suter and P. J. Flory, "Conformational energy and configurational statistics of polypropylene," *Macromolecules*, vol. 8, no. 6, pp. 765–76, 1975.

[12] W. Krigbaum and P. Flory, "Molecular weight dependence of the intrinsic viscosity of polymer solutions. II," *J Polym Sci Part A: Polym Chem*, vol. 11, no. 1, pp. 37–51, 1953.

[13] T. Orofino and J. Mickey Jr, "Dilute solution properties of linear polystyrene in θ-solvent media," *J Chem Phys*, vol. 38, no. 10, pp. 2512–2520, 1963.

[14] T. Altares, D. Wyman, and V. Allen, "Synthesis of low molecular weight polystyrene by anionic techniques and intrinsic viscosity–molecular weight relations over a broad range in molecular weight," *J Polym Sci Part A: Polym Chem*, vol. 2, no. 10, pp. 4533–4544, 1964.

[15] T. Orofino and A. Ciferri, "Temperature dependence of the unperturbed dimensions of polystyrene," *J Phys Chem*, vol. 68, no. 11, pp. 3136–3141, 1964.

[16] J. Cotton, D. Decker, H. Benoit, B. Farnoux, J. Higgins, G. Jannink, R. Ober, C. Picot, and J. Des Cloizeaux, "Conformation of polymer chain in the bulk," *Macromolecules*, vol. 7, no. 6, pp. 863–872, 1974.

[17] S. Kar and M. L. Greenfield, "Sizes and shapes of simulated amorphous cis- and trans-1,4-polybutadiene," *Polymer*, vol. 62, pp. 129–138, 2015.

[18] P. Flory, J. Mark, and A. Abe, "Random-coil configurations of vinyl polymer chains. the influence of stereoregularity on the average dimensions," *J Am Chem Soc*, vol. 88, no. 4, pp. 639–650, 1966.

[19] A. Abe, "Unperturbed dimensions of vinyl polymer chains," *Polym J*, vol. 1, no. 2, pp. 232–244, 1970.

[20] R. H. Boyd and S. M. Breitling, "Conformational properties of polypropylene," *Macromolecules*, vol. 5, no. 3, pp. 279–286, 1972.

[21] T. Asakura, I. Ando, and A. Nishioka, "Calculation of the characteristic ratio of polypropylene containing chemical inversions (head-to-head and tail-to-tail units)," *Macrom Chem Phys*, vol. 177, no. 5, pp. 1493–1500, 1976.

[22] Y. Fujiwara and P. Flory, "Second and fourth moments of vinyl polymer chains," *Macromolecules*, vol. 3, no. 3, pp. 280–288, 1970.

[23] D. Y. Yoon, P. R. Sundararajan, and P. J. Flory, "Conformational characteristics of polystyrene," *Macromolecules*, vol. 8, no. 6, pp. 776–83, 1975.

[24] R. F. Rapold and U. W. Suter, "Conformational characteristics of polystyrene," *Macrom Theory Simul*, vol. 3, no. 1, pp. 1–17, 1994.

[25] A. Gitsas and G. Floudas, "Pressure dependence of the glass transition in atactic and isotactic polypropylene," *Macromolecules*, vol. 41, no. 23, pp. 9423–9429, 2008.

[26] R. J. Andrews and E. A. Grulke, "Glass transition temperatures of polymers," *Wiley Database of Polymer Properties*, 2003.

[27] M. P. Allen and D. J. Tildesley, *Computer Simulation of Liquids.* Oxford Univ. Press, 1987.

[28] D. N. Theodorou and U. W. Suter, "Shape of unperturbed linear polymers: polypropylene," *Macromolecules*, vol. 18, no. 6, pp. 1206–14, 1985.

[29] J. Brandrup, E. H. Immergut, and Editors, *Polymer Handbook, Fourth Edition.* Wiley, 1998.

[30] J. E. Mark, "Interpretation of random-coil configurations of trans-1,4-polybutadiene and trans-1,4-polyisoprene," *J Am Chem Soc*, vol. 89, no. 26, pp. 6829–35, 1967.

[31] N. Kuwahara, S. Saeki, S. Konno, and M. Kaneko, "Temperature dependence of polymer chain dimensions in the polystyrene-cyclopentane system," *Polymer*, vol. 15, no. 2, pp. 66–68, 1974.

[32] P. Debye, "The intrinsic viscosity of polymer solutions," *J Chem Phys*, vol. 14, no. 10, pp. 636–639, 1946.

CHAPTER 5

"Fitting Viscoelastic Models to Bitumen Shear Rheometry Data to Predict Rheological Properties"

by

Suvrajyoti Kar[a], Julie L Cuddigan[a], Toby Bohannon[b], Michael L Greenfield[a,*]

[a]Department of Chemical Engineering, University of Rhode Island, Kingston, RI - 02881, USA

[b]Rhode Island Department of Transportation, Providence, RI - 02903, USA

is prepared for submission to Construction and Building Materials

*Corresponding author email: greenfield@uri.edu

Abstract

Viscoelastic models were fit to experimental rheological data to compute asphalt binder properties over a wide range of frequencies, temperatures and sample preparations. Binders were obtained from different sources and aged using rolling thin-film oven (RTFO) and pressure aging vessel (PAV) procedures. Rheological and bending beam rheometer experiments were carried out at the Rhode Island Department of Transportation. Time-temperature superposition and Williams-Landel-Ferry (WLF) equation were applied to experimental rheological data to produce master curves using horizontal and vertical shift factors. Binder stiffness increased with aging, discrete and continuous models of complex modulus and phase angle were in excellent agreement with experimental results. The contributions from aging processes at shorter relaxation times were similar, while greater contributions were observed for PAV-aging at longer relaxation times. Results predicted from our rheological model for PAV-aged binder resistance to low temperature thermal cracking were in decent agreement with bending beam rheometer experimental data.

Keywords: asphalt, aging, time-temperature superposition, modeling, moduli, compliance, relaxation time

5.1 Introduction

The single largest use of asphalt is in construction of roads and highways encompassing approximately 85% of total asphalt production [1]. Roads are paved with hot mix asphalt (HMA), which is a combination of stone, sand, or gravel held together by asphalt binder [1]. In its simplest form, asphalt binders are residues produced from crude-oil blends which are then processed with additives, usually polymers, to enhance their properties as thermoplastic adhesives for paving [2]. The lifetime of roads is closely related to the rheological properties of binders in response to deformation and temperature over time. These binders are characterized for roadway applications according to the Superpave performance-grading (PG) system from the Strategic Highway Research Program (SHRP) based on their environmental conditions of use [1]. This grading takes into account the magnitude and temperature dependence of binder viscoelastic properties [3, 4]. Over time binders age, harden, and embrittle, contributing significantly to the deterioration of paved surfaces [5]. This loss of durability has been linked to short-term aging from high temperature processing conditions as well as long-term aging during service life [6, 7, 8].

Rolling thin-film oven (RTFO) simulates short-term aging of binders. It is

used to represent changes in binder during HMA production and placement due to oxidation [6, 7, 9, 10]. Long-term aging is represented through use of a pressure aging vessel (PAV) to simulate in-service aging from combined effects of time, traffic and environment [6, 7, 9, 10].

Stress-strain studies on aged binders can yield information pertaining to stiffness, resistance to fatigue and thermal cracking over different periods of time and temperature [11]. It is crucial both from a financial and practical perspective to predict asphalt durability and viscoelastic properties before investing in a material of construction meant to last a significant amount of time. Molecular modeling is a useful tool that is used to cheaply and efficiently compute and predict viscoelastic properties of asphalt binders, sometimes at time and temperature scales which are difficult and expensive to obtain experimentally.

The objective of this work was to define a self-consistent physics-based asphalt-specific model to characterize and predict mechanical behavior of binders such as those used in Rhode Island. Viscoelastic properties were obtained experimentally using a rheometer and the data was fit using time-temperature superposition [12], a technique dating back to the 1940's and 50's when Leaderman [13], Andrews [14], and Tobolsky [15] used it to predict polymer properties. Time-temperature

superposition allowed predicting viscoelastic properties of binders over a broader range of time scales than experimentally measured. Modeling asphalt behavior over wide ranges of temperature, stress, and strain conditions through a well-defined physical basis allows for the prediction of macroscopic properties from microscopic behavior [16, 17] with the potential of enhancing pavement designs.

Deformation measured through stress-strain behavior leads to quantifiable moduli [12, 11]. As strain is repeatedly applied to a binder sample, the complex shear modulus ($G*$) can be considered to be the sample's total resistance to the deformation, while phase angle δ is the lag between the applied strain and measured stress [12]. Since complex modulus ($G*$) and tan δ can be related to storage (G') and loss moduli (G'') through $|G^*| = G'^2 + G''^2$ and tan $\delta = G''/G'$, modeling complex modulus is equivalent to modeling storage and loss moduli [12]. Well-established Maxwell models [11, 12] accurately predict storage and loss moduli over a continuous distribution of frequencies and relaxation times, and were used in this work. The frequency dependence in complex modulus arises from the relation between experimental time scales and binder relaxation times [12].

Relaxation time distributions can relate rheological parameters to chemical change effects on the molecular level [16]. The approach of our model is such

that all viscoelastic properties can be determined in the linear viscoelastic region through a well-defined distribution of relaxation times [12, 16]. Zhang and Greenfield [18, 19] used this approach and identified typical molecular relaxation times in binders. Jongepier and Kuilman [20, 21] proposed a log normal distribution of relaxation times. Instead of following such a Gaussian distribution, our relaxation times were restricted within finite limits [16]. Dickinson and Witt [22] computed storage and loss moduli at different frequencies and developed a relaxation spectra. They proposed a hyperbolic relationship between complex modulus and frequency, and concluded that their spectra was not consistent with Jongepier and Kuilman's [21] assumption of log normal distribution of relaxation times.

As roads are subjected to cyclical stresses from traffic, the strain in the arrangement of binder molecules fluctuates and ultimately reaches a residual limit with time [12]. As temperatures drop, pavements contract and build up additional internal stresses which without sufficient time to relax can lead to cracking. Bending beam rheometer (BBR) measures the low temperature thermal resistance or flexibility of PAV-aged binders. In the BBR experiment, a constant load is applied to the the center of a PAV-aged binder beam for a fixed period of time, and the beam deflection and stiffness are measured as a function of time (AASHTO

T 313). In this work, creep compliance computations from viscoelastic models fit to rheological data, along with stress-strain relations, allowed for prediction of low temperature thermal cracking resistance of PAV-aged binders. Additionally, molecular motion and stiffness of binders were qualitatively and quantitatively computed and compared using moduli master curves, relaxation and retardation time distributions, and stress relaxation modulus.

5.2 Methods

5.2.1 Experimental

The Rhode Island Department of Transportation (RIDOT) acquire asphalt binder samples in unaged form from multiple sources. In this work, we have analyzed binders from three sources: Cardi, Bitumar, and Allstate. Bitumar and Allstate are suppliers of asphalt while Cardi is a construction company that uses the asphalt to pave roads. The Bitumar and Allstate binders were known to be modified with styrene-butadiene-styrene (SBS) co-polymer while the Cardi binder did not have polymer modification. Unaged asphalt binders are used to determine mixing and compacting temperatures based on viscosity (AASHTO T 316) and used in hot mix asphalt (HMA). Strain sweep and frequency sweep tests were performed on asphalt binders under three conditions: unaged or original, aged

using rolling thin-film oven (RTFO) (AASHTO T 240), and aged using pressure aging vessel (PAV) (AASHTO R 28). Asphalt binder samples and their sources are listed in table 8.

Table 8: Asphalt binder sample details

Binder ID	PG	Source
PAV-1	PG 64S-28	Cardi
Original-2	PG 64E-28	Bitumar
RTFO-2	PG 64E-28	Bitumar
PAV-2	PG 64E-28	Bitumar
Original-3	PG 64E-28	Allstate

Strain sweep and frequency sweep tests were performed using a Discovery HR-1 dynamic shear rheometer (DSR) from TA Instuments. Strain sweeps were carried out at a single temperature over 0.1 - 12% at angular frequencies (ω) of 0.1, 1, 10, and 100 rad/s. At the conclusion of 100 rad/s, further strain sweeps were done at 1 and 10 rad/s to detect for signs of sample damage. Strain sweeps were done from 10°C to PG+6°C, at intervals of 12°C, in order to determine the range of linear viscoelasticity [12] of the binder samples at different temperatures. A strain % was chosen from the linear viscoelastic range to perform frequency sweeps from 0.1 - 100 rad/s at different temperatures at intervals of 6°C. 8 mm parallel plates with a 2 mm gap were used from 10°C to 34°C, while 25 mm parallel plates with

a 1 mm gap were used from 34°C to PG+6°C. For Bitumar samples, additional frequency sweeps were carried out at 28°C, 31°C, 37°C, and 43°C using 25 mm plates along with multiple tests at certain temperatures for data reproducibility.

For both strain and frequency sweep tests, the samples were allowed to equilibrate for 10 minutes prior to testing. If the test temperature was lower than 46°C, the samples were loaded in the rheometer at 46°C, trimmed, cooled to the test temperature, and equilibrated prior to testing. For test temperatures of 46°C and higher, the samples were loaded at the test temperature, trimmed, equilibrated, and tested. Additionally, compliance testing was done on the PAV-aged samples. Flexural creep strain of PAV-aged binders was determined using a Cannon Model TE-Bending Beam Rheometer (BBR) (AASHTO T 313).

5.2.2 Modeling

Time-Temperature Superposition

Time-temperature superposition interrelates modulus, density, and temperature at times t and $a_T = t/t_r$ or frequencies ω and $T = \omega/\omega_r$ by assuming a common functional form [12, 16, 23]

$$G/\rho T = G_r/\rho_r T_r = f(t/a_T) \tag{90}$$

where a_T is the horizontal or frequency shift factor, T_r is the reference temperature, and t_r is the reference time. This technique extends beyond measurement time scales in order to predict binder mechanical properties and molecular motions at experimentally unfeasible conditions.

The same physical processes were assumed to apply across the temperature range between T and T_r [12]. Density and temperature prefactors were accounted for in the time-temperature superposition by means of the vertical shift factor b_T ($b_T = \rho T/\rho_r T_r$) [12]. The same density was assumed across all binders and varied with temperature, leading to the same thermal expansion coefficient and b_T across all binders. Combinations of a_T and b_T were used to shift experimentally obtained moduli, compliance and tan δ data at all temperatures to obtain master curves.

The a_T were chosen based on the moduli master curves and a linear form of the Williams-Landel-Ferry (WLF) equation [24]

$$\frac{1}{\log a_T} = -\frac{C_2}{C_1}\frac{1}{(T - T_r)} - \frac{1}{C_1} \tag{91}$$

The reference temperature was chosen to be 34°C, considering strain and frequency sweeps were done at this temperature using both 8 mm and 25 mm plates, and assigned a_T and b_T of 1. The same shift factors per sample were applied to generate

the tan δ and compliance master curves because their time-temperature frequency shifts originate from the same mechanism [16, 23].

Models for Determining Viscoelastic Properties

Maxwell models are used to represent viscoelastic properties of polymers. These models are based on the spring and dashpot concept where spring represents the elastic segment and dashpot represents the viscous segment of the viscoelastic material. The Maxwell model assumes the spring and dashpot to be in series and is used for computing moduli (G) and stress relaxation. The Voigt model assumes the spring and dashpot to be in parallel and is used for computing creep compliance (J) [11].

Discrete viscoelastic models are well-defined physical models that approximate modulus by using n terms [12]

$$G'(\omega) = \sum_i \frac{G_i \omega^2 \tau_i^2}{1 + \omega^2 \tau_i^2} \tag{92}$$

$$G''(\omega) = \sum_i \frac{G_i \omega \tau_i}{1 + \omega^2 \tau_i^2} \tag{93}$$

$$J'(\omega) = \sum_i \frac{J_i}{1 + \omega^2 \tau_i^2} \tag{94}$$

$$J''(\omega) = \sum_i \frac{J_i \omega \tau_i}{1 + \omega^2 \tau_i^2} \tag{95}$$

The above equations contain binder dependent prefactors (G_i, J_i, τ_i) manually chosen to give good fits for the master curves. Details of these prefactors are included in tables 9 and 10.

Table 9: G_i (Pa) for each binder sample from discrete Maxwell model

$\tau_i(s)$	PAV-1	Original-2	RTFO-2	PAV-2	Original-3
10^{-9}				6.76×10^{8}	
10^{-8}	1.15×10^{7}	1.11×10^{9}	4.85×10^{8}	4.17×10^{8}	1.17×10^{9}
10^{-7}	1.95×10^{7}	4.24×10^{8}	2.56×10^{8}	2.34×10^{8}	3.96×10^{8}
10^{-6}	2.51×10^{7}	1.45×10^{8}	1.19×10^{8}	1.20×10^{8}	1.24×10^{8}
10^{-5}	2.45×10^{7}	4.42×10^{7}	4.90×10^{7}	5.62×10^{7}	3.55×10^{7}
10^{-4}	1.82×10^{7}	1.20×10^{7}	1.78×10^{7}	2.40×10^{7}	9.38×10^{6}
10^{-3}	1.02×10^{7}	2.91×10^{6}	5.70×10^{6}	9.33×10^{6}	2.28×10^{6}
10^{-2}	4.37×10^{6}	6.29×10^{5}	1.61×10^{6}	3.31×10^{6}	5.11×10^{5}
10^{-1}	1.41×10^{6}	1.21×10^{5}	4.04×10^{5}	1.07×10^{6}	1.05×10^{5}
10^{0}	3.47×10^{5}	2.09×10^{4}	8.91×10^{4}	3.16×10^{5}	2.00×10^{4}
10^{1}	6.46×10^{4}	3.21×10^{3}	1.74×10^{4}	8.51×10^{4}	3.48×10^{3}
10^{2}	9.12×10^{3}	4.39×10^{2}	2.99×10^{3}	2.09×10^{4}	5.60×10^{2}
10^{3}	9.77×10^{2}	5.37×10^{1}	4.55×10^{2}	4.68×10^{3}	8.28×10^{1}
10^{4}	7.94×10^{1}	5.85×10^{0}	6.11×10^{1}	9.55×10^{2}	1.13×10^{1}
10^{5}	4.90×10^{0}	5.69×10^{-1}	7.24×10^{0}	1.78×10^{2}	1.41×10^{0}

Table 10: J_i (1/Pa) for each binder sample from discrete Voigt model

$\tau_i(s)$	PAV-1	Original-2	RTFO-2	PAV-2	Original-3
10^{-7}	3.05 x 10^{-9}	1.68 x 10^{-9}	2.26 x 10^{-9}	2.95 x 10^{-9}	2.36 x 10^{-9}
10^{-6}	5.20 x 10^{-9}	5.13 x 10^{-9}	5.25 x 10^{-9}	5.50 x 10^{-9}	6.64 x 10^{-9}
10^{-5}	1.00 x 10^{-8}	1.68 x 10^{-8}	1.33 x 10^{-8}	1.12 x 10^{-8}	2.02 x 10^{-8}
10^{-4}	2.17 x 10^{-8}	5.89 x 10^{-8}	3.72 x 10^{-8}	2.51 x 10^{-8}	6.64 x 10^{-8}
10^{-3}	5.30 x 10^{-8}	2.21 x 10^{-7}	1.14 x 10^{-7}	6.17 x 10^{-8}	2.36 x 10^{-7}
10^{-2}	1.46 x 10^{-7}	8.91 x 10^{-7}	3.80 x 10^{-7}	1.66 x 10^{-7}	9.08 x 10^{-7}
10^{-1}	4.53 x 10^{-7}	3.85 x 10^{-6}	1.40 x 10^{-6}	4.90 x 10^{-7}	3.78 x 10^{-6}
10^{0}	1.58 x 10^{-6}	1.78 x 10^{-5}	5.62 x 10^{-6}	1.58 x 10^{-6}	1.70 x 10^{-5}
10^{1}	6.25 x 10^{-6}	8.81 x 10^{-5}	2.48 x 10^{-5}	5.62 x 10^{-6}	8.26 x 10^{-5}
10^{2}	2.78 x 10^{-5}	4.68 x 10^{-4}	1.20 x 10^{-4}	2.19 x 10^{-5}	4.35 x 10^{-4}
10^{3}	1.39 x 10^{-4}	2.66 x 10^{-3}	6.38 x 10^{-4}	9.33 x 10^{-5}	2.47 x 10^{-3}
10^{4}	7.87 x 10^{-4}	1.62 x 10^{-2}	3.72 x 10^{-3}	4.37 x 10^{-4}	1.52 x 10^{-2}
10^{5}	5.01 x 10^{-3}	1.06 x 10^{-1}	2.37 x 10^{-2}	2.24 x 10^{-3}	1.01 x 10^{-1}
10^{6}	3.60 x 10^{-2}	7.41 x 10^{-1}	1.66 x 10^{-1}	1.26 x 10^{-2}	7.28 x 10^{-1}
10^{7}	2.91 x 10^{-1}	5.56 x 10^{0}	1.27 x 10^{0}	7.76 x 10^{-2}	5.66 x 10^{0}

Continuous distributions of relaxation and retardation times were obtained and used to model the storage and loss viscoelastic properties through [12]

$$G'(\omega) = \int_{\tau_l}^{\tau_u} H(\tau) \frac{\omega^2\tau^2}{1+\omega^2\tau^2} d\ln\tau \tag{96}$$

$$G''(\omega) = \int_{\tau_l}^{\tau_u} H(\tau) \frac{\omega\tau}{1+\omega^2\tau^2} d\ln\tau \tag{97}$$

$$J'(\omega) = \int_{\tau_l}^{\tau_u} \frac{L(\tau)}{1+\omega^2\tau^2} d\ln\tau \tag{98}$$

$$J''(\omega) = \int_{\tau_l}^{\tau_u} L(\tau) \frac{\omega\tau}{1+\omega^2\tau^2} d\ln\tau \tag{99}$$

Probability densities of the discrete Maxwell model were regressed to a simple

empirical quadratic function for $H(\tau)$,

$$log\ H(\tau) = a(log\tau)^2 + b(log\tau) + c\ \ at\ \tau_l < \tau < \tau_u;\ H(\tau) = 0\ \ \text{otherwise} \quad (100)$$

as used in our prior work [16]. Thus, relaxation time distribution $H(\tau)$ is represented by 5 model parameters: a, b, c, τ_u, and τ_l. The relaxation and retardation time distributions are interrelated and describe viscoelastic mechanisms across different regions of time or frequency scales [12]. An approximate expression for the retardation time distribution $L(\tau)$ can be related from known $H(\tau)$, $G'(\omega)$, and $G''(\omega)$ [12] through

$$L(\tau) = \frac{H(\tau)}{(G'(\omega) - G''(\omega) + 1.37H(\tau)^2) + (\pi H(\tau))^2} \quad (101)$$

where $\omega = 1/\tau$. Gauss-Legendre integration was used to integrate equations [16, 25].

Stress relaxation modulus $G(t)$ and creep compliance $J(t)$ from continuous and discrete models are given by [12]

$$G(t) = \sum_i G_i \exp(-t/\tau_i) = \int_{\tau_l}^{\tau_u} H(\tau) \exp(-t/\tau) d\ \ln\tau \quad (102)$$

$$J(t) = \sum_i J_i (1 - \exp(-t/\tau_i)) = \int_{\tau_l}^{\tau_u} L(\tau)(1 - \exp(-t/\tau)) d\ \ln\tau \quad (103)$$

The plateau modulus at very low temperatures or high frequencies, where the polymer exhibits glassy behavior, is known as glassy modulus (G_g) [12]. Zero-shear viscosity (η_0) can be defined as the viscosity of a sample at very low shear rates when the angular frequency is almost zero [12]. Both glassy modulus and zero shear viscosity [12] were computed using the continuous Maxwell model

$$G_g = \int_{\tau_l}^{\tau_u} H(\tau) d \ln \tau \tag{104}$$

$$\eta_0 = \int_{\tau_l}^{\tau_u} H(\tau) \tau d \ln \tau \tag{105}$$

Additionally, zero-shear viscosity can be defined by [12]

$$\eta_0 = \lim_{\omega \to 0} \frac{dG''(\omega)}{d\omega} \tag{106}$$

and determined from lowest frequency range of loss moduli master curves.

5.3 Results and Discussion

5.3.1 Sample Damage

Strain sweeps yield strain ranges over which binders are in the linear viscoelastic region. Additionally, they give indication of binder stability when subjected to shear. A fresh binder sample was used at each temperature over the angular frequency range. Phase angles (δ) and complex moduli (G^*) can be used to deter-

mine viscoelastic properties such as storage and loss moduli (G' and G'') as well as storage, loss, and complex compliance (J', J'', and J^*). Stability of binders is indicated by agreement between initial and final strain sweep data at 1 and 10 rad/s respectively, with disagreement signaling sample damage. Figure 42 shows good agreement between initial and final data sets at 70°C and disagreement at 10°C. Over all temperatures tested, sample damage was maximum at 10°C and no damage was observed from 34°C upward for all samples. The linear viscoelastic region, indicated by phase angle δ being independent of strain amplitude, spans a more broad strain range at higher temperatures for all angular frequencies. Molecular motion is restricted at lower temperatures; samples are less flexible and get damaged when subjected to high shear as indicated by disagreement between initial and final data sets at 10°C in figure 42. This is also indicated by a more pronounced change in phase angle with strain at lower temperatures [23]. Sample stability is desirable at higher temperatures considering that processing conditions such as hot mix asphalt for roads are carried out at elevated temperatures.

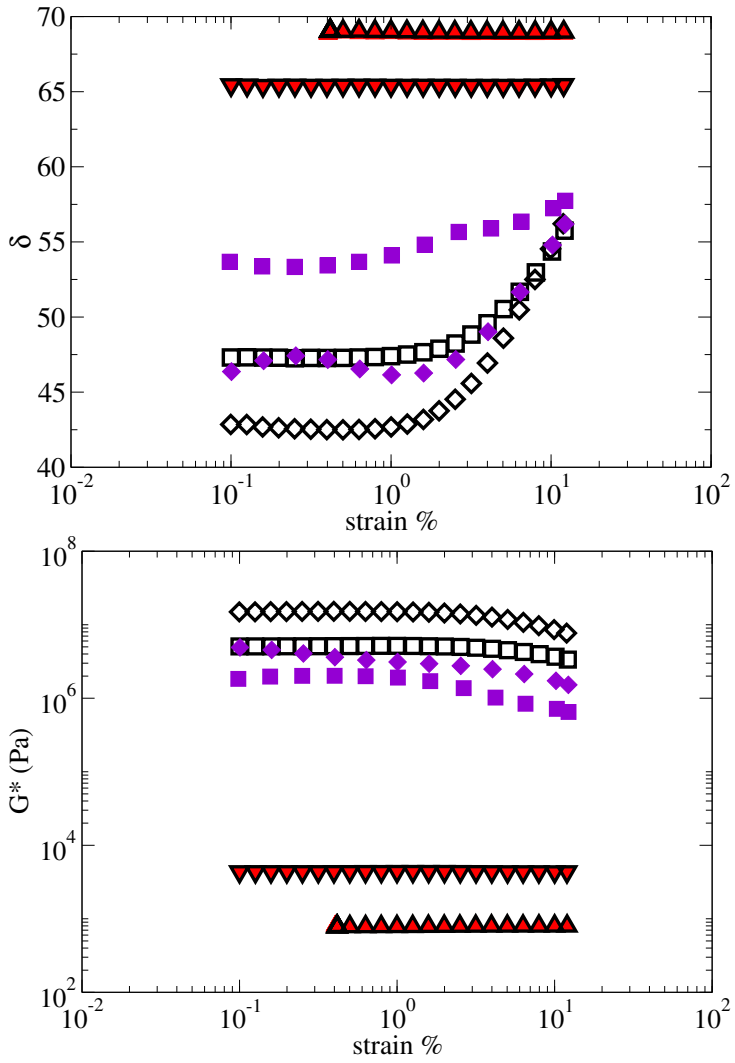

Figure 42: Phase angle δ and Complex modulus G^* vs strain % for RTFO-2. Data at 70°C ($\triangle$) for 1 rad/s, ($\triangledown$) for 10 rad/s. Data at 10°C ($\square$) for 1 rad/s, ($\diamond$) for 10 rad/s. Unfilled black symbols are for set 1/initial run and filled symbols are for set 2/final run.

5.3.2 Time-Temperature Superposition and Viscoelastic Models

Horizontal (a_T) and vertical (b_T) shift factors were applied to experimental storage and loss moduli data relative to the reference temperature 34°C. Details of these shift factors are given in table 11.

Table 11: Horizontal and vertical shift factors (a_T and b_T)

T($^\circ C$)	PAV-1	Original-2	RTFO-2	PAV-2	Original-3	b_T
10	992.29	609.77	716.99	1049.81	476.34	0.934
16	152.75	99.61	116.13	157.21	84.82	0.951
22	26.01	18.79	21.25	26.35	17.15	0.968
28	4.87	4.06	4.36	4.89	3.91	0.984
31		1.98	2.06	2.19		0.992
34	1	1	1	1	1	1.000
37		0.52	0.49	0.47		1.008
40	0.22	0.278	0.254	0.223	0.285	1.016
43		0.153	0.133	0.108		1.024
46	0.054	0.086	0.071	0.054	0.089	1.032
52	0.014	0.030	0.022	0.014	0.031	1.048
58	0.004	0.0117	0.0073	0.0039	0.0118	1.063
64	0.0012	0.0049	0.0027	0.0012	0.0049	1.079
70	0.00039	0.0023	0.0011	0.00036	0.0022	1.094

The horizontal shift factors were modeled using the WLF equation to produce well-fit master curves. The WLF parameters for all binders are listed in table 13. Figure 43 shows decreasing slope with aging i.e. maximum slope for original or unaged binder and minimum for PAV-aged. The increasing range of a_T with aging results in flatter slopes and decreased ratio of WLF parameters (C_2/C_1). The temperature dependence of horizontal shift factor a_T can yield an Arrhenius relationship with $1/T$ through [12]

$$\Delta H = R\frac{d\ \ln a_T}{d(1/T)} \tag{107}$$

where ΔH can be interpreted as the activation energy for viscoelastic relaxation

and R is the universal gas constant. From table 12 and the flatter slopes in figure 43, it can be inferred that greater activation energies are required for molecular motion of aged binders.

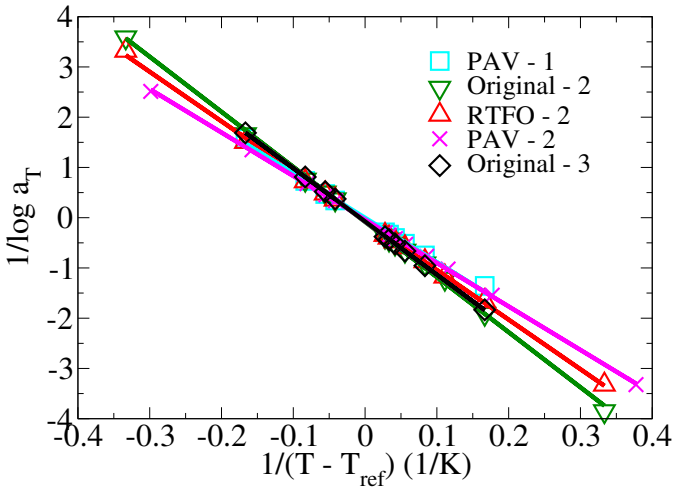

Figure 43: WLF plot of horizontal shift factors a_T

Table 12: Activation energy

Activation energy	PAV-1	Original-2	RTFO-2	PAV-2	Original-3
$\Delta H(kcal/mol)$	47.45	40.18	43.69	47.76	39.51

Modulus indicates binder stiffness at each frequency [12]. Figure 44 clearly shows aged binders have greater stiffness which can be attributed to oxidation from the aging process. PAV-aged binders show similar stiffness at medium to high frequencies while PAV-2 was stiffer at lower frequencies. Similarly, original binders also showed close agreement with Original-3 being slightly stiffer over

lower frequencies. The continuous (equations 96, 97) and discrete Maxwell models (equations 92, 93) applied to experimental moduli data showed great agreement as a result of the choice of $2n$ parameters for the discrete model and resultant 5 parameters for the continuous. The parameters from the continuous Maxwell model allowed for computing glassy modulus (equation 104) and zero-shear viscosity (equation 105), with results listed in table 13.

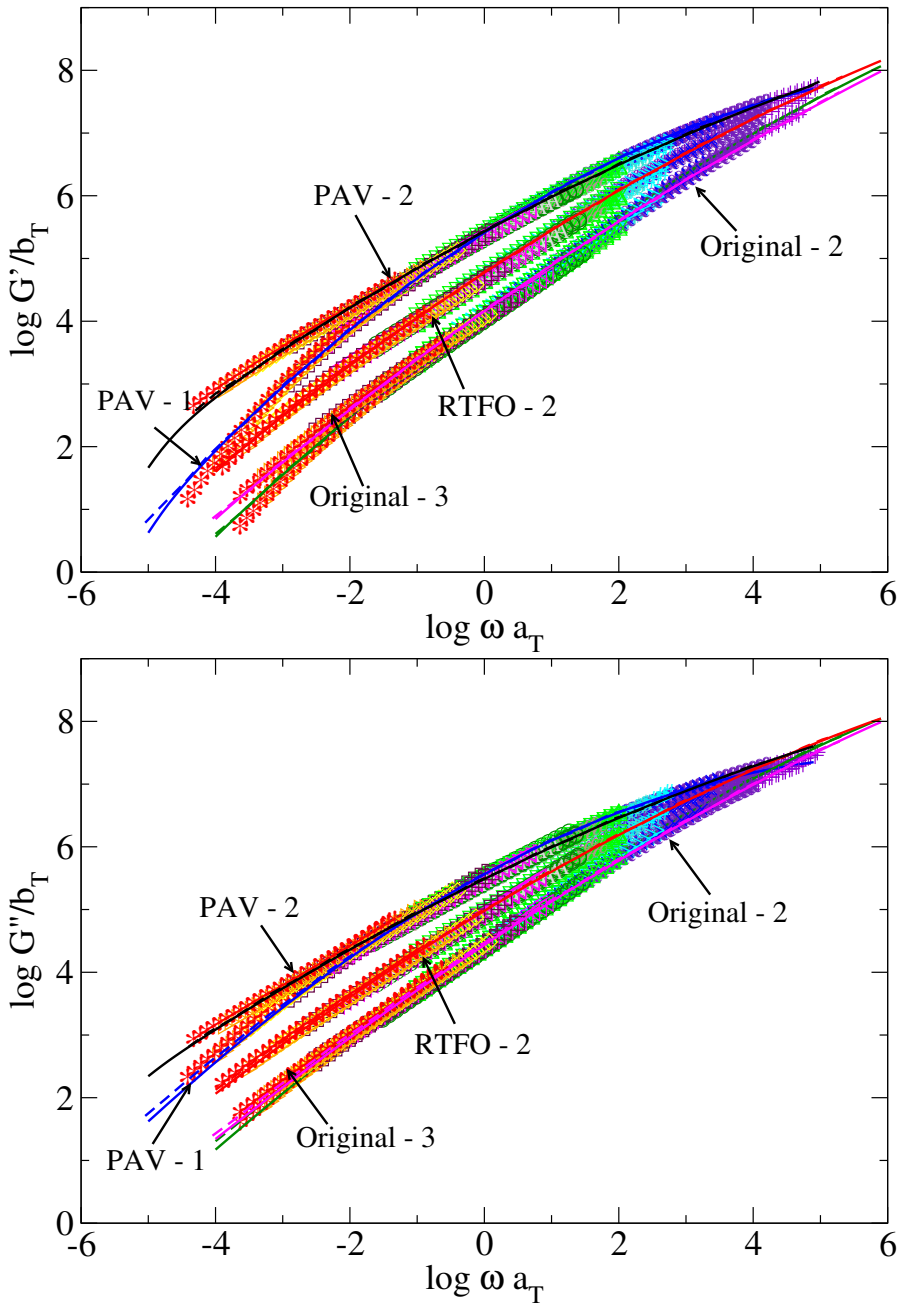

Figure 44: Storage and loss moduli G', G'' for all samples after applying time-temperature superposition; data originate from measurements at 70°C ($*$ red), 64°C ($\triangleright$ orange), 58°C ($\diamond$ yellow), 52°C ($\square$ maroon), 46°C ($\triangleleft$ magenta), 43°C (A grey), 40°C ($\circ$ dark green), 37°C (% brown), 34°C ($\triangle$ green, large plate), 34°C ($\triangledown$ green, small plate), 31°C ($ turquoise), 28°C (# cyan, large plate), 28°C ($<$ cyan, small plate), 22°C (X blue), 16°C (& indigo), 10°C ($+$ violet). Lines indicate continuous model and dashed lines indicate discrete Maxwell model fits.

Table 13: WLF parameters, Continuous Maxwell Model parameters, Glassy modulus, Zero-shear viscosity

Parameters	PAV-1	Original-2	RTFO-2	PAV-2	Original-3
C_1	26.04	12.41	16.61	25.64	14.77
C_2 (K)	233.91	128.06	161.64	229.45	156.44
τ_l (s)	10^{-8}	10^{-8}	10^{-8}	10^{-9}	10^{-8}
τ_u (s)	10^5	10^5	10^5	10^5	10^5
a	-0.06	-0.025	-0.027	-0.02	-0.018
b	-0.67	-0.789	-0.683	-0.55	-0.740
c	5.18	3.96	4.59	5.14	3.94
G_g (GPa)	0.11	1.10	0.67	1.18	1.05
η_0 (Pa.s)(continuous)	4.14 x 10^6	2.61 x 10^5	2.05 x 10^6	N/A	3.94 x 10^5
η_0 (Pa.s)(experimental)	4.23 x 10^6	1.33 x 10^5	1.20 x 10^6	N/A	1.91 x 10^5

Glassy moduli of Original-2, PAV-2, and Original-3 are typical for bitumens ($\sim$1.1 GPa) [22, 23, 26]. PAV-1 shows a much lesser G_g which could be attributed to the absence of polymer modifier. Zero-shear viscosity increased with aging due to restricted rotational motion of molecules as a consequence from increased binder stiffness due to oxidation. Experimental zero-shear viscosities at different temperatures were obtained from the loss moduli master curves (equation 106). Figure 45 shows decreasing viscosities with increasing temperature as a result of increasing molecular motion, i.e binder flexibility with heating. Original binders had comparable viscosities at all temperatures. RTFO-2 and PAV-1 approach similar η_0 at higher temperatures. In case of PAV-2, the frequencies were not low enough to accurately predict experimental η_0 as shown in figure 46. Further

frequency sweep tests at higher temperatures could possibly provide low enough frequency ranges for accurate predictions from linear regression.

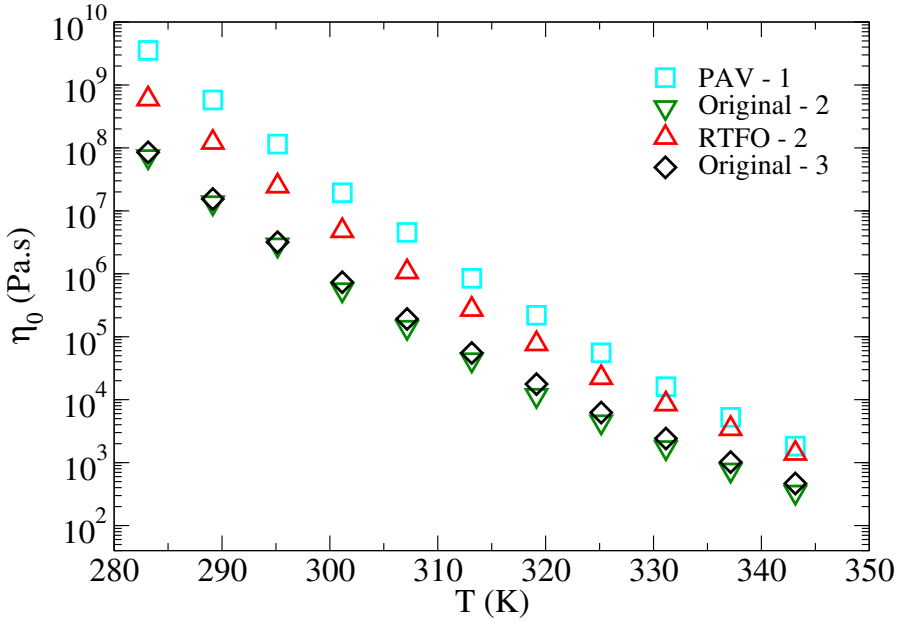

Figure 45: Experimental η_0 for all binders.

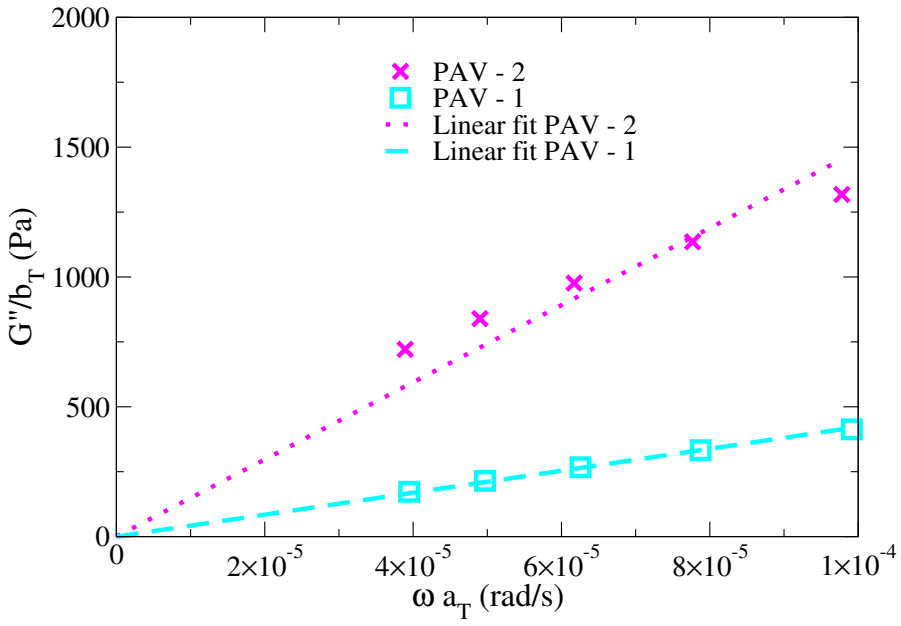

Figure 46: Experimental η_0 for PAV-2 and PAV-1 at 34°C.

Ratio of loss to storage modulus i.e. tan δ was plotted and fit using the same horizontal shift factors (a_T) as moduli. As shown in figure 47, tan δ decreased with decreasing temperature for all binders and increasing frequency for most binders, except at certain temperatures for PAV-2 and Original-3 binders. For RTFO-2 and PAV-2 imperfect overlaps were observed resulting from multiple frequency sweep data sets at certain temperatures using different plates. For PAV-2 at 28°C using 25 mm parallel plates, tan δ appears to slightly increase with frequency. This could be due to this data set being an outlier where larger plates were used for a low temperature resulting in greater viscous flow at high frequencies. Viscous losses decreased with aging as indicated from figures 47(a) to (c). For Original-3 overlap was not good at certain frequencies which could indicate that the 6°C temperature difference between frequency sweeps were insufficient for obtaining good data superposition. Same combination of shift factors from moduli master curves were used to fit compliance data at the same reference temperature. Compliance master curves have not been shown here.

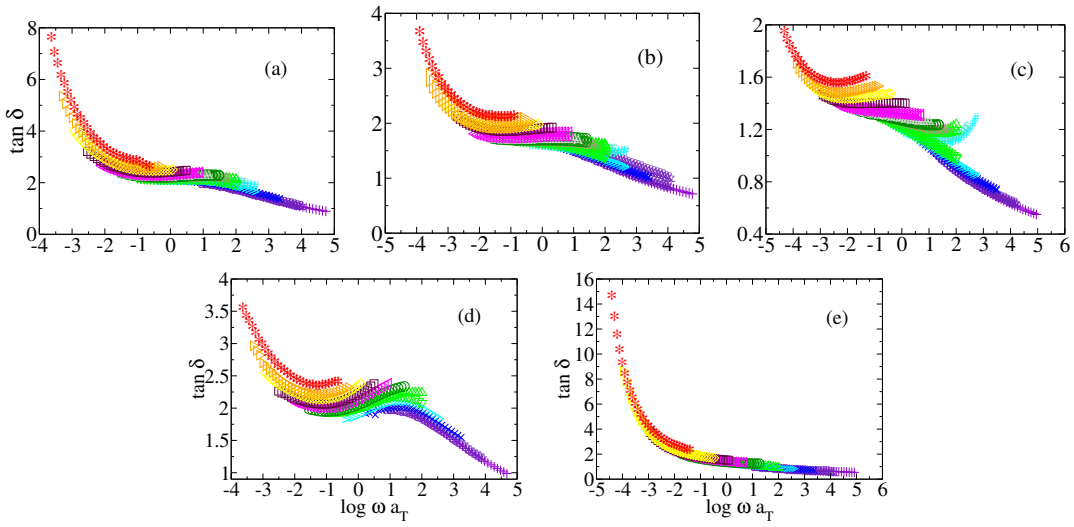

Figure 47: Tan δ vs. frequency fitted with horizontal shift factors: (a) Original-2, (b) RTFO-2, (c) PAV-2, (d) Original-3, (e) PAV-1. Colors and symbols follow convention shown in figure 44.

The relaxation time distributions $H(\tau)$ for all binders were computed for the continuous Maxwell model. Retardation time distributions $L(\tau)$ were computed from $H(\tau)$, $G'(\omega)$ and $G''(\omega)$ using equation 101. $H(\tau)$ and $L(\tau)$ are spectra used to interconvert between viscoelastic properties [12]. Figure 48 shows that $H(\tau)$ and $L(\tau)$ span several magnitudes and wide ranges of time in their contributions to binder modulus and compliance respectively. $H(\tau)$ decreased monotonically with relaxation time within the nonzero domain, especially for Original-2, RTFO-2, PAV-2 and Original-3 binders, similar to the shape predicted by Dickinson and Witt [16, 22]. The contributions from aging processes at shorter relaxation times were similar, while greater contributions were observed for PAV-aging at longer

relaxation times. This indicated that aging of binders yield additional relaxation mechanisms while retaining faster relaxations, as inferred earlier for other asphalt binders [16]. Original-2 and Original-3 showed highest contribution to modulus at lowest relaxation times and least at highest relaxation times, indicated by a sharp monotonic decrease. PAV-1 showed a slightly different shape than other binders and seemed to have peaked around $\sim 10^{-4}$ seconds. Analogous to $H(\tau)$, the contributions from aging processes at shorter relaxation times were similar while greater contributions from PAV-aging were observed at longer relaxation times for $L(\tau)$.

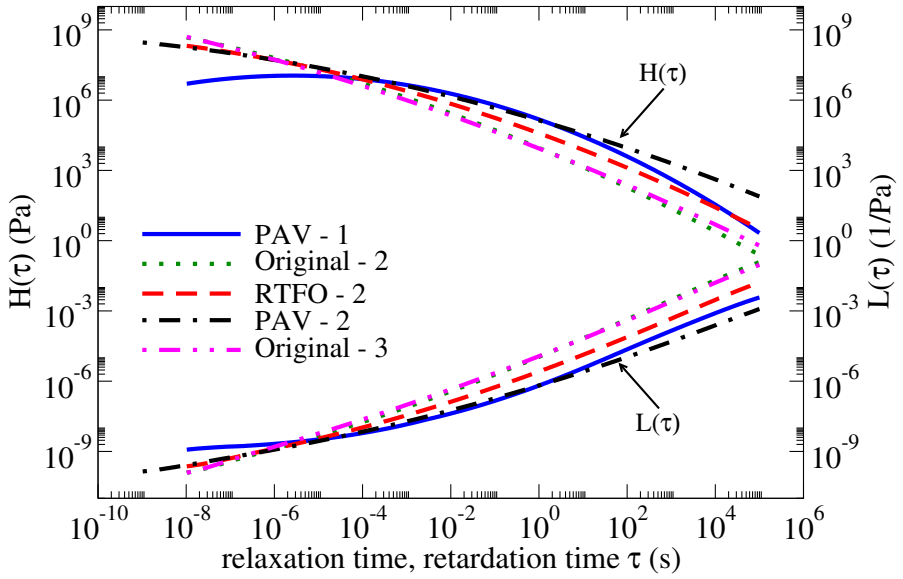

Figure 48: Relaxation and retardation time distributions vs. relaxation/retardation time for all samples.

Using parameters from the continuous models, stress relaxation modulus $G(t)$

and creep compliance $J(t)$ were computed. Discrete data were in excellent agreement with continuous but were not included here. Figure 49 shows that at lower times $G(t)$ are closely spaced for all binders and decrease with time. Original binders relax the fastest followed by RTFO-aged and then PAV-aged binders. Aging increases binder stiffness which is corroborated by PAV-aged binders having higher $G(t)$ than RTFO-aged and original binders over the entire time scale. All binders show closely related $J(t)$ at shorter times and increase with time due to contribution from viscous flow [12]. Original-2 and Original-3 show similar $J(t)$ over the entire time scale while $G(t)$ shows minor differences, with Original-2 being higher at shorter times and Original-3 higher at longer times. Low $J(t)$ at shorter times correspond to absence of any configurational re-arrangements in the microstructure of asphalt binders [12]. Aged samples creep slower than unaged ones. $G(t)$ can be predicted to reach zero at infinitely long times.

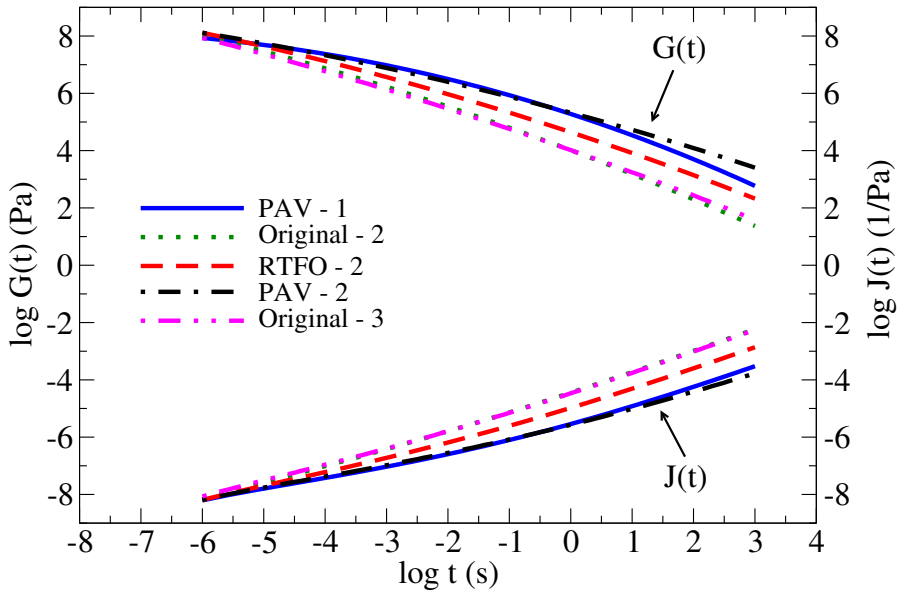

Figure 49: Stress relaxation modulus and creep compliance vs. time for all samples.

5.3.3 Bending Beam Rheometer (BBR)

$J(t)$ was used to make a model comparison with experimental compliance data from BBR experiment. PAV-1 and PAV-2 binders were tested using BBR at -18°C for resistance to low temperature thermal cracking. Binders were contained in beams and immersed in a cold solution bath before a constant load was applied for 240 seconds to measure beam deflection as a function of time. Calculations were averaged over two experimental runs for each binder. Maximum bending stress and strain were computed based on load, beam dimensions and deflections (AASHTO T 313). For the model comparison, compliance data were shifted to

-18°C using the WLF equation. Strain ($\gamma(t)$) was calculated

$$\gamma(t) = \sigma_0 \int_0^t J(t)\ dt \tag{108}$$

where σ_0 is the maximum bending stress applied experimentally on the binders. Figure 50 shows similar strain for PAV-1 and PAV-2 across the time scale from experimental measurements. The model for PAV-1 showed great agreement with BBR results over the entire time scale. The PAV-2 model predicted lower strain values than experimental at shorter times but had great agreement at medium to longer time scales. Both PAV-aged binders showed comparable flexibilities at low temperature. Asphalt binders that exhibit higher strains at low temperatures are more desirable since they are able to withstand more thermal stresses.

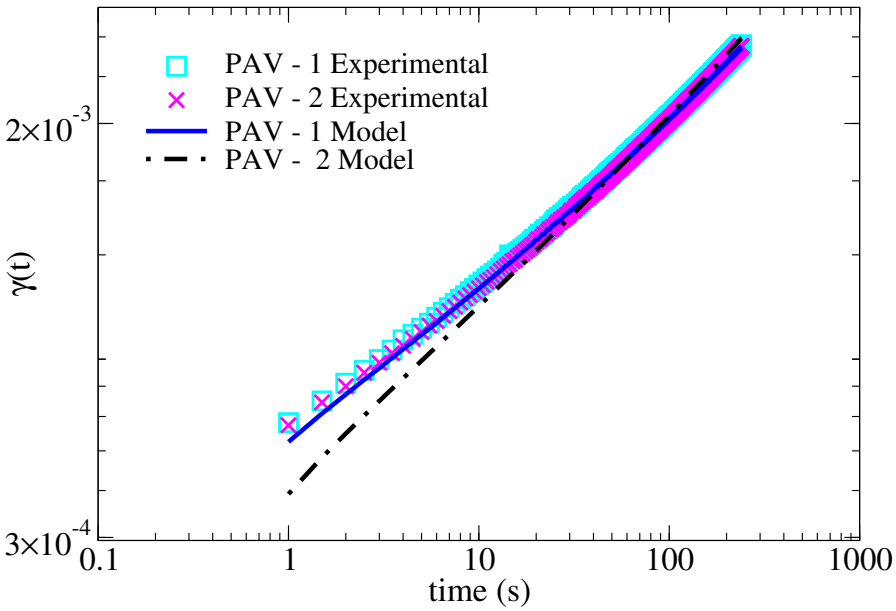

Figure 50: Strain as a function of time for BBR data on PAV-aged binders.

5.4 Conclusions

Asphalt binders from three sources were analyzed using experimental and modeling techniques. The PAV-1 binder was not polymer modified while Original-2, RTFO-2, PAV-2, and Original-3 binders were known to be modified with styrene-butadiene-styrene (SBS) co-polymer. Well-defined viscoelastic models that we employed were excellent fits to the experimental rheological data.

Shift factors, horizontal or frequency (a_T) and vertical or density and temperature (b_T), were obtained by constructing viscoelastic master curves at a particular reference temperature (34°C) to determine binder properties beyond experimentally feasible conditions. Horizontal shift factor a_T varied largely with temperature

due to greater variations in relaxation rates with temperature and sample preparation [16] while vertical shift factor b_T showed minor variations with temperature. WLF model and Arrhenius dependence of a_T on $1/T$ suggested aged binders needed greater activation energies for rotational motion of their molecules. Signs of sample damage were observed across all samples at low temperatures while no such signs were observed at relatively higher temperatures. The restriction of molecular motions was greater at low temperatures thus resulting in sample deterioration with shear.

Moduli master curves indicated increase in sample stiffness with aging. This was corroborated by the relaxation time distribution and stress relaxation modulus. Discrete and continuous models provided excellent fits to experimental results. Glassy moduli for all samples were within typical bitumen values, except PAV-1 which was lower than expected. This could be attributed to the lack of polymer modifier within the binder. Zero-shear viscosity decreased with heating for all binders due to increased molecular motion and thus increased flexibility. Frequency ranges were not low enough to accurately predict zero-shear viscosity for PAV-2. Tan δ decreased with decreasing temperature for all binders and increasing frequency for most binders, except at certain temperatures for PAV-2 and Original-

3 binders.

From relaxation and retardation time distributions, it was observed that the contributions from aging processes at shorter relaxation times were similar while greater contributions from PAV-aging were observed at longer relaxation times. At shorter times, stress relaxation moduli and creep compliance were closely spaced across all binders with original binders relaxing the fastest and PAV-aged binders relaxing the slowest. Low creep compliance at shorter times corresponded to absence of any configurational re-arrangements in the microstructure of the asphalt binders.

Compliance data from our model was shifted to -18°C, using WLF, to compare rheological measurements for PAV-1 and PAV-2 binders with bending beam rheometer data. Our model showed good agreement with experimental results for PAV-1 over the entire time scale. For PAV-2, there was great agreement between model and experimental results at medium to longer times and slight deviation at shorter times. Both PAV-1 and PAV-2 binders showed comparable flexibilities at low temperature.

5.5 Acknowledgments

We would like to thank the Rhode Island Department of Transportation and especially Michael Byrne and Michael Sock for financially supporting this work. We would also like to thank Christopher Spencer for his help in sample preparation.

List of References

[1] Asphalt Insititute, *The Asphalt Handbook (MS-4).* Asphalt Institute, Lexington KY, 2007.

[2] D. Anderson, J. Youtcheff, and M. Zupanick, *Asphalt binders*, 2000, Transportation Research Board (TRB) Committee on Characteristics of Bituminous Materials, TRB Millennium Paper Series.

[3] J. Petersen, R. Robertson, J. Branthaver, P. Harnsberger, J. Duvall, S. Kim, D. Anderson, D. Christiansen, and H. Bahia, *Binder characterization and evaluation: Volume 1*, 1994, Rep. No. SHRP-A-367, Strategic Highway Research Program, National Research Council, Washington, DC.

[4] T. W. Kennedy, G. A. Huber, E. T. Harrigan, R. J. Cominsky, C. S. Hughes, H. Von Quintus, and J. S. Moulthrop, *Superior performing asphalt pavements (Superpave): The product of the SHRP asphalt research program.* Strategic Highway Research Program, National Research Council Washington, DC, USA, 1994, no. SHRP-A-410.

[5] C. Baek, B. Underwood, and Y. Kim, "Effects of oxidative aging on asphalt mixture properties," *Transp Res Rec: J Transp Res Board*, no. 2296, pp. 77–85, 2012.

[6] C. A. Bell, *Aging of asphalt-aggregate systems*, SR-OSU-A-003A-89-2, Summary Report, SHRP, National Research Council, Washington DC, USA.

[7] C. A. Bell, Y. AbWahab, M. Cristi, and D. Sosnovske, *Selection of laboratory aging procedures for asphalt-aggregate mixtures.* Strategic Highway Research Program, 1994, SHRP-A-383.

[8] Y. S. Kumbargeri and K. P. Biligiri, "Understanding aging behaviour of conventional asphalt binders used in India," *Transp Res Proc*, vol. 17, pp. 282–290, 2016.

[9] R. N. Traxler, *Durability of asphalt cements*, 1963, vol. 32, Assoc Asphalt Paving Technol Proc.

[10] D. Lee, *Asphalt durability correlation in Iowa*, 1973, vol. 468, Transp Res Rec.

[11] N. G. McCrum, C. P. Buckley, and C. B. Bucknall, *Principles of Polymer Engineering, 2nd Edition.* Oxford Univ Press, 1997.

[12] J. D. Ferry, *Viscoelastic Properties of Polymers. 3rd Ed.* Wiley, 1980.

[13] H. Leaderman, *Elastic and creep properties of filamentous materials and other high polymers.* The Textile Foundation, 1943.

[14] R. Andrews, N. Hofman-Bang, and A. Tobolsky, "Elastoviscous properties of polyisobutylene. I. Relaxation of stress in whole polymer of different molecular weights at elevated temperatures," *J Polym Sci Part A: Polym Chem*, vol. 3, no. 5, pp. 669–692, 1948.

[15] A. V. Tobolsky, "Stress relaxation studies of the viscoelastic properties of polymers," *J Appl Phys*, vol. 27, no. 7, pp. 673–685, 1956.

[16] J. V. Badami and M. L. Greenfield, "Maxwell model analysis of bitumen rheological data," *J Mater Civ Eng*, vol. 23, no. 10, pp. 1387–1395, 2011.

[17] L. Zhang and M. L. Greenfield, "Analyzing properties of model asphalts using molecular simulation," *Energy fuels*, vol. 21, no. 3, pp. 1712–1716, 2007.

[18] L. Zhang and M. L. Greenfield, "Relaxation time, diffusion, and viscosity analysis of model asphalt systems using molecular simulation," *J Chem Phys*, vol. 127, no. 19, p. 194502, 2007.

[19] L. Zhang and M. L. Greenfield, "Rotational relaxation times of individual compounds within simulations of molecular asphalt models," *J Chem Phys*, vol. 132, no. 19, p. 184502, 2010.

[20] R. Jongepier, B. Kuilman, R. Schmidt, V. Puzinauskas, and F. Rostler, "Characteristics of the rheology of bitumens," *J Assoc Asphalt Paving Technol*, vol. 38, pp. 98–122, 1968.

[21] R. Jongepier and B. Kuilman, "Dynamic shear modulus of bitumens as a function of frequency and temperature," *Rheol Acta*, vol. 9, no. 1, pp. 102–10, 1970.

[22] E. Dickinson and H. Witt, "The dynamic shear modulus of paving asphalts as a function of frequency," *J Rheo*, vol. 18, no. 4, pp. 591–606, 1974.

[23] M. O. Marasteanu, T. Clyne, J. McGraw, X. Li, and R. Velasquez, "High-temperature rheological properties of asphalt binders," *Transp Res Rec*, vol. 1901, pp. 52–59, 2005.

[24] M. L. Williams, R. F. Landel, and J. D. Ferry, "The temperature dependence of relaxation mechanisms in amorphous polymers and other glass-forming liquids," *J Am Chem Soc*, vol. 77, pp. 3701–7, 1955.

[25] M. Abramowitz and I. A. Stegun, *Handbook of mathematical functions*. Dover, Mineola, NY, 1964.

[26] M. O. Marasteanu and D. A. Anderson, "Comparison of moduli for asphalt binders obtained from different test devices," *Asphalt Paving Technol*, vol. 69, pp. 574–606, 2000.

APPENDIX A

Discussion on statistical weights, statistical weight matrices, partition function and transformation matrices for generation of RIS chains

A.1 Statistical weights and statistical weight matrices

Statistical weights are relative probabilities of occurence for bonds in rotational isomeric states. Statistical weights are dependent on the torsional energy around the bonds,

$$\alpha = \exp(-E_\alpha / k_b T) \tag{A.1}$$

In eqn A.1, α is a statistical weight based on the torsional energy E_α. The statistical weights are arranged in statistical weight matrices with the row and column elements being statistical weights for successive torsional bonds. Row elements are statistical weights around bond i and column elements are statistical weights around bond $i+1$ [1] as shown in figures 1, 34 and 35.

Discrete rotational isomeric states were chosen corresponding to regions of potential energy minima for each torsional bond [1]. Six discrete rotational states were chosen for polybutadiene [2, 3, 4], five for polypropylene [5, 6], and two for polystyrene [6, 7, 8]. Statistical weights were arranged in $M \times M$ statistical weight

matrices , where M is the number of discrete rotational isomeric states. Each repeat unit of polybutadiene has three torsional bonds while polypropylene and polystyrene have two torsional bonds, thus three statistical weight matrices were used for polybutadiene [2, 3, 4] and two each were used for polypropylene [5, 6] and polystyrene [6, 7, 8] respectively.

A.2 Partition function

Partition function (z) can be defined as the sum of the unnormalized probabilities for all possible discrete rotational isomeric states [1]. It is used in the computation of bond pair probability as

$$z = J^{\star} U^{\gamma\prime} (U^{\gamma})^{x-2} U^{\gamma\prime\prime} J \tag{A.2}$$

$$J^{\star} = (1, 0, 0, 0, 0, 0) \tag{A.3}$$

$$J = col(1, 1, 1, 1, 1, 1) \tag{A.4}$$

where $J^{\star}$ and J are row and column matrices for chain start and end respectively, $U^{\gamma\prime}$, U^{γ}, and $U^{\gamma\prime\prime}$ are statistical weight matrices for bonds preceding, of and fol-

lowing repeat units, and x is the number of repeat units in a polymer chain [1]. Carrying out the matrix multiplication in equation A.2 provides one term in z for each possible combination of rotational isomeric states. The probability of a single conformation equals its contribution to z, divided by z.

A.3 Transformation matrices

Transformation matrices are used to transform bond vectors from one reference state to another one. According to Flory [1], the transformation matrix used to transform bond vectors from $i+1$ frame to i frame (refer figures 1, 34 and 35) can be given as

$$T_i = \begin{pmatrix} \cos\theta_i & \sin\theta_i & 0 \\ \sin\theta_i\cos\phi_i & -\cos\theta_i\cos\phi_i & \sin\phi_i \\ \sin\theta_i\sin\phi_i & -\cos\theta_i\sin\phi_i & -\cos\phi_i \end{pmatrix} \tag{A.5}$$

where θ_i and ϕ_i are bond angle supplements and torsional angles respectively. These matrices depend on the torsional bonds in a repeat unit of a polymer chain.

List of References

[1] P. J. Flory, *Statistical Mechanics of Chain Molecules*. Wiley Interscience, 1969.

[2] J. E. Mark, "Random-coil configurations of cis-l,4-polybutadiene and cis-1,4-polyisoprene. Theoretical interpretation," *J Am Chem Soc*, vol. 88, no. 19, pp. 4354–9, 1966.

[3] J. E. Mark, "Interpretation of random-coil configurations of trans-1,4-polybutadiene and trans-1,4-polyisoprene," *J Am Chem Soc*, vol. 89, no. 26, pp. 6829–35, 1967.

[4] S. Kar and M. L. Greenfield, "Sizes and shapes of simulated amorphous cis- and trans-1,4-polybutadiene," *Polymer*, vol. 62, pp. 129–138, 2015.

[5] U. W. Suter and P. J. Flory, "Conformational energy and configurational statistics of polypropylene," *Macromolecules*, vol. 8, no. 6, pp. 765–76, 1975.

[6] S. Kar, J. L. Cuddigan, and M. L. Greenfield, "Size distribution analysis of simulated amorphous vinyl polymer chains: Polypropylene and polystyrene," 2017, to be submitted.

[7] D. Y. Yoon, P. R. Sundararajan, and P. J. Flory, "Conformational characteristics of polystyrene," *Macromolecules*, vol. 8, no. 6, pp. 776–83, 1975.

[8] R. F. Rapold and U. W. Suter, "Conformational characteristics of polystyrene," *Macrom Theory Simul*, vol. 3, no. 1, pp. 1–17, 1994.

APPENDIX B

Equibiaxial deformation and shear force and stress plots

Force and stress plots for trans-1,4-polybutadiene chains, of different repeat unit sizes and over a range of temperatures, under equibiaxial deformation and shear are shown here. Results from the tensile stress plots have been used in the moduli plots (figure 28) shown in chapter 3. Results for cis-1,4-polybutadiene chains are similar to trans-1,4-polybutadiene chains, and have not been included here.

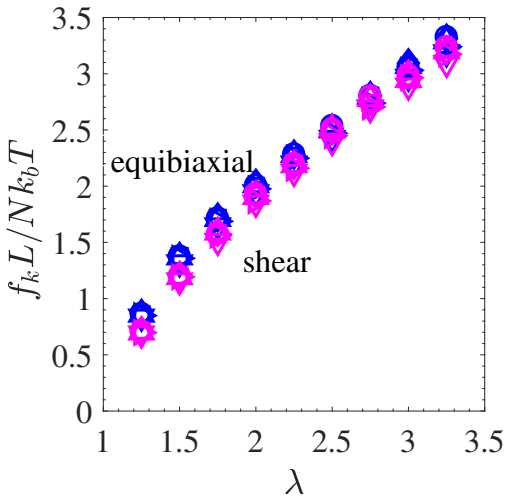

Figure B.1: Forces on trans-1,4-polybutadiene chains under equibiaxial deformation and shear at 343 K for repeat unit sizes of x = 15, 25, 50, 75, 100 and 120. Equibiaxial tension force f_x or f_y, shear force f_x. Symbols: x = 15 ($\triangledown$), 25 ($\triangleright$), 50 ($\triangle$), 75 ($\square$), 100 ($\diamond$), and 120 ($\circ$). Colors: equibiaxial (blue) and shear (magenta).

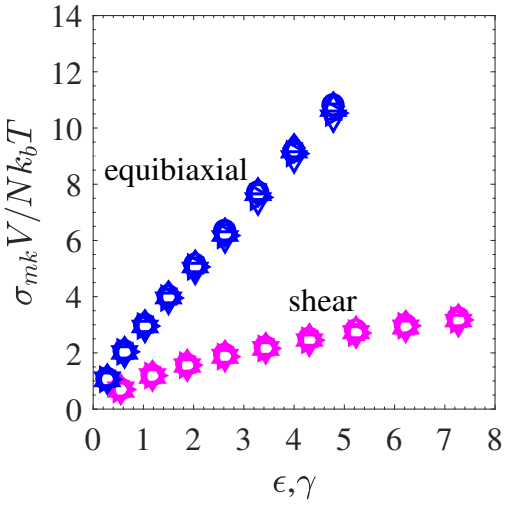

Figure B.2: Stresses on trans-1,4-polybutadiene chains under equibiaxial deformation and shear at 343 K for repeat unit sizes of x = 15, 25, 50, 75, 100 and 120. Equibiaxial: σ_{xx} or σ_{yy}, and shear: σ_{yx}. Symbols and colors follow convention of figure B.1.

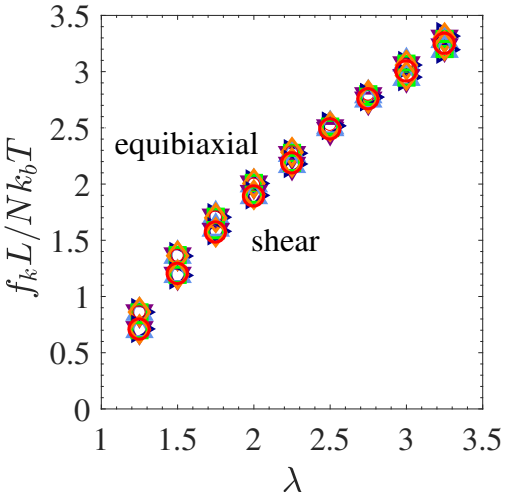

Figure B.3: Forces on trans-1,4-polybutadiene chains under equibiaxial deformation and shear for x = 50 repeat units at T = 275 K, 300 K, 323 K, 343 K, 375 K, and 400 K. Equibiaxial tension force f_x or f_y, shear force f_x. Symbols and colors: T = 275 K ($\triangledown$ violet), 300 K ($\triangleright$ indigo), 323 K ($\triangle$ blue), 343 K ($\square$ green), 375 K ($\diamond$ orange), and 400 K ($\circ$ red).

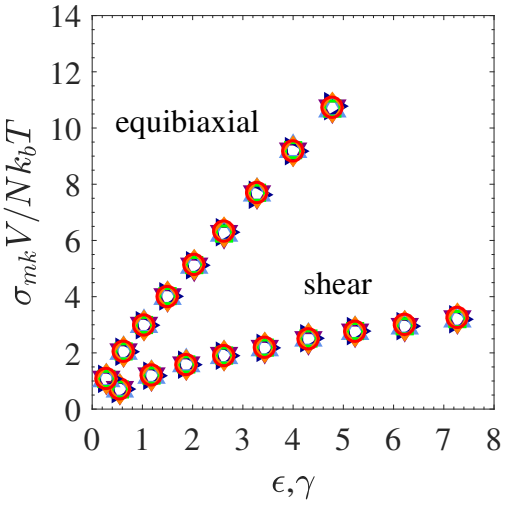

Figure B.4: Stresses on trans-1,4-polybutadiene chains under equibiaxial deformation and shear for x = 50 repeat units at T = 275 K, 300 K, 323 K, 343 K, 375 K, and 400 K. Equibiaxial: σ_{xx} or σ_{yy}, and shear: σ_{yx}. Symbols and colors follow convention of figure B.3.

BIBLIOGRAPHY

Abe, A., "Unperturbed dimensions of vinyl polymer chains," *Polym J*, vol. 1, no. 2, pp. 232–244, 1970.

Abe, M. and Fujita, H., "Binary mixtures of theta-solvents," *J Phys Chem*, vol. 69, no. 10, pp. 3263–7, 1965.

Abe, Y. and Flory, P. J., "Configurational statistics of 1,4-polybutadiene chains," *Macromolecules*, vol. 4, no. 2, pp. 219–29, 1971.

Abramowitz, M. and Stegun, I. A., *Handbook of mathematical functions.* Dover, Mineola, NY, 1964.

Allen, M. P. and Tildesley, D. J., *Computer Simulation of Liquids.* Oxford Univ. Press, 1987.

Altares, T., Wyman, D., and Allen, V., "Synthesis of low molecular weight polystyrene by anionic techniques and intrinsic viscosity–molecular weight relations over a broad range in molecular weight," *J Polym Sci Part A: Polym Chem*, vol. 2, no. 10, pp. 4533–4544, 1964.

Anderson, D., Youtcheff, J., and Zupanick, M., *Asphalt binders*, 2000, Transportation Research Board (TRB) Committee on Characteristics of Bituminous Materials, TRB Millennium Paper Series.

Andrews, R., Hofman-Bang, N., and Tobolsky, A., "Elastoviscous properties of polyisobutylene. I. Relaxation of stress in whole polymer of different molecular weights at elevated temperatures," *J Polym Sci Part A: Polym Chem*, vol. 3, no. 5, pp. 669–692, 1948.

Andrews, R. J. and Grulke, E. A., "Glass transition temperatures of polymers," *Wiley Database of Polymer Properties*, 2003.

Asakura, T., Ando, I., and Nishioka, A., "Calculation of the characteristic ratio of polypropylene containing chemical inversions (head-to-head and tail-to-tail units)," *Macrom Chem Phys*, vol. 177, no. 5, pp. 1493–1500, 1976.

Asphalt Insititute, *The Asphalt Handbook (MS-4)*. Asphalt Institute, Lexington KY, 2007.

Badami, J. V. and Greenfield, M. L., "Maxwell model analysis of bitumen rheological data," *J Mater Civ Eng*, vol. 23, no. 10, pp. 1387–1395, 2011.

Baek, C., Underwood, B., and Kim, Y., "Effects of oxidative aging on asphalt mixture properties," *Transp Res Rec: J Transp Res Board*, no. 2296, pp. 77–85, 2012.

Bahar, I., "Local relaxation of polymers in dense media: Cooperative kinematics theory and applications," *Macro Theory Simul*, vol. 6, no. 5, pp. 881–906, 1997.

Ball, R. C., Doi, M., Edwards, S. F., and Warner, M., "Elasticity of entangled networks," *Polymer*, vol. 22, no. 8, pp. 1010–1018, 1981.

Bates, F., Cohen, R., and Berney, C., "Small-angle neutron scattering determination of macrolattice structure in a polystyrene-polybutadiene diblock copolymer," *Macromolecules*, vol. 15, no. 2, pp. 589–592, 1982.

Baysal, C., Bahar, I., Erman, B., and Monnerie, L., "Kinematics of polymer chains in dense medium. 4. Effect of backbone geometry and application to polybutadiene," *Macromolecules*, vol. 29, no. 8, pp. 2980–8, 1996.

Becker, R. H., Yu, C. U., and Mark, J. E., "Thermoelastic studies of diene polymers in elongation and compression," *Polymer J*, vol. 7, no. 2, pp. 234–240, 1975.

Bell, C. A., *Aging of asphalt-aggregate systems*, no. SR-OSU-A-003A-89-2, Summary Report, SHRP, National Research Council, Washington DC, USA.

Bell, C. A., AbWahab, Y., Cristi, M., and Sosnovske, D., *Selection of laboratory aging procedures for asphalt-aggregate mixtures.* Strategic Highway Research Program, 1994, no. SHRP-A-383.

Blow, C. M. and Hepburn, C., *Rubber Technology and Manufacture.* Plastics and Rubber Institute, London, 1982.

Boyd, R. H. and Breitling, S. M., "Conformational properties of polypropylene," *Macromolecules*, vol. 5, no. 3, pp. 279–286, 1972.

Brandrup, J., Immergut, E. H., and Editors, *Polymer Handbook, Fourth Edition.* Wiley, 1998.

Brinke Ten, J. W., Litvinov, V. M., Wijnhoven, J. E. G. J., and Noordermeer, J. W. M., "Interactions of stober silica with natural rubber under the influence of coupling agents, studied by ^{1}H NMR T_2 relaxation analysis," *Macromolecules*, vol. 35, no. 27, pp. 10 026–37, 2002.

Burkhart, C. W., "Structurally realistic modeling of elastomers," *Rubber Chem Tech*, vol. 71, no. 3, pp. 342–406, 1998.

Cakmak, U. D. and Major, Z., "Experimental thermomechanical analysis of elastomers under uni- and biaxial tensile stress state," *Exp Mech*, vol. 54, no. 4, pp. 653–663, 2013.

Cohen Addad, J., Thanh, B. P., and Montes, H., "Evidence for a linear NMR-Elasticity interrelationship in polymeric gels," *Macromolecules*, vol. 30, no. 15, pp. 4374–4380, 1997.

Cotton, J., Decker, D., Benoit, H., Farnoux, B., Higgins, J., Jannink, G., Ober, R., Picot, C., and Des Cloizeaux, J., "Conformation of polymer chain in the bulk," *Macromolecules*, vol. 7, no. 6, pp. 863–872, 1974.

Crespi, G. and Flisi, U., "Contribution of the internal energy to the retractive force of vulcanized cis-1,4 polybutadiene," *Makromol Chem*, vol. 60, pp. 191–201, 1963.

Danusso, F., Moraglio, G., and Gianotti, G., "cis-Tactic Polybutadiene: Solubility $[\eta]-M$ Relations in Different Solvents, and Molecular Conformation," *J Polym Sci*, vol. 51, pp. 475–485, 1961.

Debye, P., "The intrinsic viscosity of polymer solutions," *J Chem Phys*, vol. 14, no. 10, pp. 636–639, 1946.

Dickinson, E. and Witt, H., "The dynamic shear modulus of paving asphalts as a function of frequency," *J Rheo*, vol. 18, no. 4, pp. 591–606, 1974.

Dubrović, I., Klepac, D., Valić, S., and Žauhar, G., "Study of natural rubber crosslinked in the state of uniaxial deformation," *Radiat Phys Chem*, vol. 77, no. 6, pp. 811–817, 2008.

Edwards, S. and Vilgis, T., "The effect of entanglements in rubber elasticity," *Polymer*, vol. 27, no. 4, pp. 483–492, 1986.

Ferry, J. D., *Viscoelastic Properties of Polymers. 3rd Ed.* Wiley, 1980.

Flanigan, C. M., Beyer, L., Klekamp, D., Rohweder, D., Stuck, B., and Terrill, E. R., "Comparative study of silica, carbon black and novel fillers in tread compounds," *Rubber World*, vol. 245, no. 5, pp. 18–31, 2012.

Flory, P. J., *Principles of Polymer Chemistry*. Cornell University Press, 1953.

Flory, P. J., *Statistical Mechanics of Chain Molecules*. Wiley Interscience, 1969.

Flory, P., "Mean-square moments of chain molecules," *Proc Natl Acad Sci USA*, vol. 51, no. 6, pp. 1060–67, 1964.

Flory, P., Mark, J., and Abe, A., "Random-coil configurations of vinyl polymer chains. the influence of stereoregularity on the average dimensions," *J Am Chem Soc*, vol. 88, no. 4, pp. 639–650, 1966.

Fujikawa, M., Maeda, N., Yamabe, J., Kodama, Y., and Koishi, M., "Determining stress-strain in rubber with in-plane biaxial tensile tester," *Exp Mech*, vol. 54, no. 9, pp. 1639–1649, 2014.

Fujiwara, Y. and Flory, P., "Second and fourth moments of vinyl polymer chains," *Macromolecules*, vol. 3, no. 3, pp. 280–288, 1970.

Gee, R. H. and Boyd, R. H., "Conformational dynamics and relaxation in bulk polybutadienes: A molecular dynamics simulation study," *J Chem Phys*, vol. 101, no. 9, pp. 8028–38, 1994.

Gestoso, P., Nicol, E., Doxastakis, M., and Theodorou, D. N., "Atomistic Monte Carlo simulation of polybutadiene isomers: cis-1,4-polybutadiene and 1,2-polybutadiene," *Macromolecules*, vol. 36, no. 18, pp. 6925–6938, 2003.

Gitsas, A. and Floudas, G., "Pressure dependence of the glass transition in atactic and isotactic polypropylene," *Macromolecules*, vol. 41, no. 23, pp. 9423–9429, 2008.

Gkourmpis, T. and Mitchell, G. R., "Three dimensional picture of the local structure of 1,4-polybutadiene from a complete atomistic model and neutron scattering data," *Macromolecules*, vol. 44, no. 8, pp. 3140–3148, 2011.

Hadjichristidis, N., Xu, Z., Fetters, L. J., and Roovers, J., "The characteristic ratios of stereoirregular polybutadiene and polyisoprene," *J Polym Sci, Polym Phys Ed*, vol. 20, no. 4, pp. 743–50, 1982.

Haliloglu, T., Bahar, I., Erman, B., Kim, E.-G., and Mattice, W. L., "A dynamic rotational isomeric state approach for extension of the time scale of the local dynamics observed in fully atomistic molecular dynamics simulations: Application to polybutadiene," *J Chem Phys*, vol. 104, pp. 4828–4834, 1996.

Hariharaputhiran, H. and Saravanan, U., "A new set of biaxial and uniaxial experiments on vulcanized rubber and attempts at modeling it using classical hyperelastic models," *Mech Mater*, vol. 92, pp. 211–222, 2016.

Heatley, F., Salovey, R., and Bovey, F., "Polymer Nuclear Magnetic Resonance Spectroscopy. XVIII. The Nuclear Magnetic Resonance Spectrum, Dimensions, and Steric Interactions of Isotactic Polypropylene," *Macromolecules*, vol. 2, no. 6, pp. 619–623, 1969.

Heinrich, G., Straube, E., and Helmis, G., "Rubber elasticity of polymer networks: Theories," *Adv Polym Sci*, vol. 85, pp. 33–87, 1988.

Hiemenz, P. C. and Lodge, T. P., *Polymer Chemistry, 2nd Edition*. CRC Press, Taylor & Francis Group, 2007.

Inagaki, H., Miyamoto, T., and Ohta, S., "The unperturbed dimensions of polypropylene and polyethylene," *J Phys Chem*, vol. 70, no. 11, pp. 3420–3431, 1966.

James, H. M. and Guth, E., "Theory of the elasticity of rubber," *J Appl Phys*, vol. 15, no. 4, pp. 294–303, 1944.

Jongepier, R. and Kuilman, B., "Dynamic shear modulus of bitumens as a function of frequency and temperature," *Rheol Acta*, vol. 9, no. 1, pp. 102–10, 1970.

Jongepier, R., Kuilman, B., Schmidt, R., Puzinauskas, V., and Rostler, F., "Characteristics of the rheology of bitumens," *J Assoc Asphalt Paving Technol*, vol. 38, pp. 98–122, 1968.

Kajiwara, K. and Burchard, W., "Rotational isomeric state calculations of the dynamic structure factor and related properties of some linear chains. 1. The $\rho = \langle S^2 \rangle^{1/2} \langle R_H^{-1} \rangle$ parameter," *Macromolecules*, vol. 17, no. 12, pp. 2669–73, 1984.

Kajiwara, K. and Burchard, W., "Rotational isomeric state calculations of the dynamic structure factor and related properties of some linear chains. 2. First cumulant of the dynamic structure factor," *Macromolecules*, vol. 17, no. 12, pp. 2674–8, 1984.

Kameda, T. and Asakura, T., "Structure and dynamics in the amorphous region of natural rubber observed under uniaxial deformation monitored with solid-state ^{13}C NMR," *Polymer*, vol. 44, no. 24, pp. 7539–7544, 2003.

Kar, S. and Greenfield, M. L., "Sizes and shapes of simulated amorphous cis- and trans-1,4-polybutadiene," *Polymer*, vol. 62, pp. 129–138, 2015.

Kennedy, T. W., Huber, G. A., Harrigan, E. T., Cominsky, R. J., Hughes, C. S., Von Quintus, H., and Moulthrop, J. S., *Superior performing asphalt pavements (Superpave): The product of the SHRP asphalt research program.* Strategic Highway Research Program, National Research Council Washington, DC, USA, 1994, SHRP-A-410.

Kim, E. and Mattice, W. L., "Local chain dynamics of bulk amorphous polybutadienes: a molecular dynamics study," *J Chem Phys*, vol. 101, no. 7, pp. 6242–54, 1994.

Kim, E., Misra, S., and Mattice, W. L., "Atomistic models of amorphous polybutadienes. 2. Poly(1,4-trans-butadiene), poly(1,2-butadiene), and a random copolymer of 1,4-trans-butadiene, 1,4-cis-butadiene, and 1,2-butadiene," *Macromolecules*, vol. 26, no. 13, pp. 3424–31, 1993.

Kinsinger, J. B. and Hughes, R., "The unperturbed dimensions of atactic and isotactic polypropylene," *J Phys Chem*, vol. 67, no. 9, pp. 1922–1923, 1963.

Kinsinger, J. and Hughes, R., "Intrinsic viscosity-molecular weight relationships for isotactic and atactic polypropylene," *J Phys Chem*, vol. 63, no. 12, pp. 2002–2007, 1959.

Krigbaum, W. and Flory, P., "Molecular weight dependence of the intrinsic viscosity of polymer solutions. II," *J Polym Sci Part A: Polym Chem*, vol. 11, no. 1, pp. 37–51, 1953.

Kumbargeri, Y. S. and Biligiri, K. P., "Understanding aging behaviour of conventional asphalt binders used in India," *Transp Res Proc*, vol. 17, pp. 282–290, 2016.

Kuwahara, N., Saeki, S., Konno, S., and Kaneko, M., "Temperature dependence of polymer chain dimensions in the polystyrene-cyclopentane system," *Polymer*, vol. 15, no. 2, pp. 66–68, 1974.

Leaderman, H., *Elastic and creep properties of filamentous materials and other high polymers.* The Textile Foundation, 1943.

Lee, D., *Asphalt durability correlation in Iowa*, 1973, 468, Transp Res Rec.

Li, Y. and Mattice, W. L., "Atom-based modeling of amorphous 1,4-cis-polybutadiene," *Macromolecules*, vol. 25, no. 19, pp. 4942–47, 1992.

Marasteanu, M. O. and Anderson, D. A., "Comparison of moduli for asphalt binders obtained from different test devices," *Asphalt Paving Technol*, vol. 69, pp. 574–606, 2000.

Marasteanu, M. O., Clyne, T., McGraw, J., Li, X., and Velasquez, R., "High-temperature rheological properties of asphalt binders," *Transp Res Rec*, vol. 1901, pp. 52–59, 2005.

Mark, J. E., "Random-coil configurations of cis-l,4-polybutadiene and cis-1,4-polyisoprene. Theoretical interpretation," *J Am Chem Soc*, vol. 88, no. 19, pp. 4354–9, 1966.

Mark, J. E., "Interpretation of random-coil configurations of trans-1,4-polybutadiene and trans-1,4-polyisoprene," *J Am Chem Soc*, vol. 89, no. 26, pp. 6829–35, 1967.

Mark, J. E., "Thermoelastic properties of rubberlike networks and their thermodynamic and molecular interpretation," *Rubber Chem Technol*, vol. 46, no. 3, pp. 593–618, 1973.

Mark, J. E., Abou-Hussein, R., Sen, T. Z., and Kloczkowski, A., "Some simulations on filler reinforcement in elastomers," *Polymer*, vol. 46, no. 21, pp. 8894–8904, 2005.

Mark, J. E. and Erman, B., *Rubberlike Elasticity: A Molecular Primer*. Wiley Interscience, 1988.

McCrum, N. G., Buckley, C. P., and Bucknall, C. B., *Principles of Polymer Engineering, 2nd Edition*. Oxford Univ Press, 1997.

Meissner, B. and Matjka, L., "Comparison of recent rubber-elasticity theories with biaxial stress-strain data: The slip-link theory of Edwards and Vilgis," *Polymer*, vol. 43, no. 13, pp. 3803–3809, 2002.

Moraglio, G., "Cistactic polybutadiene: unperturbed molecular dimensions at various temperatures," *Eur Polym J*, vol. 1, no. 2, pp. 103–9, 1965.

Nakajima, A. and Saijyo, A., "Unperturbed chain dimensions of isotactic polypropylene in theta solvents," *J Polym Sci Part B: Polym Phys*, vol. 6, no. 4, pp. 735–744, 1968.

Ogden, R. W., "Large deformation isotropic elasticity - On the correlation of theory and experiment for incompressible rubberlike solids," *Proc R Soc Lond A*, vol. 326, no. 1567, pp. 565–584, 1972.

Okada, O. and Furuya, H., "Molecular dynamics simulation of cis-1,4-polybutadiene. 1. Comparison with experimental data for static and dynamic properties," *Polymer*, vol. 43, no. 3, pp. 971–976, 2001.

Okada, O., Furuya, H., and Kanaya, T., "Molecular dynamics simulation of cis-1,4-polybutadiene. 2. Chain motion and origin of the fast process," *Polymer*, vol. 43, no. 3, pp. 977–982, 2001.

Orofino, T. and Ciferri, A., "Temperature dependence of the unperturbed dimensions of polystyrene," *J Phys Chem*, vol. 68, no. 11, pp. 3136–3141, 1964.

Orofino, T. and Mickey Jr, J., "Dilute solution properties of linear polystyrene in θ-solvent media," *J Chem Phys*, vol. 38, no. 10, pp. 2512–2520, 1963.

Ott, M., Pérez-Aparicio, R., Schneider, H., Sotta, P., and Saalwächter, K., "Microscopic study of chain deformation and orientation in uniaxially strained

polymer networks: NMR results versus different network models," *Macromolecules*, vol. 47, no. 21, pp. 7597–7611, 2014.

Pancheri, F. Q. and Dorfmann, L., "Strain-controlled biaxial tension of natural rubber: New experimental data," *Rubber Chem Technol*, vol. 87, no. 1, pp. 120–138, 2014.

Paul, D. and DiBenedetto, A., "Diffusion in amorphous polymers," *J Polym Sci: Part C*, no. 10, pp. 17–44, 1965.

Petersen, J., Robertson, R., Branthaver, J., Harnsberger, P., Duvall, J., Kim, S., Anderson, D., Christiansen, D., and Bahia, H., *Binder characterization and evaluation: Volume 1*, 1994, Rep. No. SHRP-A-367, Strategic Highway Research Program, National Research Council, Washington, DC.

Ragab, A. R. A. and Bayoumi, S. E. A., *Engineering solid mechanics: fundamentals and applications*. CRC Press, 1998.

Rapold, R. F. and Suter, U. W., "Conformational characteristics of polystyrene," *Macromol Theory Simul*, vol. 3, no. 1, pp. 1–17, 1994.

Reuvekamp, L. A. E. M., Debnath, S. C., Brinke Ten, J. W., Van Swaaij, J. P., and Noordermeer, J. W. M., "Effect of zinc oxide on the reaction of TESPT silane coupling agent with silica and rubber," *Rubber Chem Tech*, vol. 77, no. 1, pp. 34–49, 2004.

Rivlin, R. S. and Saunders, D., "Large elastic deformations of isotropic materials. VII. Experiments on the deformation of rubber," *Phil Trans R Soc Lond A*, vol. 243, no. 865, pp. 251–288, 1951.

Rubinstein, M. and Colby, R. H., *Polymer physics*. Oxford University Press New York, 2003.

Rubinstein, M. and Panyukov, S., "Nonaffine deformation and elasticity of polymer networks," *Macromolecules*, vol. 30, no. 25, pp. 8036–8044, 1997.

Schlögl, S., Trutschel, M. L., Chasśe, W., Riess, G., and Saalwächter, K., "Entanglement effects in elastomers: Macroscopic vs microscopic properties," *Macromolecules*, vol. 48, no. 8, p. 2855, 2014.

Smith, G. D., Borodin, O., Bedrov, D., Paul, W., Qiu, X., and Ediger, M. D., "13c NMR spin-lattice relaxation and conformational dynamics in a 1,4-polybutadiene melt," *Macromolecules*, vol. 34, no. 15, pp. 5192–5199, 2001.

Smith, G. D., Borodin, O., and Paul, W., "A molecular-dynamics simulation study of dielectric relaxation in a 1,4-polybutadiene melt," *J Chem Phys*, vol. 117, no. 22, pp. 10 350–10 359, 2002.

Smith, G. D. and Paul, W., "United atom force field for molecular dynamics simulations of 1,4-polybutadiene based on quantum chemistry calculations on model molecules," *J Phys Chem A*, vol. 102, no. 7, pp. 1200–1208, 1998.

Starkova, O. and Aniskevich, A., "Poisson's ratio and the incompressibility relation for various strain measures with the example of a silica-filled SBR rubber in uniaxial tension tests," *Polym Test*, vol. 29, no. 3, pp. 310–318, 2010.

Subhani, P. M. and Kumar, R. K., "A new stored energy function for rubber like materials for low strains," *Mech Adv Mater Struct*, vol. 16, no. 5, pp. 402–416, 2009.

Suter, U. W. and Flory, P. J., "Conformational energy and configurational statistics of polypropylene," *Macromolecules*, vol. 8, no. 6, pp. 765–76, 1975.

ten Brinke, J. W, Litvinov, V. M., Wijnhoven, J. E. G. J., and Noordermeer, J. W. M., "Interactions of stober silica with natural rubber under the influ-

ence of coupling agents, studied by ^{1}H NMR T_2 relaxation analysis," *Macromolecules*, vol. 35, no. 27, pp. 10 026–37, 2002.

Theodorou, D. N. and Suter, U. W., "Shape of unperturbed linear polymers: polypropylene," *Macromolecules*, vol. 18, no. 6, pp. 1206–14, 1985.

Tobolsky, A. V., "Stress relaxation studies of the viscoelastic properties of polymers," *J Appl Phys*, vol. 27, no. 7, pp. 673–685, 1956.

Traxler, R. N., *Durability of asphalt cements*, 1963, 32, Assoc Asphalt Paving Technol Proc.

Treloar, L. R. G., *The physics of rubber elasticity.* Oxford University Press, USA, 1975.

Treloar, L., "Stress-strain data for vulcanised rubber under various types of deformation," *Trans Faraday Soc*, vol. 40, pp. 59–70, 1944.

Tsolou, G., Mavrantzas, V. G., and Theodorou, D. N., "Detailed atomistic molecular dynamics simulation of cis-1,4-poly(butadiene)," *Macromolecules*, vol. 38, no. 4, pp. 1478–1492, 2005.

Valanis, K. C. and Landel, R. F., "The strain-energy function of a hyperelastic material in terms of the extension ratios," *J Appl Phys*, vol. 38, no. 7, pp. 2997–3002, 1967.

Valić, S., "Orientational motions of chain segments in natural rubber crosslinked under uniaxial deformation," *Radiat Phys Chem*, vol. 97, pp. 393–397, 2014.

Vieyres, A., Pérez-Aparicio, R., Albouy, P. A., Sanseau, O., Saalwächter, K., Long, D. R., and Sotta, P., "Sulfur-cured natural rubber elastomer networks: correlating cross-link density, chain orientation, and mechanical response by combined techniques," *Macromolecules*, vol. 46, no. 3, pp. 889–899, 2013.

Wagner, M., "Analysis of small-angle neutron scattering data on poly (dimethylsiloxane) network unfolding," *Macromolecules*, vol. 27, no. 18, pp. 5223–5226, 1994.

Ward, I. M. and Sweeney, J., *Mechanical properties of solid polymers*. John Wiley & Sons, 2012.

White, J. L., *Rubber Processing: Technology, Materials, and Principles*. Hanser, Munich, 1995.

Williams, M. L., Landel, R. F., and Ferry, J. D., "The temperature dependence of relaxation mechanisms in amorphous polymers and other glass-forming liquids," *J Am Chem Soc*, vol. 77, pp. 3701–7, 1955.

Yoon, D. Y., Sundararajan, P. R., and Flory, P. J., "Conformational characteristics of polystyrene," *Macromolecules*, vol. 8, no. 6, pp. 776–83, 1975.

Zhan, Y. and Mattice, W. L., "Molecular dynamics simulation of the collapse of poly(1,4-trans-butadiene) to globule and to a thin film," *Macromolecules*, vol. 27, no. 24, pp. 7056–62, 1994.

Zhang, L. and Greenfield, M. L., "Analyzing properties of model asphalts using molecular simulation," *Energy fuels*, vol. 21, no. 3, pp. 1712–1716, 2007.

Zhang, L. and Greenfield, M. L., "Relaxation time, diffusion, and viscosity analysis of model asphalt systems using molecular simulation," *J Chem Phys*, vol. 127, no. 19, p. 194502, 2007.

Zhang, L. and Greenfield, M. L., "Rotational relaxation times of individual compounds within simulations of molecular asphalt models," *J Chem Phys*, vol. 132, no. 19, p. 184502, 2010.